"THE DETERMINATION OF NUCLEAR DECAY SCHEMES BY ABSORPTION AND COINCIDENCE MEASUREMENTS"

by

John Patrick
J. P. LONERGAN B. Sc.

(Thesis Submitted for the Degree of M. Sc. in Physics)

28. 2. 1951.

Note on the Numbering of Equations.

In this thesis equations are numbered in sequence in each section of a chapter. Thus equation (3.2, 1) is the first equation in section 3.2, (3.4, 10) is the 10th equation in section 3.4.

The examiners have pointed out to the author that the equations might have been numbered in sequence throughout a chapter. Such a system would simplify the notation and would possibly shorten the task of finding any particular equation.

C O N T E N T S

PLATES.

1. Coincidence Unit

2. (a) Preamplifier
   (b) Coincidence Circuit - front view
   (c) Coincidence Circuit - under chassis wiring
   (d) Scaler - front view
   (e) Scaler - under chassis wiring
   (f) Recorder

3. Geiger Counters
   (a) Conventional Cu-cathode Gamma Counter
   (b) G.E.C. Beta Counters, EHM2 and GM4
   (c) Beta Counter - Physics Dept., Sydney
   (d) Double Window Beta Counter - Physics Dept., Sydney

4. (a) Experimental Set-up for β-γ Coincidences
   (b) Experimental Set-up for Compton Electron Coincidences

5. Miscellaneous Supports and Attachments
   (a) Support for Counters : β-γ Measurements
   (b) Support for Counters : Compton Coincidences
   (c) Support for End Window Beta Counter, and Fittings
   (d) Source Holder and Absorber Holder
   (e) Absorber

I N T R O D U C T I O N

The radiations from heavy naturally occurring isotopes were observed by Becquerel in 1896[1]. The identification of the radiations - Alpha Particles, Beta Rays and Gamma Rays -, their nuclear origin and their properties, the stability of the nucleus and its mode of transformation constitute the essential topics of "Natural Radioactivity".[2] Radiations from lighter isotopes produced by the transmutation of certain stable elements irradiated with nuclear particles were observed for the first time in 1933 by the Joliots[3]. The subject matter of this "Artificial Radioactivity" includes the topics already mentioned for "Natural Radioactivity" and, in addition, the study of the production of unstable nuclei. The chief differences between the two types of radioactivity are, of course, the absence of radioactive series and the occurrence of positron emission and electron capture in the case of unstable nuclei produced artificially.

Characteristic of a particular nuclear transformation are its decay scheme and its half life. The former involves the emission of nuclear particles of energy equal to the energy difference between the "levels" of the initial and final nuclear states and includes the possibility of alternative modes of disintegration. The transition probabilities of these possible competitive modes of transformation determine the half life.

The greater part of this paper is concerned with the determination of the disintegration schemes of artificially produced radioactive nuclei from an investigation of the emitted radiations. Such an investigation involves identification of the radiations, determination of the energies of the various components, their relative

1. Reference B1.
2. See, for example, Reference H1, Chapters 11 and 12.
3. Reference C1.

probabilities and order of emission, and finally, the weaving of the experimental data into a self consistent energy diagram. A method for determining short half-life periods is also mentioned.

Fundamental to these investigations is the task of counting accurately the radiations emitted. Accordingly, after a preliminary Chapter on Radioactivity, this topic is discussed first. The methods of determining the energies of the radiations and the decay schemes are then described, and, finally, a detailed account of experiments on the isotopes Co^{60} and Ag^{110} is given.

CHAPTER 1.

THE FUNDAMENTALS OF RADIOACTIVITY

1.1. The Radiations.

The radiations of interest in the experiments reported here are beta rays (high speed electrons) and gamma rays (electromagnetic waves). Either type is specified by its energy usually expressed in electron volts[1], and, whilst monoenergetic gamma rays are observed, a continuous energy distribution up to a well defined maximum is found among the beta particles. It is assumed that the nuclear transformation corresponding to the emission of a beta particle involves an energy loss equal to the maximum energy W_o observed in the beta spectrum. A hypothetical particle, the neutrino, having no charge and very small mass takes away an amount of energy equal to the difference between W_o and the energy observed for any particular beta particle[2].

Both beta particles and gamma rays can penetrate matter although the range of the gammas may be very much greater than that of the betas. Beta rays can also produce ionisation in a gas.

The continuous absorption of gamma rays in matter is due to three processes

(1) Photo-electric Effect

(2) Compton electron scattering

(3) Pair Production.

The first of these involves the ejection of an electron from the K, L or M shell of an atom and the complete absorption of the incident gamma ray. The photoelectrons are monoenergetic, their

1. One electron volt = 1.591×10^{-12} erg.
   10^6 electron volts (1 M.E.V.) = 931 M.U. (mass units)
   = 1.768×10^{-27} grm.
   For gamma radiation, the energy and frequency are related by Planck's equation $\mathcal{E} = h\nu$.
2. For a discussion of the Fermi Theory of Beta decay, see K1, C2, or M1 pp. 40 et seq.

kinetic energy being equal to the difference between the energy of the incident gamma ray and the binding energy of the electron in the atom. The second process may be regarded as one of elastic collision between a gamma ray and an electron[1]. The Compton recoil electrons are found to have a continuous distribution of energies up to a sharp maximum W_c which is related to the energy W_γ of the gamma radiation by the formula[2]

$$W_c = \frac{2W_\gamma^2}{m_0c^2 + 2W_\gamma} \qquad (1.1,1)$$

In the third process the gamma ray disappears and a positron-electron pair is formed. Such a transformation is only possible when the energy of the gamma rays is greater than 1.02 M.e.v. and in the neighbourhood of a heavy nucleus. The threshold energy corresponds to the rest mass of an electron-positron pair.

The intensity of a monochromatic beam of gamma rays, passing through matter decreases exponentially.

$$I = I_0 e^{-\mu x} \qquad (1.1,2)$$

where the absorption coefficient, μ, can be expressed as a sum of partial coefficients

$$\mu = \mu_{photo} + \mu_{compton} + \mu_{pair} \qquad (1.1,3)$$

If N be the number of absorber atoms per sq. cm., the cross section per atom is[3]

$$\sigma = \mu/N \qquad (1.1,4)$$

The cross sections for the processes (1), (2) and (3) have been calculated by Heitler[4]. For a given absorber element process (1) is the most important at low energies, process (2) at intermediate energies and process (3) at very high energies. Where process (2) predominates, μ is proportional to NZ (there being Z electrons per atom); thus μ is approximately proportional

1. See, for example, Reference S1, p. 281.
2. Reference D1, p. 85.
3. One has $dI = -\mu I_0 e^{-\mu x} dx = -\mu I\, dx$, which may be compared with the defining equation (See Ref. H1, p. 325) of the "Cross Section"
4. Reference H2, Sections 13, 16 and 20 resp.

to ρ, the density of the absorber. Consequently a "mass absorption coefficient", μ/ρ, which is practically constant for all elements may be defined[1]. The photoelectric absorption coefficient at a great distance from the absorption edge[2] is proportional to Z^5 and to $\varepsilon^{-7/2}$. For gamma energies in excess of 1.02 M.e.v. where pair production is possible, μ_{pair} is proportional to Z^2 and increases rapidly with energy.

These features are displayed in Fig. 1.1 copied from Heitler.

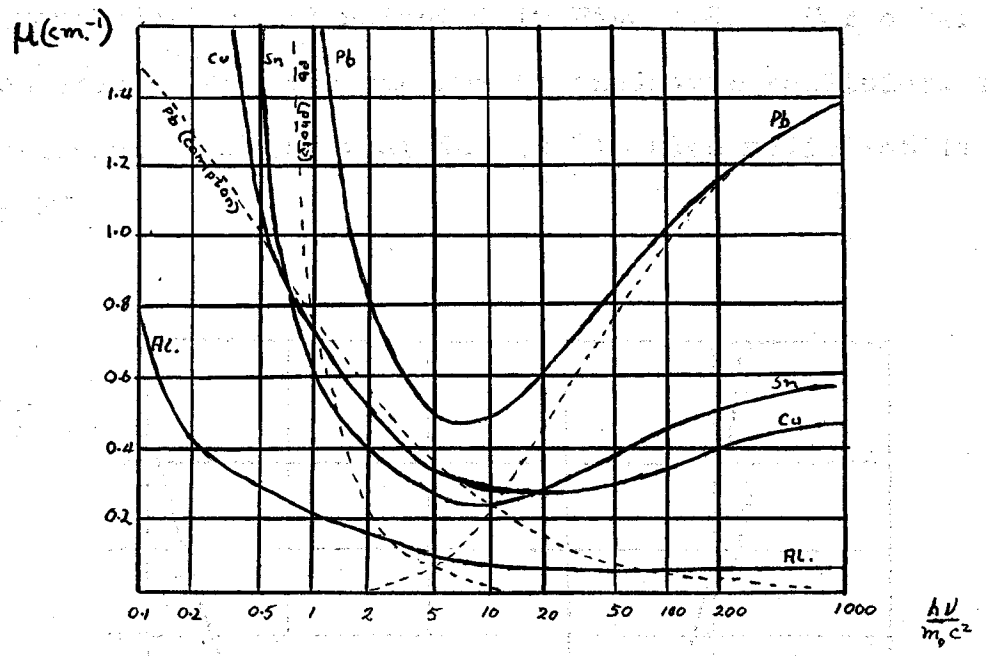

FIG. 1.1 Absorption coefficient μ as a function of gamma ray energy for different absorbers. The components μ_{photo}, $\mu_{compton}$ and μ_{pair} for lead are shown dotted.

1. The significance is that one can express the absorption as a function of grms per sq. cm. of absorber without specifying the absorber.
2. The "Absorption Edge" is defined to be that point on the Absorption coefficient v. quantum energy curve where the ionisation potential is equal to the energy of the gamma ray.

In passing through matter, fast charged particles lose energy following deflections in the fields of nuclei and as a result of inelastic collisions with atoms. According to the classical theory, the accelerations produced in the former process are accompanied by radiation, whilst on the quantum theory there exist definite probabilities that light quanta be emitted. The inelastic collisions involve excitation and ionisation of atoms. The cross sections for these two processes as a function of energy have been calculated by Heitler[1], and the energy loss per cm. as a function of primary energy of electrons passing through lead is illustrated in Fig. 1.2. For other absorbers, the energy loss per cm. due to inelastic collisions is proportional to Z and that due to "impulse radiation" is proportional to Z^2.

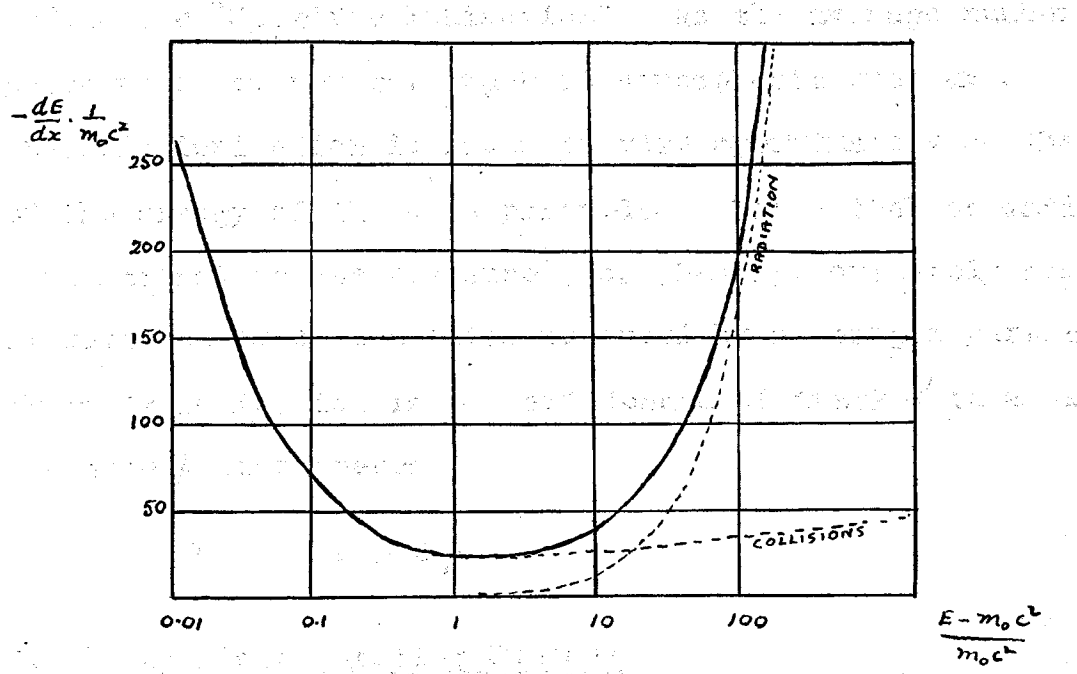

FIG. 1.2 Energy loss per cm. in lead as a function of primary energy of electrons.

Whilst a definite range can be calculated for fast monoenergetic electrons[2], the difficulty in obtaining a range-energy curve for beta particles lies in the continuous distribution of energy amony them. It is found that the mean angle

1. Reference H2, Sections 17 and 23.
2. Reference H2, p. 223.

of deflection of beta particles after passage through an absorber layer increases with the atomic number of the absorber. For thin layers the mean angle of deflection is proportional to the square root of the thickness, but, as the latter is increased, tends to a constant value. "Back scattering", i.e. deflection through more than 90°, may occur. The intensity of the radiation after passage through thickness x of absorber is found to obey a law

$$\frac{dN}{dx} = -\mu(x).N \qquad (1.1,5)$$

Thus, in investigating the intensity distribution of a beta source, mounted on suitable backing, one is faced with the problems of allowing for back scattering and for self absorption in the source.

The density of ionisation produced by a beta particle in a gas varies along the track of the particle. However, one may define the "Specific Ionisation" as the average number of ion pairs produced per cm. track at atmospheric pressure. The specific ionisation is found to vary approximately as the inverse of the energy of the beta particle. Since the ionisation is proportional to the pressure[1], one has approximately for the average number of ion pairs produced by a charged particle whose specific ionisation is σ, and length of track ℓ in a gas of pressure p atmospheres

$$I = \sigma \ell p \qquad (1.1,6)$$

1.2. The Disintegrating Nucleus.

If one assumes[2] that the number of nuclei disintegrating per second is proportional to the number of nuclei present, i.e.

$$\frac{dN}{dt} = -\lambda N \qquad (1.2,1)$$

1. Deviations from this proportionality are sometimes found, particularly at higher pressures.
2. The Rutherford-Soddy Theory of Transformations. See, for example, H1, p. 244.

one obtains, by integration, the well known formula

$$N = N_0 e^{-\lambda t} \qquad (1.2,2)$$

for the activity at time t. Equation (1.2, 1) may be expressed in another way - the probability that a nucleus disintegrate in a time interval dt is proportional to dt.

$$P(dt) = \lambda\, dt \qquad (1.2,3)$$

Thus λ is a "transition probability"[1]. If several modes of disintegration are possible

$$\lambda = \lambda_1 + \lambda_2 + \cdots \qquad (1.2,4)$$

where $\lambda_1, \lambda_2 \cdots$ are the several transition probabilities. It may be deduced[2] that the mean life L of a nucleus and the half life T of an aggregate of nuclei are given by the relations

$$L = 1/\lambda \qquad (1.2,5)$$

$$\text{and} \quad T = \frac{\log_e 2}{\lambda} = \frac{0.693}{\lambda} \qquad (1.2,6)$$

The existence of discrete energy levels within the nucleus is inferred from the monoenergetic alpha particles and gamma rays observed in radioactive decay. The difficulty of reconciling the continuous distribution of energy found among the beta particles with this hypothesis has been mentioned.

The energy of the parent must be equal to the energy of the product plus the total energies of the disintegration particles. In mass units,

Mass of Parent = Mass of Product + Mass of Particles + Kinetic Energies of Particles

Fig. 1.3 shows the well known disintegration scheme of Co^{60} and Fig. 1.4 that proposed by Rutledge et al[3] for the isotope Ag^{110}. The latter is unusually complicated and provides

1. λ is often called the "transformation constant"
2. $L = \int_0^\infty t e^{-\lambda t} \lambda\, dt = 1/\lambda$
   $\frac{1}{2}N_0 = N_0 e^{-\lambda T}$, $\therefore \lambda T = \log_e 2$.
3. Reference R1.

an excellent illustration of the piecing-together of information obtained by observations of the emitted gamma radiations. The overall agreement between the observed gamma energies and the differences between nuclear levels is very good. The branching ratios[1] of the alternative modes of decay are inferred from the relative intensities of the observed particles[2]. Recent measurements[3] indicate a half life of 270 days for the isomer Ag^{110}.

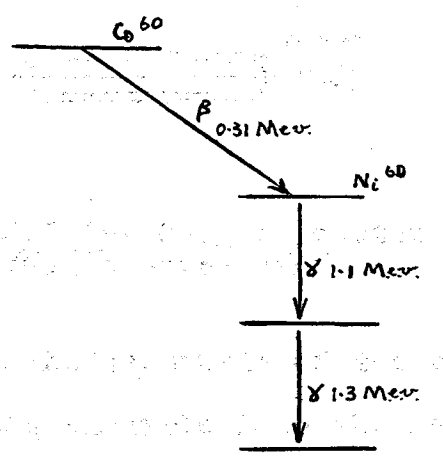

FIG. 1.3 Decay Scheme of Co^{60}.

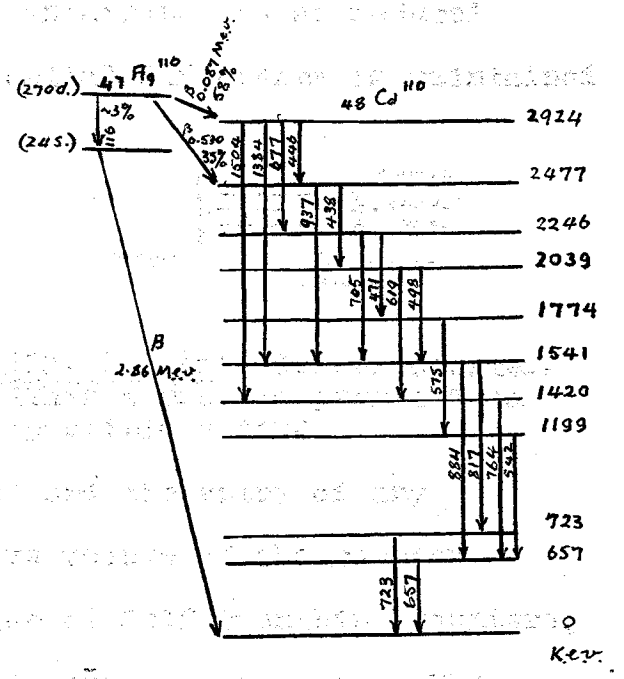

FIG. 1.4 Decay Schemes of Ag^{110} proposed by Rutledge et al.

Decay schemes of the type shown in Fig. 1.3 where there is only one beta ray per disintegration are called "Simple". Those of the type of Fig. 1.4 where two distinct half lives are observed are called "Compound"; that from the metastable level[4] (T = 270 days) in which transitions may occur from the initial nuclear state to alternative levels in the product nucleus is called "Complex".

1. Ratios of the transition probabilities.
2. Reference S2.
3. Reference G1.
4. "Metastable level" = Long lived excited state.

CHAPTER 2.

THE FUNDAMENTALS OF COUNTING NUCLEAR RADIATIONS

2.1. Self Quenching Geiger Counters.

A type of counter commonly used for detecting beta and gamma rays consists of an outer cylinder, the cathode, and a centre wire in a glass envelope containing gas at reduced pressure (Fig. 2.1). A large potential difference is maintained

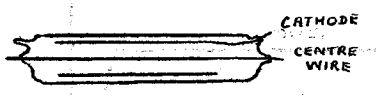

FIG. 2.1 (a) Geiger Counter (Glass envelope)

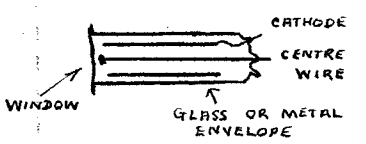

FIG. 2.1 (b) Geiger Counter. (Thin window to permit beta particle entry.)

across the terminals of the counter and the entry of any ionising particle into the sensitive volume of the counter initiates a discharge. In the case of Self Quenching Counters, the discharge is terminated by an internal mechanism. The primary ionisation may be caused by beta particles directly, provided the beta particles can penetrate the walls of the counter and reach the sensitive volume. Counters with thin mica windows, thin duralumin windows and glass bubble windows have been constructed for this purpose (Fig. 2.1(b)). Gamma rays are detected from ionisation produced by Compton or Photo electrons ejected from the walls of the counter or the cylinder. The electrical impulse caused by the discharge of the counter is fed to an amplifier and electronic counting circuit (Fig.2.2).

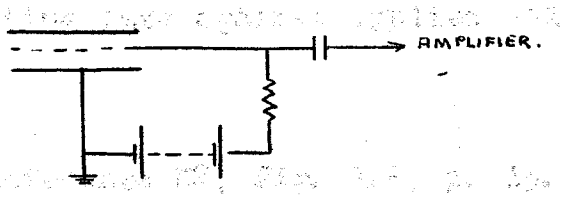

FIG. 2.2 Electrical connection to Geiger Counter.

The pulse size-voltage characteristic of a counter of the type shown in Fig. 2.1 is drawn in Fig. 2.3 for a strongly ionising alpha particle and for a weakly ionising cosmic ray[1]. The counters discussed here are operated

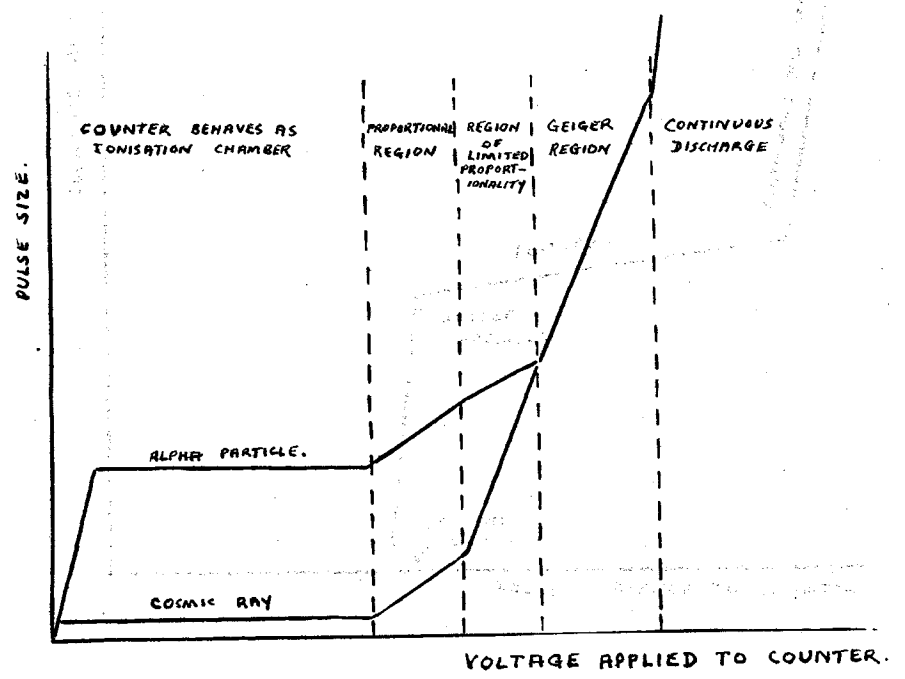

FIG. 2.3 Pulse size-voltage characteristic for a counter of the type shown in Fig. 2.1.

in the Geiger region where, for a given operating voltage, the pulse size is independent of the primary ionisation.

A self quenching Geiger counter may be constructed after the manner of Fig. 2.1. The cathode cylinder may be of copper, stainless steel, lead or gold film deposited on the glass, and the centre wire of tungsten (generally 0.003" to 0.012" diameter) which can be sealed readily to glass. The counter may be filled to approximately 10 cms. pressure with a mixture of 90% monatomic gas (e.g. argon) and 10% polyatomic gas (e.g. alcohol). If one places a source close to a newly constructed counter and plots a curve of counting rate against applied voltage, one obtains

1. See Reference K2, Fig. 1.2, p. 13.

a curve similar to that of Fig. 2.4. The correct operating

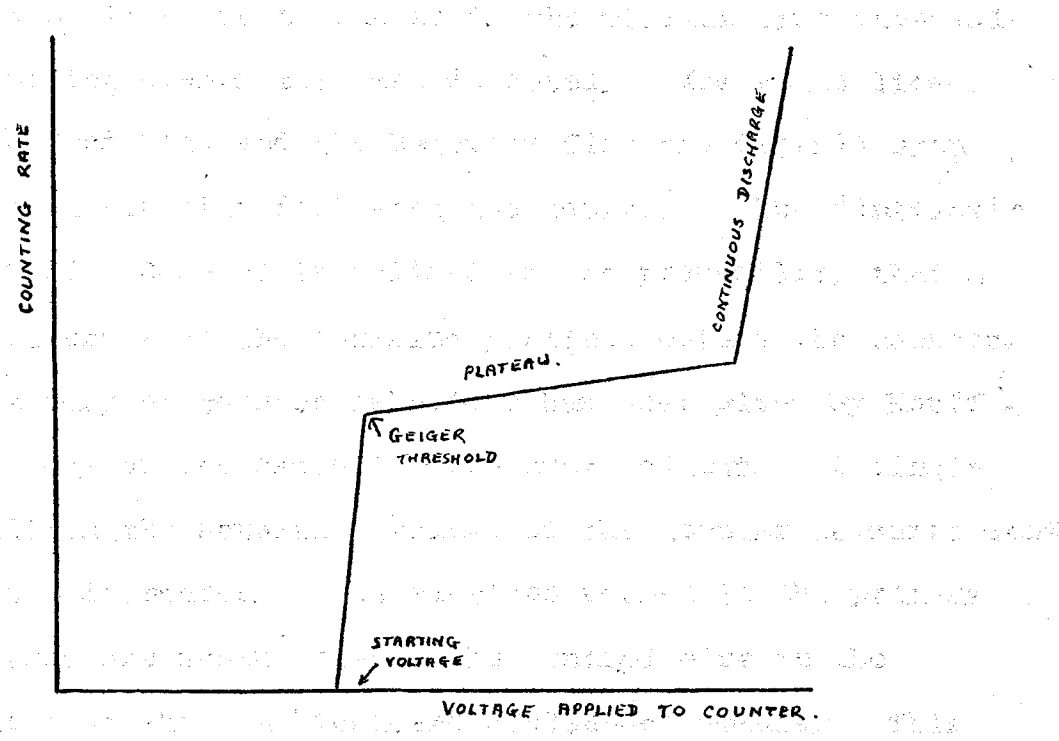

FIG. 2.4 Counting rate plotted against applied voltage for a typical Geiger Counter.

point is roughly in the centre of the plateau. When one examines the pulses obtained from the counter on a Cathode Ray Oscilloscope, one observes patterns of the type shown in Fig. 2.5. The rapid initial rise of the pulse is called the "Break", the time interval for which no pulses occur following the Break the

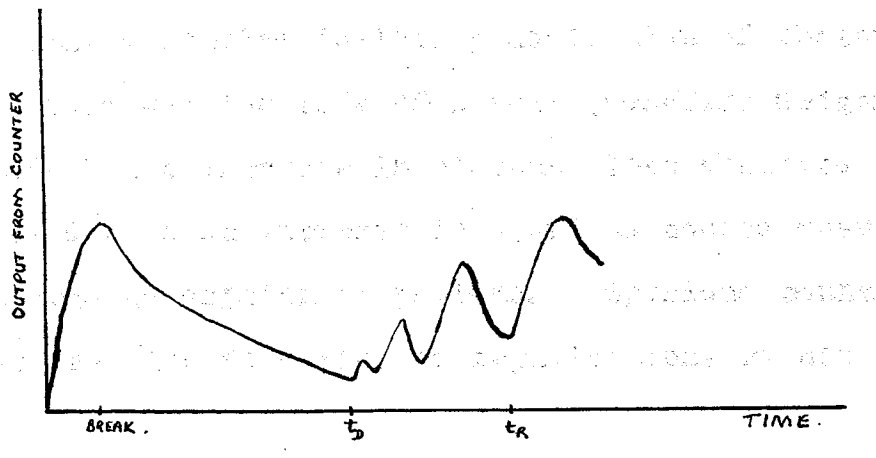

FIG. 2.5 Output pulses from Geiger Counter. The Dead Time (t_D) and the recovery time (t_R) are shown.

"Dead Time", and the time interval required for pulses following the Break to attain their full size the "Recovery Time". The "Resolving Time" of a Counter is the minimum time interval between ionising events that are detected. Its value lies between the Dead Time and the Recovery Time and depends upon the electronic circuits following the counter. The "Intrinsic Efficiency" of a Counter is defined as the probability that a discharge occurs when the ionising particle enters the counter.

The theory of counter behaviour has been given by Korff[1]. A brief summary of the essential features follows. A single electron within the sensitive volume of the counter is sufficient to initiate a discharge. The electrons formed in the primary ionising event are drawn towards the central wire in the neighbourhood of which a "Townsend Avalanche" occurs. This avalanche is complete in less than a microsecond and the positive ion sheath remaining around the central wire lowers the field in this region and terminates the discharge. Positive ions then travel out towards the cylinder, and, during this process which takes a hundred or more microseconds, the counter begins to recover. The purpose of the polyatomic molecules is to absorb photons formed in the initial avalanche and those resulting from recombination at the cathode. These photons would produce photoelectrons and perpetuate the discharge. The dissociation of the polyatomic molecules following absorption of photons is one of the reasons why the life of a self quenching Geiger counter is limited. The increase in plateau slope observed as the counter ages is due to an increase in spurious counts resulting from incomplete absorption of photons. Spurious counts may also result from the formation of negative ions within the counter.

1. See Reference K2, p. 91 et seq.

The "Intrinsic Efficiency" of the counter may be shown to be[1]

$$G = 1 - e^{-\alpha l p}$$

in the notation of Chapter 1, equation (1.1, 6). Thus, for example, for a fast electron ($\alpha \sim 30$ ions per cm. per atmosphere) traversing a path of length 2 cms. in a counter filled with gas at 8 cms. pressure.

$$G = 99.8\%$$

An expression for the recovery time in terms of constants of the counter is given by Korff[2]. The recovery time is inversely proportional to the capacity of the centre wire and associated wiring, increases with the radius of the cylinder and decreases with the radius of the centre wire.

The operating potential depends on the type and pressure of gas used and the diameter of the centre wire. The noble gases have lower starting potentials than the common diatomic gases, whilst the addition of a polyatomic gas to a monatomic gas raises the operating potential from about 800 volts to about 1100 volts. As the diameter of the centre wire is increased, the operating potential rises.

Flat plateaus are desirable and may be obtained by using a pure argon - absolute alcohol mixture[3]. Contamination with air results in the formation of negative oxygen ions which produce spurious counts and cause the plateau slope to rise.

2.2. Scaling Circuits and Recorders.

The electrical impulses from the Geiger counter must be recorded accurately and visual indication of the counts must be provided. An early method of achieving this consisted

1. See Reference K2, p. 69.
2. See Reference K2, p. 94.
3. Spatz (Reference S3) quotes a mixture of 95% argon (99.8% pure) and 5% absolute alcohol.

in amplifying and lengthening the Geiger pulses and applying them to the grid of a power tube which is normally non-conducting and which has in its plate circuit a telephone message register[1]. A big disadvantage lies in the fact that the message register will not respond to more than about ten evenly spaced impulses per second. Since the resolving time of the Geiger counter is several hundred microseconds, counting losses in the Geiger counter will be negligible compared to recording losses which are large even at low counting rates. For example, if the Geiger Counter is responding to 10 random events per second, losses in the Geiger counter will be less than 0.3% and those in the recorder 60%.

The speed of operation of an electro-mechanical register is limited electrically by the time constant L/R of the winding and mechanically by the moment of inertia of the armature and the maximum torque which can be applied to it. The latter is limited by magnetic leakage, core saturation and permissible heat dissipation in the winding. The use of short square pulses to excite the winding is suggested by the last factor.

High speed mechanical registers have been developed. Commercially, the "Cyclotron Specialties Recorder" will respond to at least 50 evenly spaced impulses per second and the "Cenco" meter to at least 120. A recorder of Swedish design and marketed by Tracerlab Inc. is capable of registering over 300 impulses per second. Several fast counting meters using the mechanism of a watch with the escapement replaced by an electrically operated release have been constructed[2]. A recorder capable of operating in about 1/2000 sec. has been described by Neher[3].

1. An electro-mechanical device used in automatic exchanges to record the number of outgoing calls initiated by a subscriber.
2. See, for example, Reference T1.
3. See Reference N1.

Electronic circuits for operating mechanical registers are discussed by Lewis[1]. A circuit designed by the writer is described in Chapter 5.

With the development of the fast[2] scale-of-2^n, the major responsibility for counting losses may be transferred to the Geiger counter with its resolving time of several hundred microseconds, and, at the same time, slow[3] mechanical recorders may be used. A Scale-of-2 may be defined as an electronic circuit[4] in which one output pulse is obtained for every two input pulses; a scale-of-2^n consists of n scales-of-2 in series. The original Thyratron scale-of-2 has the merit of simplicity but the disadvantage of a rather long resolving time. The latter is related to the deionisation time[5] which may occupy a period as large as 1 millisecond. This long resolving time may lead to counting losses or, worse, to "jamming"[6] of the scaler.

Hard tube scales-of-2 usually consist of two vacuum tubes coupled together in the manner of the Eccles-Jordan Trigger circuit[7]. A description of such a circuit due to Rotblat[8] and based on an original design by Stevenson and Getting[9] will be found in Chapter 5; this circuit contains a feed-back loop which converts the scale-of 2^4 to a scale-of-10.

1. See Reference L1, p. 92 et seq.
2. "Fast" in that its input resolving time is less than 100 μ secs.
3. (and therefore not too costly).
4. The first scale-of-2 was designed by C.E. Wynn-Williams See Reference W1.
5. A discussion of the deionisation time may be found in Reference R2, p. 398 and in Reference T2, p. 347.
6. Both thyrations remaining alight. See Reference L1, pp. 82, 83.
7. Reference E3.
8. Reference R3.
9. Reference S4.

"Ring Circuits" providing any desired scaling ratio have been described[1]. In general, these do not appear to be as reliable as hard tube scales-of-2 ; however, when driven from a cathode follower, more satisfactory operation is obtained[2].

A good general account of scalers and recorders (up to 1942) may be found in Reference L1, Chapter VIII.

2.3. Counting Losses.

In discussing counting losses one must know the distribution in time of the radiated particles and the behaviour of the detector and auxiliary apparatus when subject to such radiations. The mathematical approach to the subject of counting losses is simplified by the use of the Laplace Transformation[3], a knowledge of which is assumed in the following treatment[4].

It has been shown in Chapter 1 (equation 1.2, 3) that the probability that a nucleus disintegrate in a time interval dt is equal to λdt. For N nuclei, the probability of a disintegration is $N\lambda dt$, or $n\,dt$ where n is the average disintegration rate[5]. From this it follows[6] that the probability of exactly m disintegrations in a time interval t is

$$P_m(t) = \frac{(nt)^m}{m!} e^{-nt} \qquad (2.3,1)$$

One notes that

$$\sum_{m=0}^{\infty} P_m(t) = e^{-nt}\left[1 + nt + \frac{(nt)^2}{2!} + \cdots\right] = 1,$$ as it should.

The expected number of events, $\bar{m}$, in a time interval t is

$$\bar{m}(t) = \sum_{m=0}^{\infty} m\, P_m(t) = nt \qquad (2.3,2)$$

and the variance

$$\sigma^2 = \sum_{m=0}^{\infty} (m-\bar{m})^2 P_m(t)$$

$$= \sum_{m=0}^{\infty} (m^2 - \bar{m}^2) P_m(t)$$

$$= \sum_{m=0}^{\infty} \left[m(m-1) P_m(t) + m P_m(t)\right] - n^2 t^2$$

1. References W2 and S5.
2. Dr. K. Landecker, private communication.
3. See, for example, Reference C4.
4. The arguments used here are based on Reference E1.
5. It is assumed that N is sensibly constant over the period of observation.
6. Reference L1, p. 115.

$$\text{i.e.} \quad \sigma = \sqrt{nt} \tag{2.3, 3}$$

Equations (2.3, 2) and (2.3, 3) express the important fact that an experimental determination of n from a total number of observations m obtained in time t is subject to a fractional error $1/\sqrt{m}$.

The probability that the first disintegration occur in dt at time t from a chosen origin[1] is equal to the probability that no disintegration occurs in t and one in dt.

$$\text{i.e.} \quad \Delta P_1 = n e^{-nt}\, dt$$

$$\text{or} \quad p_1 \underset{def.}{=} \frac{\Delta P_1}{dt} = n e^{-nt} \tag{2.3, 4}$$

where p_1 is defined to be the Probability Density for the first event. One can also define the probability density for the m^{th} event[2].

$$p_m \underset{def.}{=} \frac{\Delta P_m}{dt}$$

where ΔP_m is the probability that the m^{th} disintegration occur in dt at t. Consideration of Fig. 2.6 leads to the

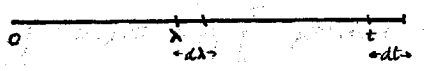

FIG. 2.6.

relation

$$\Delta P_{m_1+m_2} = \int_{\lambda=0}^{t} p_{m_1}(\lambda)\, p_{m_2}(t-\lambda)\, d\lambda\, dt$$

[3]

Thus

$$L\{p_{m_1+m_2}\} = L\{p_{m_1}\} \cdot L\{p_{m_2}\}$$

1. The origin is arbitrary and may therefore be taken at a disintegration (or "event")
2. The origin is again quite arbitrary and in the discussion of counting losses occurs at an event.
3. Reference C4, p. 37.

and hence[1]

$$L\{p_m\} = \left[L\{p_1\}\right]^m = \left(\frac{n}{n+s}\right)^m$$

from which it follows[2] that

$$p_m = \frac{n^m}{(m-1)!}\, t^{m-1} e^{-nt} \qquad (2.3,5)$$

One observes that

$$\int_0^\infty p_m(t)\,dt = \frac{n^m}{(m-1)!}\, L\left\{t^{m-1}\right\}$$

$$= 1 \qquad (2.3,6)$$

which expresses the certainty that, provided one waits long enough, the m^{th} event will be observed.

The mathematical theory of counting losses provides information on the mean time interval between events and the spread in time (standard deviation) of successive events about the mean. Provided one knows the probability density function, both of these quantities may be determined readily by means of the Laplace Transformation. One has

$$L\{p(t)\} = \int_0^\infty p(t)\, e^{-st}\,dt$$

$$= \int_0^\infty p(t)\,dt - s\int_0^\infty t\,p(t)\,dt + \frac{s^2}{2!}\int_0^\infty t^2 p(t)\,dt + \cdots + \frac{(-s)^r}{r!}\int_0^\infty t^r p(t)\,dt + \cdots \qquad (2.3,7)$$

$$= 1 - s\bar{t} + \frac{s^2}{2!}\overline{t^2} + \cdots\cdots + \frac{(-s)^r}{r!}\overline{t^r} + \cdots\cdots \qquad (2.3,8)$$

where $\overline{t^r}$ is defined to be the r^{th} moment of the distribution. One obtains $\overline{t^r}$ by expanding $L\{p(t)\}$, which is obtained from a Table of Transforms[3], in a power series in s, and equating the coefficient of s^r to $\frac{(-1)^r}{r!}\,\overline{t^r}$. The variance is obtained by recalling[4] that

$$\sigma^2 = \overline{t^2} - (\bar{t})^2 \qquad (2.3,9)$$

1. Reference C4, p. 295, Transform 8.
2. Reference C4, p. 294, Operation 11 and p. 295, Transform 3.
3. See, for example, Reference C4, pp. 294-302.
4. $\sigma^2 = \int_0^\infty (t-\bar{t})^2 p(t)\,dt$
$= \int_0^\infty t^2 p(t)\,dt - 2\bar{t}\int_0^\infty t\,p(t)\,dt + (\bar{t})^2\int_0^\infty p(t)\,dt$
$= \overline{t^2} - 2(\bar{t})^2 + (\bar{t})^2$.

For example, as far as the radioactive source is concerned

$$p_1(t) = n e^{-nt}$$

$$L\{p_1(t)\} = \frac{n}{n+s} = \left(1 + \frac{s}{n}\right)^{-1} = 1 - \frac{s}{n} + \frac{s^2}{n^2} + \cdots\cdots$$

and hence $\bar{t} = \frac{1}{n}$ (2.3, 10)

and $\sigma^2 = \frac{2}{n^2} - \frac{1}{n^2}$

or $\sigma = \frac{1}{n} = \bar{t}$ (2.3, 11)

That is, the average interval between events is equal to the reciprocal of the average disintegration rate, and the standard deviation of the interval is equal to the average interval.

The probability density function for the m^{th} event is (equation 2.3, 5)

$$p_m(t) = \frac{n^m}{(m-1)!} t^{m-1} e^{-nt}$$

$$L\{p_m(t)\} = \left(\frac{n}{n+s}\right)^m$$

$$= 1 - m\left(\frac{s}{n}\right) + \frac{m(m+1)}{1.2}\left(\frac{s}{n}\right)^2 + \cdots\cdots$$

Hence $\bar{t}_m = \frac{m}{n}$ (2.3, 12)

$$\sigma^2 = \bar{t}_m^2 - (\bar{t}_m)^2$$

$$= \frac{m}{n^2}$$

or $\sigma = \frac{\sqrt{m}}{n} = \frac{\bar{t}_m}{\sqrt{m}}$ (2.3, 13)

The significance of equations (2.3, 12) and (2.3, 13) in relation to (2.3, 10) and (2.3, 11) may be grasped from the following illustration. Suppose a perfect[1] detector is exposed to a source n and connects directly to a recording circuit. The average spacing between input pulses to the recording circuit is $\frac{1}{n}$ and the standard deviation of the spacing between successive pulses is $\frac{1}{n}$. Now suppose the source strength is increased by a factor m and that a perfect[1] scale-of-m is

1. Having zero resolving time (See definition p. 21) and therefore not subject to losses.

placed between detector and recorder. The average spacing between input pulses to the recording circuit is again $1/n$ but the standard deviation is now reduced from $1/n$ to $1/\sqrt{m} \cdot 1/n$. The effect of the scaler is to reduce the numbers of short and long intervals.

In an experimental set-up, one has a detector[1], scaling circuit and recording unit each liable to introduce counting losses. The probability density function for the events exciting the detector has been determined (equation (2.3, 4)). The density function is modified by the detector because of counting losses resulting from its finite resolving time, by the scaler because of the scaling factor (and because of counting losses if the scaler resolving time exceeds that of the detector), and by the recorder because of counting losses. The problem, then, is to determine the density function for the recorded events, the resolving characteristics of the equipment being given. From this density function one deduces the average rate at which events are recorded and the standard deviation. Allowance can then be made for counting losses and a statistical error can be assigned the corrected result. Alternatively, given certain criteria, one can deduce the optimum circuit requirements.

A "Resolving Characteristic" is ascribed to a counter, and two limiting cases occur in practice:

1) The counter records an event and is unresponsive for a definite time interval τ during which further events are lost. τ is the "Non-extended Resolving Time".

2) The counter records an event and is unresponsive for a time interval τ provided no further events occur. If, during the interval τ, an event occurs, it is lost and initiates the unresponsive time τ. τ is the "Extended Resolving Time".

1. In the experiments reported here, a Geiger counter with resolving time ~ 200 μsecs.

Experimentally one determines which type of resolving characteristic is to be ascribed to a circuit by measurements with groups of three pulses whose relative separations can be varied. It is observed that counters cannot usually be classified strictly under the one or the other of these two types. However, since most counters have a resolving characteristic tending more towards the one than the other, reliable calculations can be made on the basis of such classification.

The effect of the resolving characteristic of a counter is to introduce counting losses. Mathematically, the effect is to modify the density function[1]:

$$p(t) \longrightarrow p^*(t) \qquad (2.3,14)$$

where
$$\left.\begin{aligned} p^*(t) &= u(t-\tau)\,p(t) \\ u(t-\tau) &= 0, \quad t < \tau \\ &= 1, \quad t \geq \tau \end{aligned}\right\} \qquad (2.3,15)$$

One has $\int_0^\infty p^*(t)\,dt = A^* < 1$,

and hence the <u>normalised</u> density function[2] for counted events is $\frac{1}{A^*}\,p^*(t)$.

Now $L\left[\frac{1}{A^*}\,p^*(t)\right] = 1 - s\,\overline{t^*} + \frac{s^2}{2!}\,\overline{t^{*2}} + \ldots\ldots$ [3]

and hence $L\left[p^*(t)\right] = A^*\left[1 - s\,\overline{t^*} + \frac{s^2}{2!}\,\overline{t^{*2}} \ldots\ldots\right] \qquad (2.3,16)$

where $A^* = \int_0^\infty p^*(t)\,dt \qquad (2.3,17)$

Thus, for a non-extended resolving time, one obtains the Laplace transformation of $p^*(t)$, the un-normalised modified density function, and expands it in a power series in s. The

1. Notation: $\begin{pmatrix}\text{one}\\\text{two}\\\text{three}\end{pmatrix}$ star - output of $\begin{pmatrix}\text{first}\\\text{second}\\\text{third}\end{pmatrix}$ counting unit
2. Normalising the density function expresses the certainty of a further counted event.
3. C.f. equation (2.3, 8)

zero moment term is the reciprocal of the normalising factor. The average interval between counted events and the standard deviation of the interval between counted events are obtained as described before.

When the counter has an extended resolving time, every event, whether counted or not, initiates the dead time, and consequently the probability that an event be counted is $\int_0^\infty u(t-\tau)\, p(t)\, dt$

Thus $$n^* = nA^* \qquad (2.3,18)$$

where A^* is defined in (2.3, 17) and may be obtained from equation (2.3, 16).

It is proposed to illustrate the principles described above by considering counting losses resulting from an experimental arrangement in which a Geiger counter having a non-extended resolving time τ_1 is followed by a scale-of-m which has a non-extended resolving time τ_2 ($< \tau_1$) and which precedes a recording circuit having an extended resolving time τ_3. This is the arrangement used in the experiments described in Chapter 6.

The density function for the events fed to the Geiger counter is (equation 2.3, 4)

$$p(t) = n e^{-nt}$$

The un-normalised density function for the output of the counter is

$$p^*(t) = u(t-\tau_1)\, n e^{-nt}$$

One has[1]

$$L\{p^*(t)\} = e^{-n\tau_1}\left[e^{-\tau_2 s} \cdot \frac{n}{n+s}\right]$$

$$= e^{-n\tau_1}\left[1 - s(\tau_1 + \tfrac{1}{n}) + s^2(\tfrac{1}{n^2} + \tfrac{\tau_2^2}{2} + \tfrac{\tau_2}{n}) \cdots\right] \qquad (2.3,19)$$

Comparing this result with equation (2.3, 16), one finds

1. $u(t-\tau_1)\, n e^{-nt} = u(t-\tau_1)\, n e^{-n(t-\tau_1)}\, e^{-n\tau_1}$
$= F_{\tau_1}(t) \cdot e^{-n\tau_1}$, in the notation of Ref. C4, Theorem 1, p. 22. $F(t) = n e^{-nt}$. Hence the result quoted.

$$\left.\begin{aligned} A^* &= e^{-n\tau_1} \\ \overline{t^*} &= \tau_1 + \frac{1}{n} \\ \sigma &= \frac{1}{n} \end{aligned}\right\} \qquad (2.3,20)$$

Thus, for the Geiger counter alone, the observed output rate is

$$n^* = \frac{1}{\overline{t^*}} = \frac{n}{1+n\tau_1} .$$

The corrected disintegration rate is inferred from the observed rate by rewriting this equation in the form

$$n = \frac{n^*}{1-n^*\tau_1} \qquad (2.3,21)$$

One could calculate the probability of observing exactly m events in a time interval t by noting[1] that

$$P_m^*(t) = \frac{1}{A^*}\left[\int_0^t p_m^*(t)\,dt - \int_0^t p_{m+1}^*(t)\,dt\right]$$

and from this the standard error in m. This enables calculation of the standard error in n^* and hence of that in the value of n deduced from equation (2.3, 21). The calculation is not attempted here. One usually ascribes to n a fractional error $1/\sqrt{nt}$ (c.f. the discussion immediately following equation (2.3, 3)).

Provided τ_2 is less than τ_1, the input resolving time of the scaler does not introduce counting losses. (Mathematically, the density function is not altered by the new factor $u(t-\tau_2)$ since the factor $u(t-\tau_1)$ keeps it at zero till time $\tau_1 > \tau_2$.)

One has[2]

$$L\left\{\frac{1}{A^{**}}\,p^{**}(t)\right\} = L\left\{\frac{1}{A_m^*}\,p_m^*(t)\right\} = \left[L\left\{\frac{1}{A^*}\,p^*(t)\right\}\right]^m$$

$$= e^{-m\tau_1 s}\cdot\left(\frac{n}{n+s}\right)^m \qquad (2.3,22)$$

and hence[3]

$$\frac{1}{A^{**}}\,p^{**}(t) = u(t-m\tau_1)\,\frac{n^m}{(m-1)!}\,(t-m\tau_1)^{m-1}\,e^{-n(t-m\tau_1)} \qquad (2.3,23)$$

1. $\frac{1}{A^*}\int_0^t p_m^*(t)\,dt$ is the probability of observing m or more events in the interval $(0,t)$.
2. C.f. Fig. 2.6 and the discussion pertaining thereto.
3. Ref. C4, Operations 11 and 12, p. 294, and Transform 3, p. 295. See also footnote 1, p. 23.

If, now, $\tau_3 < m\tau_1$, the recording circuit does not introduce further loss. One may expand equation (2.3, 22):

$$L\left\{\frac{1}{A^{**}}\, p^{**}(t)\right\} = \left[\left(1 - \tau_1 m s + \frac{(\tau_1 m)^2}{2!} s^2 \cdots\right)\left(1 - \frac{ms}{n} + \frac{m(m+1)}{1\cdot 2}\frac{s^2}{n^2} \cdots\right)\right]$$

$$= 1 - s\left(\frac{m}{n} + m\tau_1\right) + \frac{s^2}{2!}\left[(m\tau_1)^2 + \frac{m(m+1)}{1\cdot 2} + \frac{2m^2\tau_1}{n}\right] + \cdots \qquad (2.3,24)$$

Comparison with equation (2.3, 16) and use of (2.3, 9) yield

$$\left.\begin{aligned} \overline{t^{**}} &= m\left(\tau_1 + \tfrac{1}{n}\right) \\ \sigma^{**} &= \sqrt{m}/n \end{aligned}\right\} \qquad (2.3,25)$$

Thus

$$\left.\begin{aligned} n^{**} &= \frac{1}{\overline{t^{**}}} = \frac{n}{m(1+n\tau_1)} \\ \text{or} \quad n &= \frac{mn^{**}}{1 - mn^{**}\tau_1} \end{aligned}\right\} \qquad (2.3,26)$$

The fractional error in n is taken as $1/\sqrt{nt}$.[1]

On the other hand, if $\tau_3 > m\tau_1$, losses in the recording circuit must be taken into account. It is assumed that τ_3 is an extended resolving time. This is roughly the case when the mechanical recorder is of the message register type. The density function for the recorded event is[2]

$$p^{***}(t) = u(t-\tau_3)\frac{n^m}{(m-1)!}(t - m\tau_1)^{m-1} e^{-n(t-m\tau_1)} \qquad (2.3,27)$$

with Laplace Transform[3]

$$L\left\{p^{***}(t)\right\} = n^m e^{-\tau_3 s - n(\tau_3 - m\tau_1)} \cdot \sum_{r=0}^{m-1} \frac{(\tau_3 - m\tau_1)^r}{r!}\left(\frac{1}{s+n}\right)^{m-r} \qquad (2.3,28)$$

Expansion of the right hand side of equation (2.3, 28) in a power series in s , and comparison with equation (2.3, 16) gives

$$A^{***} = e^{-n(\tau_3 - m\tau_1)} \sum_{r=0}^{m-1} \frac{n^r(\tau_3 - m\tau_1)^r}{r!} \qquad (2.3,29)$$

1. More accurately this could be calculated as outlined previously
2. $p^{***}(t) = u(t-\tau_3)\frac{1}{A^{**}}\, p^{**}(t)$. The factor $u(t-m\tau_1)$ can be omitted for the same reason that $u(t-\tau_3)$ was omitted in the preceding case.
3. Reference E1, equations (38) and (39).

The observed counting rate is calculated from equation (2.3, 18) where the input rate is given by the reciprocal of $\overline{t^{**}}$ in equation (2.3, 25). Thus

$$n^{***} = \frac{n}{m(1+n\tau_1)} \cdot e^{-n(\tau_3 - m\tau_1)} \cdot \sum_{r=0}^{m-1} \frac{n^r (\tau_3 - m\tau_1)^r}{r!} \qquad (2.3,30)$$

In practice, one multiplies the observed rate by the scaling ratio, and hence the overall efficiency G in per cent is

$$G_{(\tau_3 > m\tau_1)} = \frac{100}{1+n\tau_1} \cdot e^{-n(\tau_3 - m\tau_1)} \cdot \sum_{r=0}^{m-1} \frac{n^r (\tau_3 - m\tau_1)^r}{r!} \qquad (2.3,31)$$

or, from equation (2.3, 26),

$$G_{(\tau_3 < m\tau_1)} = \frac{100}{1+n\tau_1} \qquad (2.3,32)$$

Alaoglu and Smith[1] show that equation (2.3, 31) may be expressed in terms of the incomplete Gamma function[2] which is tabulated[3].

$$G = \frac{100}{1+n\tau_1} \left[1 - I\{n(\tau_3 - m\tau_1), m\}\right] \qquad (2.3,33)$$

The efficiency of the recorder alone is

$$G_{recorder} = 100\left[1 - I\{n(\tau_3 - m\tau_1), m\}\right] \qquad (2.3,34)$$

Considering the hypothetical case where $\tau_1 = 0$, Alaoglu and Smith draw, for different values of m, two series of graphs, one relating G and $n\tau_3$, and the other, G and $n\tau_3/m$. n/m is the rate at which impulses are fed to the recorder[4] and so the latter series of graphs shows the efficiency of the recorder for the same average input rate from scaling circuits of different scaling factors. From equation (2.3, 25) one has

$$\frac{\sigma^{**}}{t^{**}} = \frac{1}{\sqrt{m}}$$

and so there are relatively more of the longer and shorter intervals for lower scaling factors. This causes a relative reduction in efficiency for $\frac{n\tau_3}{m} < 1$, but an increase for

1. Reference A1.
2. $I(\mu t, n) = \dfrac{\int_0^{\mu t} e^{-x} x^{n-1} dx}{\Gamma(n)}$

   $\Gamma(n) = \int_0^{\infty} e^{-x} x^{n-1} dx$
3. Reference P1.
4. See equation (2.3, 26); $\tau_1 = 0$.

$\frac{n\tau_3}{m} > 1$. Hence the rather surprising cross-over of the graphs at $\frac{n\tau_3}{m} = 1$.

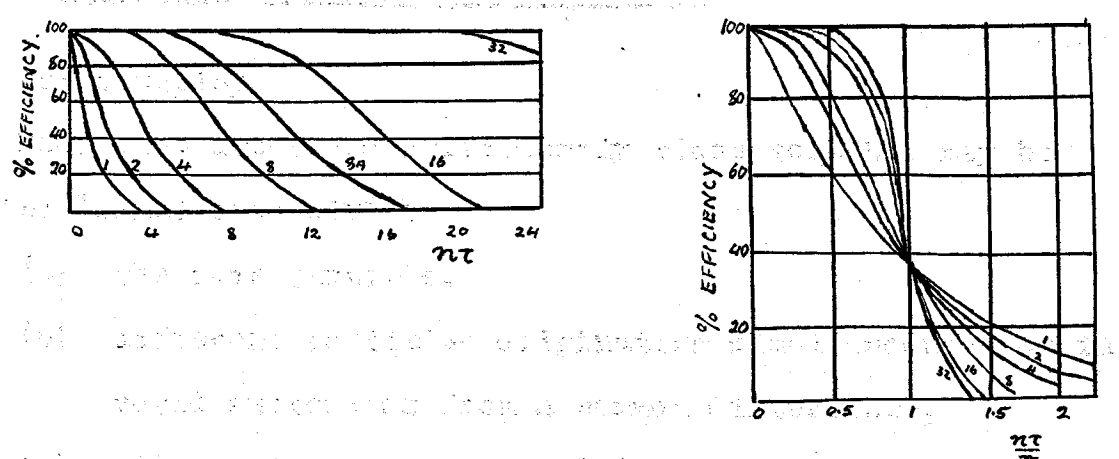

FIG. 2.7 Efficiency of Recorder plotted against (1) $n\tau$, (2) $n\tau/m$ for different values of m . n is average input rate to Geiger counter, m is scaling factor and τ is resolving time of recorder.

In the experiments described in Chapter 6, a scaling factor of 100 was employed. Since the resolving time of the Geiger counters used was never less than 150 μsecs. and the resolving time of the recorder was about 15 milliseconds, the counting rate n was obtained from (2.3, 26) and the fractional error in n was taken as $1/\sqrt{nt}$.

CHAPTER 3.

THE COINCIDENCE COUNTING TECHNIQUE

3.1. Introduction.

Radiation detectors sufficiently close together may be actuated "simultaneously" by

(a) the same particle,

(b) different particles originating simultaneously or in rapid succession from a common disturbance,

and (c) different particles resulting from different causes.

The registration of a "Coincidence" due to any of these causes may be effected by connecting two or more detectors to an electronic circuit[1] which is designed to give an output pulse whenever all the detectors are actuated within a time interval called the "Coincidence Resolving Time" of the apparatus.

Coincidences of type (a) may be used for determining gamma ray energies; in this, corrections for coincidences of types (b) and (c) are necessary. Coincidences of type (b) may result from nuclear disintegrations or from Cosmic rays; in quantitative investigations, corrections for all types of unwanted coincidences must be made. Coincidences of type (c) are "Chance Coincidences", the counting of which has application to the accurate determinatior of the coincidence resolving time of a two channel system.

3.2. Chance Coincidences.

Chance Coincidences involve coincidences of type (c), and occur whenever all channels of a coincidence circuit are receiving input pulses. Consequently, in counting coincidences of types (a) or (b), one must be able to determine quickly, or to

1. The design of a suitable circuit is discussed in Section 5.2., and the description of the circuit designed by the author is given in the appendix.

calculate readily the contribution of chance coincidences to the total coincidence rate. In this connection, the importance of using electronic circuits which posses a constant resolving time will be apparent from the following discussion which is a modified account of the treatment by Eckart and Shonka[1].

Consider an n-fold coincidence circuit and suppose that the excitation of the i^{th} detector by an incident particle at time t_i produces at the input from the i^{th} to the mixing stage a square pulse beginning at t_i and of length τ_i, constant and thus independent of t_i and of the nature of the incident particle. Suppose, further, that the i^{th} detector is such that re-excitation within time τ_i is not possible, i.e. the resolving time of the detector is greater than τ_i. In addition, let the counting rate in the i^{th} detector be such that counting losses due to the resolving time of the detector are negligible. Finally, suppose that a coincidence is observed at time t if, firstly, at this time, whilst pulses are being fed to the mixer from each of $(n-1)$ channels, a particle is detected in the remaining channel, and if, secondly, the time overlap of all n pulses at the mixer is not less than ρ.

For an n-fold coincidence circuit, "chance coincidences of the first kind" are defined as coincidences due to the superposition of mixer input pulses, no two of which are related causally; chance coincidences of the second kind are those in which two events are causally simultaneous and $(n-2)$ events are accidentally simultaneous; other types of coincidences may be defined similarly.

On the basis of what has been said above, the probability $P(t)\,dt$ that a coincidence[2] is observed in a time increment dt at t is equal to the product of the probability that a particle is detected in one of the channels in dt at t and the probability

1. Reference E2.
2. (OF THE FIRST KIND)

that, at t, there are being fed to the mixer stage from each of the other $(n-1)$ channels pulses whose time distribution is such that all of the n pulses persist at least till time $t+\rho$. Thus the m^{th} channel must have been actuated in the interval $(t+\rho-\tau_m, t)$, the probability of which is $N_m \cdot \{t-(t+\rho-\tau_m)\}$, where N_m is the average input rate. Hence

$$\begin{aligned} P(t)dt &= N_1 dt\,[N_2(\tau_2-\rho)\cdot N_3(\tau_3-\rho)\cdots\cdots N_n(\tau_n-\rho)] \\ &\quad + N_2 dt\,[N_1(\tau_1-\rho)\cdot N_3(\tau_3-\rho)\cdots\cdots N_n(\tau_n-\rho)] \\ &\quad + \cdots\cdots\cdots\cdots \\ &\quad + N_n dt\,[N_1(\tau_1-\rho)\cdot N_2(\tau_2-\rho)\cdots\cdots N_{n-1}(\tau_{n-1}-\rho)] \end{aligned}$$

$$\text{or} \quad P(t) = N_1(\tau_1-\rho)\cdot N_2(\tau_2-\rho)\cdots\cdots N_n(\tau_n-\rho)\left[\frac{1}{\tau_1-\rho}+\frac{1}{\tau_2-\rho}+\cdots\right] \quad (3.2,1)$$

For a two-fold circuit where chance coincidences of the first kind only occur, this becomes

$$P(t) = N_1 N_2\,[(\tau_1-\rho)+(\tau_2-\rho)] \quad (3.2,2)$$

The term in the square brackets is obviously twice the coincidence resolving time[2], and if this is to be a constant, the pulse widths must be constant (independent of counting rate, detected particle etc.) and the minimum overlap time must be constant. On the other hand, the resolving time may be varied by altering the pulse widths at the mixer input, or by altering the mixer circuit so that ρ is changed.

Equation (3.2,2) expresses the fact that the chance coincidence rate C is given by

$$\left.\begin{aligned} C &= N_1 N_2\,[(\tau_1-\rho)+(\tau_2-\rho)] \\ &= N_1 N_2 \cdot 2\tau \end{aligned}\right\} \quad (3.2,3)$$

Obviously, the resolving time may be determined by observing simultaneously the chance coincidence rate and both channel impulse rates when the detectors are excited from independent

1. See the second paragraph in Section 2.3.
2. It is assumed equally probable that each counter be actuated first.

sources. Experimental verification of the constancy of the fraction C/N_1N_2 for the equipment designed by the author is described in Section 6.1; the dependence of C on τ_1 and τ_2 is also verified. Several circuits have been described in the literature in which the resolving time is altered by varying ρ.[1]

Thus the significance of equation (3.2, 2) is that, firstly, it provides a means of determining the resolving time of a coincidence circuit, and secondly, once the resolving time has been determined, the contribution of chance coincidences to the total observed number of coincidences, may be calculated quickly. More exactly, the contribution of the chance coincidence rate to the total observed coincidence rate would be

$$C = (N_1 - G)(N_2 - G) \cdot 2\tau \qquad (3.2,4)$$

where G is the coincidence rate of events related causally.

For triple coincidence, the probability of a coincidence of the first kind in dt at t, is, from equation (3.2, 1)

$$P(t)\,dt = N_1 N_2 N_3 \left[(\tau_1-\rho)(\tau_2-\rho) + (\tau_1-\rho)(\tau_3-\rho) + (\tau_2-\rho)(\tau_3-\rho)\right] dt$$

The probability of coincidences of the second kind also must be deduced, and is found to be[2]

$$\begin{aligned} Q(t) = {} & N_{12} N_3 \left[(\tau_{12}-\rho) + (\tau_3-\rho)\right] \\ & + N_{23} N_1 \left[(\tau_{23}-\rho) + (\tau_1-\rho)\right] \\ & + N_{31} N_2 \left[(\tau_{31}-\rho) + (\tau_2-\rho)\right] \end{aligned} \qquad (3.2,5)$$

where τ_{ij} is the smaller of τ_i and τ_j

and N_{ij} is the rate of simultaneous actuation of detectors i and j by particles related causally.

3.3. Coincidence Absorption Measurements of Gamma Ray Energies.

The experimental technique, Fig. 3.1, consists firstly in the production by the gamma rays from the source S of Compton electrons in a suitable radiator R [3], and secondly in the measurement of rate of electron coincidences (type (a)) as a function of

1. See, for example, Reference B7.
2. Reference E2.
3. Section 1.1.

the thickness of an absorber A between the two detectors, β_1, a double window Beta Counter, and β_2, a single window Beta Counter[1].

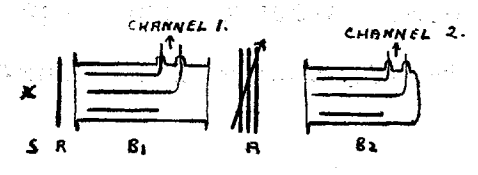

FIG. 3.1 Experimental Arrangement for measuring Compton electron Coincidences. See also Plate 4b.

Corrections to the observed coincidence rate for cosmic coincidences, for possible gamma-gamma coincidences and for chance coincidences must be made. Determination of the contribution of the Cosmic rate together with the gamma-gamma rate is effected by increasing A till the observed rate falls to a constant value. The chance coincidence rate may be evaluated from equation (3.2, 3).

The evaluation of the energy of the hardest gamma ray may be effected by comparison with the graph of Curran, Dee and Petrzilka, in which Compton electron range is related to incident gamma ray energy[2].

A second method for investigating the gamma spectrum consists in using the method of Fig. 3.1, and in determining the thickness of absorber necessary to reduce the coincidence rate to one half, one quarter, - - - - of the zero absorber rate. The way in which the spectrum is resolved from these observations is described in Chapter 4.

3.4. Nuclear Disintegration Schemes.

(i) The experimental technique. This involves the following steps -

(A) Determination of background for each counter used.

1. The beta counters used in the experiments of Chapter 6 are reproduced in Plate 3, (b), (c), (d).
2. See Reference C3.

(B) Determination of the cosmic coincidence rate for each pair of counters connected in coincidence in the succeeding steps[1].

(C) The single Beta counting rate is determined as a function of thickness of absorber placed between source and counter.

(D) Gamma-Gamma coincidences are investigated.

(E) The Beta-gamma coincidence rate is observed as a function of thickness of absorber placed before the beta counter.

(F) The energy of the gamma rays is investigated by the methods outlined in Sections 3.3 and 4.2.

Step (C) yields the absorption curve for the whole Beta ray spectrum. The thickness of absorber necessary to stop all beta rays provides a measure of the energy of the hardest beta ray[2], and, if, beyond this point, a steady counting rate above the background is observed, one can infer that the disintegration involves at least one gamma ray.

Two beta counters may be used to determine whether gamma-gamma coincidences occur; sufficient absorber is placed between each counter and the source to remove all beta particles. In determining the gamma-gamma rate, one allows for cosmic coincidences, and for chance coincidences whose contribution to the coincidence rate may be calculated from equation (3.2, 3).

The beta ray absorber in front of one of the counters used in the preceding step is removed and step (E) is carried out. Allowance is made for the cosmic rate, the chance rate and the gamma-gamma rate which has been determined in the preceding step. To interpret the experimental results, it is convenient, at this point, to consider special disintegration schemes.

1. The counters are placed in a horizontal plane to keep the cosmic rate to a minimum, and should be used in the same geometry throughout the experiment.
2. See Chapter 4.

(ii) <u>One Beta Particle, One Gamma Ray.</u> In the first place, suppose that a nucleus of the isotope being investigated decays with the emission of one beta particle to an excited state of the product which loses its excess energy by the radiation of one gamma ray, (Fig. 3.2).

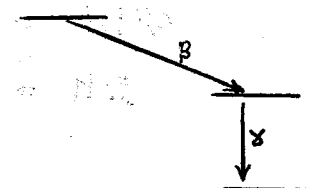

FIG. 3.2.

Step (C) has given the beta ray end point energy and has shown the presence of at least one gamma ray. Step (D) has shown that there are no gamma-gamma coincidences. This does not mean necessarily that there is only one gamma ray per disintegration. Now let us suppose that there are N disintegrations per second and let the net efficiencies of the counters be ϵ_1^γ and ϵ_2^γ for gamma rays and ϵ_1^β and ϵ_2^β for beta particles. The net efficiency is given by

$$\epsilon = \frac{1}{4\pi}\int_0^{4\pi} \ell_\omega \, d\omega \qquad (3.4,1)$$

where ℓ_ω is the intrinsic efficiency of the counter for the detection of the radiation in the element of solid angle $d\omega$ subtended at the source. The following relations hold:[1]

$${}_cN_1(x) = {}_cN_1^\beta(x) + {}_cN_1^\gamma = N\epsilon_1^\beta F(x) + N\epsilon_1^\gamma \qquad (3.4,2)$$

where $F(x)$ is the fraction of beta particles penetrating the thickness x of absorber.

1. The prefix identifies the step, the superscript, the radiation, and the subscript, the counter. The expressions on the left are counting rates and they represent the corrected observed rate in each case e.g.
   ${}_cN_1(x)$ refers to counter 1 in step (C) and represents the total observed counting rate (corrected for background) for absorber thickness x.
   ${}_E N_{12}^{\beta\gamma}(x)$ represents the observed coincidence rate in step (E) corrected for Cosmic, Chance and γ-γ coincidences.

$$_{D}N_{12}^{\beta\gamma} = 0 \qquad (3.4,3)$$

$$_{D}N_{1}^{\gamma} = N\epsilon_{1}^{\gamma} \qquad (3.4,4)$$

$$_{D}N_{2}^{\gamma} = N\epsilon_{2}^{\gamma} \qquad (3.4,5)$$

$$_{E}N_{12}^{\beta\gamma}(x) = N\epsilon_{1}^{\beta}F(x)\epsilon_{2}^{\gamma} \qquad (3.4,6)$$

$$_{E}N_{1}^{\beta}(x) = N\epsilon_{1}^{\beta}F(x) \qquad (3.4,7)$$

$$_{E}N_{2}^{\gamma} = N\epsilon_{2}^{\gamma} \qquad (3.4,8)$$

From the last three relations, one deduces

$$\frac{_{E}N_{12}^{\beta\gamma}(x)}{_{E}N_{1}^{\beta}(x)} = \epsilon_{2}^{\gamma} \qquad (3.4,9)$$

$$\frac{_{E}N_{1}^{\beta}(x).\ _{E}N_{2}^{\gamma}}{_{E}N_{12}^{\beta\gamma}(x)} = N \qquad (3.4,10)$$

We may summarise the case of one beta particle, one gamma ray per disintegration by noting:

Step (C) gives the absorption curve of the beta ray and its end point energy, and indicates the presence of gamma rays.

Step (D) shows that there are no gamma-gamma coincidences.

From step (E), one finds that the ratio $N^{\beta\gamma}/N^{\beta}$ plotted as a function of absorber thickness is a constant, and is, in fact, equal to the net efficiency of counter 2 for the emitted gamma ray. One may calculate also, from equation (3.4, 10), the source strength.

Finally, extrapolation of the curve $_{c}N_{1}(x)$ to $x = 0$ enables the net efficiency ϵ_{1}^{β} to be determined, whilst ϵ_{1}^{γ} may be determined from equation (3.4, 4).

(iii) Complex Beta Ray Spectrum, One Gamma Ray per Disintegration. In this scheme, the nucleus has an alternative method of decay, (Fig. 3.3).

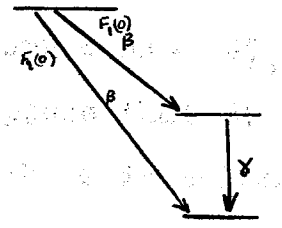

FIG. 3.3 Complex Beta Spectrum. $F_1(o)$ is the fraction of nuclei decaying by way of β-γ transition.

In the previous notation, the relations which hold are:

$$_{C}N_1(x) = N\epsilon_1^{\beta}\left[F_1(x) + F_2(x)\right] + N\epsilon_1^{\gamma} \qquad (3.4,11)$$

$$_{D}N_{12}^{\gamma\gamma} = 0 \qquad (3.4,12)$$

$$_{D}N_1^{\gamma} = N\epsilon_1^{\gamma} \qquad (3.4,13)$$

$$_{D}N_2^{\gamma} = N\epsilon_2^{\gamma} \qquad (3.4,14)$$

$$_{E}N_{12}^{\beta\gamma}(x) = N\epsilon_1^{\beta}F_1(x)\epsilon_2^{\gamma} \qquad (3.4,15)$$

$$_{E}N_1^{\beta}(x) = N\epsilon_1^{\beta}\left[F_1(x) + F_2(x)\right] \qquad (3.4,16)$$

$$_{E}N_2^{\gamma} = N\epsilon_2^{\gamma} \qquad (3.4,17)$$

Hence

$$\frac{_{E}N_{12}^{\beta\gamma}(x)}{_{E}N_1^{\beta}(x)} = \frac{F_1(x)}{F_1(x)+F_2(x)}\epsilon_2^{\gamma} = \frac{\frac{F_1(x)}{F_2(x)}}{\frac{F_1(x)}{F_2(x)}+1}\epsilon_2^{\gamma}, \qquad (3.4,18)$$

$$\frac{_{E}N_{12}^{\beta\gamma}(x)}{_{E}N_2^{\gamma}} = \epsilon_1^{\beta}F_1(x) \qquad (3.4,19)$$

and

$$\frac{_{E}N_1^{\beta}\cdot{}_{E}N_2^{\gamma}}{_{E}N_{12}^{\beta\gamma}(x)} = \frac{N\left[F_1(x)+F_2(x)\right]}{F_1(x)} \qquad (3.4,20)$$

One additional relation holds, namely

$$F_1(\omega) + F_2(\omega) = 1 \qquad (3.4,21)$$

If one examines these equations, one finds that there are six unknowns - ϵ_1^β, ϵ_1^γ, $F_1(\omega)$, $F_2(\omega)$, ϵ_2^γ, N. Now one may suppose that ϵ_1^β has been determined in a previous experiment, such as described in the preceding section[1]. Then by extrapolating $\epsilon N_1^\beta(x)$ to $x=0$, and noting equation (3.4, 21) one determines N. From equations (3.4, 13) and (3.4, 14), one evaluates ϵ_1^γ and ϵ_2^γ respectively. Then, by extrapolation of $\frac{\epsilon N_{12}^{\beta\gamma}(x)}{\epsilon N_1^\gamma}$ to $x=0$, one obtains $F_1(\omega)$ and hence $F_2(\omega)$.

The information obtained may be summarised:

Step (C) gives the total beta absorption curve and the end point of the energy of the harder beta particle and indicates the presence of at least one gamma ray.

Step (D) shows that there are no gamma-gamma coincidences.

As a consequence of step (E), equation (3.4, 19), one obtains the absorption curve for the softer beta ray and hence its end point energy. The ratio $N^{\beta\alpha}/N^\beta$ decreases to zero as the thickness of the absorber increases.[2]

Other quantities of interest are deduced as described above.

(iv) <u>One Beta Particle, Several Gamma Rays per Disintegration</u>. The simplest case of two gamma rays is illustrated in Fig. 3.4.

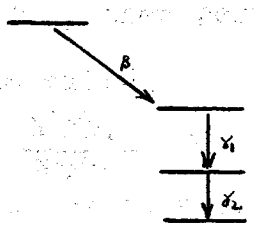

FIG. 3.4.

1. The intrinsic efficiency for beta particle detection does not depend upon beta ray energy and is practically equal to unity, so that this assumption is justified provided the same geometry is used.
2. *c.f.* the case (section (IV)) where the Beta spectrum is simple : $\frac{N^{\beta\gamma}}{N^\beta}(x)$ = a constant.

Relations of interest are:

$$ {}_{c}N_{1}(x) = N\epsilon_{1}^{\beta} F(x) + \left(N\epsilon_{1}^{\gamma_1} + N\epsilon_{1}^{\gamma_2} + \cdots\cdots\right) \qquad (3.4,22) $$

$$ {}_{D}N_{12}^{\beta\gamma} = N\left\{\epsilon_{1}^{\gamma_1}\left[\epsilon_{2}^{\gamma_2} + \epsilon_{2}^{\gamma_3} + \cdots\cdots\right] + \epsilon_{1}^{\gamma_2}\left[\epsilon_{2}^{\gamma_1} + \epsilon_{2}^{\gamma_3} + \cdots\cdots\right] \right. $$

$$ + \cdots\cdots\cdots\cdots\cdots\cdots\cdots\cdots\cdots\cdots\cdots\cdots $$

$$ \left. + \epsilon_{1}^{\gamma_n}\left[\epsilon_{2}^{\gamma_1} + \epsilon_{2}^{\gamma_2} + \cdots\cdots + \epsilon_{2}^{\gamma_{n-1}}\right]\right\} $$

$$ {}_{D}N_{1}^{\gamma} = N\left\{\epsilon_{1}^{\gamma_1} + \epsilon_{1}^{\gamma_2} + \cdots\cdots + \epsilon_{1}^{\gamma_n}\right\} $$

and

$$ {}_{D}N_{2}^{\gamma} = N\left\{\epsilon_{2}^{\gamma_1} + \epsilon_{2}^{\gamma_2} + \cdots\cdots + \epsilon_{2}^{\gamma_n}\right\} $$

If one makes the assumption that $\epsilon_{1}^{\gamma_1} = \epsilon_{1}^{\gamma_2} = \cdots\cdots = \epsilon_{1}^{\gamma_n} = \bar{\epsilon}_{1}^{\gamma}$ and $\epsilon_{2}^{\gamma_1} = \epsilon_{2}^{\gamma_2} = \cdots\cdots = \epsilon_{2}^{\gamma_n} = \bar{\epsilon}_{2}^{\gamma}$, [1] these equations reduce to

$$ {}_{D}N_{12}^{\gamma\gamma} = N_n (n-1)\, \bar{\epsilon}_{1}^{\gamma}\, \bar{\epsilon}_{2}^{\gamma} \qquad (3.4,23) $$

$$ {}_{D}N_{1}^{\gamma} = N_n\, \bar{\epsilon}_{1}^{\gamma} \qquad (3.4,24) $$

$$ {}_{D}N_{2}^{\gamma} = N_n\, \bar{\epsilon}_{2}^{\gamma} \qquad (3.4,25) $$

Other relations of interest are

$$ {}_{E}N_{12}^{\beta\gamma}(x) = N\epsilon_{1}^{\beta} F(x)\, n\bar{\epsilon}_{2}^{\gamma} \qquad (3.4,26) $$

$$ {}_{E}N_{1}^{\beta}(x) = N\epsilon_{1}^{\beta} F(x) \qquad (3.4,27) $$

and

$$ {}_{E}N_{2}^{\gamma} = N_n\, \bar{\epsilon}_{2}^{\gamma} \qquad (3.4,28) $$

The ratio $\frac{N^{\beta\gamma}}{N^{\beta}}$ is thus a constant, equal to $n\,\bar{\epsilon}_{2}^{\gamma}$, independent of absorber thickness. $\frac{N^{\beta\gamma}}{N^{\gamma}}(x)$ equal to $\epsilon_{1}^{\beta} F(x)$ traces out the shape of the beta spectrum and gives the end point energy; extrapolation to $x=0$ gives ϵ_{1}^{β}. Extrapolation of ${}_{E}N_{1}^{\beta}(x)$ to $x=0$, then permits a determination of the source strength N. The ratio

$$ R = \frac{N^{\beta\gamma}/N^{\gamma}}{N^{\beta\gamma}/N^{\beta}} = 1 - \frac{1}{n} \qquad (3.4,29) $$

gives the number of gamma rays per disintegration; the average quantum efficiencies may be deduced, now, from equations (3.4,24) and (3.4, 25).

1. This assumption is justified only when the energies of the several gamma rays do not differ greatly.

To summarize, we observe that Step (C) provides the beta ray energy and indicates the presence of at least one gamma ray. Step (D) indicates that there are gamma coincidences, whilst Step (E) shows that the beta spectrum is simple. Interpretation of the results leads to information concerning the number of gamma rays per disintegration, the source strength and the net quantum efficiencies.

(v) Complex Beta Spectrum and Several Gamma Rays per Disintegration. Coincidence absorption measurements alone are not sufficient to determine completely disintegration schemes of this type. Valuable information, however, can be obtained, and this, together with data from a magnetic lens or beta ray spectrograph, enables the decay scheme to be resolved.

The information that can be obtained from the coincidence-absorption technique includes

(a) The total beta absorption curve, the energy of the hardest beta ray and the presence of gamma rays (Step (C))

(b) The presence of gamma-gamma coincidences (Step (D))

(c) Whether the spectrum is complex and, if it is, whether the hardest beta ray leads to the ground state of the product. (Step (E)). It is not difficult to show that, in general, if the spectrum is complex the graph of $\frac{N^{\beta\gamma}}{N^{\beta}}(x)$ decreases as x increases[1]; if it decreases uniformly to zero, the hardest beta ray leads to the ground state of the product, whilst, on the other hand, if it decreases uniformly to a constant value, the hardest beta ray lead to an excited state of the product.

3.5. Half-Life Measurements (Delayed Coincidences).

In cases where the product of a radioactive transition has a short half life (10^{-7} sec. to 10^{-2} sec.), the technique of counting delayed coincidences provides a method for the accurate determination of the half life. The half lives of isomeric states formed from beta decay have been investigated

1. EXCEPTIONAL CASES ARE DISCUSSED IN REF. W3.

in this way, and, in fact, many isomers have been discovered by this technique.

The registration of a delayed coincidence may be effected either by delaying the first pulse or by lengthening it. The former method has been called the "Differential" method and the latter the "Integral" Method. Since the probability that a nucleus disintegrate in dt at t is[1] $\lambda e^{-\lambda t} dt$, it follows that, if the pulse (of width dt) corresponding to the initial beta particle be delayed for time t, the probability that it be in "delayed coincidence" with that corresponding to the particle subsequently radiated from the short lived product, is also $\lambda e^{-\lambda t} dt$. Thus the genuine delayed coincidence rate is proportional to $e^{-\lambda t}$. On the other hand, if the length of the pulse corresponding to the beta particle be τ, the probability that a delayed coincidence be registered is $\int_0^\tau \lambda e^{-\lambda t} dt = 1 - e^{-\lambda \tau}$. Thus, from a plot of the delayed coincidence rate against either the delay time or the pulse length, one deduces λ and hence the half life.

An upper limit to the half life that can be determined in this way is set by the chance coincidence rate. With the Integral method, for example, the condition that the chance coincidence rate be less than the genuine rate is equivalent to the condition[2]

$$N < \sim \frac{1 - e^{-\lambda \tau}}{\tau}$$

and, since one must plot the genuine rate over at least one half-life (i.e. $\tau \sim \frac{1}{\lambda}$), this condition is

$$N < \sim \lambda.$$

A source strength less than 100 disintegrations per second would give too small a counting rate for reliable results to be obtained. Consequently an upper limit to the half life is roughly 10^{-2} sec.

1. Equation (2.3, 4) $n = N\lambda = \lambda$, the transformation constant satisfying equations (1.2, 5) and (1.2, 6).
2. Reference R4.

The effect of time delays in the counters are discussed in Reference B3. The fluctuation of intrinsic time delays in the counters sets a lower limit to the half life that can be measured. Calculations of the sensitivities of the methods are given in References B3 and D2.

3.6. Optimum Conditions for a Coincidence Experiment.

Let us consider for simplicity a coincidence experiment in which a decay scheme of the type of Fig. 3.2 is being investigated with a coincidence circuit whose resolving time τ is known accurately. The genuine coincidence rate, G is [1]

$$G(o) = N^{\beta\gamma}(o) = N\epsilon_1^{\beta}\epsilon_2^{\gamma}$$

and the chance rate, C, is

$$C = 2N^2\epsilon_1^{\beta}\epsilon_2^{\gamma}\tau$$

Hence
$$\frac{C}{G} = 2N\tau \qquad (3.6,1)$$

and, for a given resolving time, this ratio increases with the source strength.

The standard error in an observed coincidence rate is[2]

$$\delta = \frac{(C+G)^{1/2}}{T^{1/2}} \qquad (3.6,2)$$

and, consequently, the fractional error, f, in G (C being known accurately) is

$$f = \frac{(1+\frac{C}{G})^{1/2}}{T^{1/2}\,G^{1/2}}$$

which may be reduced to the form

$$f = \frac{(2\tau)^{1/2}}{T^{1/2}(\epsilon^{\beta}\epsilon^{\gamma})^{1/2}}\left(1+\frac{1}{2N\tau}\right)^{1/2} \qquad (3.6,3)$$

or
$$f = f_L\left(1+\frac{1}{2N\tau}\right)^{1/2} \qquad (3.6,4)$$

where
$$f_L = \frac{(2\tau)^{1/2}}{T^{1/2}(\epsilon^{\beta}\epsilon^{\gamma})^{1/2}} \qquad (3.6,5)$$

1. Equation (3.4, 6)
2. See equations (2.3, 2) and (2.3, 3) and the discussion pertaining thereto.

is the limiting value of the fractional error in G when a very strong source is used.

It is obvious that no great advantage is obtained by increasing N beyond the value for which $\frac{C}{G}\,(=2N\tau)=1$.[1] In fact, if τ be small, a value of N satisfying this relation may not be permissible since the counting rates in the single channels may be too high.

One deduces from equation (3.6, 3) that, for a given fractional error f, the time of experiment T is

$$T = \frac{2\tau}{\epsilon^{\beta}\epsilon^{\gamma}f^{2}}\left(1+\frac{1}{2N\tau}\right) \qquad (3.6,6)$$

Consequently, to keep the time of experiment to a minimum, one strives to use counters of high net efficiencies, and a coincidence circuit of short resolving time.

1. For example, if $\frac{C}{G}=1$, $f = 1.4\,f_{\infty}$
   If $\frac{C}{G}=2$, $f = 1.2\,f_{\infty}$

CHAPTER 4.

ENERGY MEASUREMENTS BY ABSORPTION

4.1. Beta Rays.

It has been pointed out in Chapter 1 that the thickness of absorber required to stop all beta rays from a source provides a measure of the maximum energy of the beta rays. In contrast to other methods[1], the determination may be carried out quickly, the experimental arrangement and procedure are quite simple, and comparatively weak sources may be used. On the other hand, however, the estimation of the end point (particularly when gamma rays are present) is largely subjective[2] and it is difficult to allot a standard error to the point so chosen. Further, it is not possible from the absorption curve alone to determine the energies and relative intensities of any softer components present.

Before an estimate of the energy of the hardest beta ray can be made with any certainty from absorption measurements, one must have a reliable range-energy relation, and one must be able to determine accurately the range. Moreover, if the absorption method is to compete with the spectrographic method, a means of determining the relative intensities and the respective end points of the several components from the absorption data must be found.

An empirical range-energy relation proposed by Feather[3] is

$$R = aE + b$$

This relation has been found to hold quite well for energies above about 0.8 M.e.v. Estimates of the constants a and b vary, but a recent determination by Bleuler and Zunti[4] appears the most reliable. They quote

$$R = 0.571\,E - 0.161\,, \quad E > 1\ \text{Mev.} \qquad (4.1,1)$$

where R is in gms. per sq. cm. and E in M.e.v.

1. Magnetic Spectrograph or Cloud Chamber.
2. Most early determinations were too low.
3. Reference F1.
4. Reference B4.

To enable accurate determination of the range from absorption measurements, several methods of treating the observed data have been proposed. Champion and Widdowson[1] suggest that a polynomial

$$y = \Sigma a_n (x_0 - x)^n \qquad (4.1,2)$$

represents a good approximation to the observed characteristics of an absorption curve. y is the ratio of the number of beta particles penetrating absorber thickness x to the number observed for zero thickness, x_0 is the end point and a_n is a constant. They find that, for a given experimental arrangement, a single term ($n \sim 3$ or 4) is adequate. x_0 is obtained by producing the straight line drawn through the points ($y^{1/n}$ v. x) to cut the x-axis. A standard error (including only errors due to fluctuations in the source) can be assigned to x_0 .

An extension of the method just described has been made recently by Katz and his associates[2]. An absorption curve

$$y = K (E_0 - E)^n \qquad (4.1,3)$$

is assumed. One has

$$\log y = K' + n \log (E_0 - E) \qquad (4.1,4)$$

and

$$y^{\frac{1}{n}} = K'' (E_0 - E) \qquad (4.1,5)$$

From the experimental absorption curve, an upper energy value E_0' is assumed. A plot of log. y against log. ($E_0' - E$) yields a value n' of n. $y^{1/n'}$ is now plotted against E and a new value E_0'' of E_0 is obtained. This process is repeated until E_0 is determined with sufficient accuracy.

A different approach to the problem has been made by Feather[3]. The procedure involves the use of the absorption curve (log. y v. x) of the beta rays from a standard source[4]. The range R of the latter is divided into ten equal parts ($d_n = \frac{n}{10} R$) and the corresponding fractions y_n of the zero

1. Reference C5.
2. Reference K3.
3. Reference F2.
4. In Feather's Case, $R \propto E$.

absorber intensity are obtained. The value d_n' of absorber density necessary to reduce the beta intensity of the source under investigation to the fraction y_n is observed and the sequence

$$\frac{d_n'}{d_n} \quad , \quad n = 1, 2, \ldots\ldots$$

tends towards the ratio of the ranges R'/R. An abrupt change in slope of the ratio d_n'/d_n indicates that the spectrum is complex. When sufficient data are available, the ranges and relative intensities of the several components may be determined.

Weaknesses inherent in Feather's comparison method have been pointed out by Bleuler and Zunti[1]. In the first place, R_aE is not a good standard[2]. The reason is that the form of the beta spectrum depends upon the character of the transition and, in the case of forbidden transitions, as for R_aE, the spectrum contains a relatively large number of slow electrons. As a result the sequence d_n'/d_n may decrease rapidly, and, if the absorption curve of the unknown cannot be followed far enough, as may be the case when gamma rays are present, the limiting value of d_n'/d_n, and hence the ratio R'/R, may be difficult to determine accurately. Further, the curvature of the logarithmic absorption curve increases markedly with the energy and depends a good deal on the nuclear charge.

The form of the absorption curve for allowed spectra has been calculated semi-empirically by Bleuler and Zunti[1]. The results for beta particles emitted from a source for which $Z = 20$, have been presented in the convenient form of Fig. 4.1. To use these curves, one determines from the measured absorption curve the absorber thickness d_n necessary to reduce the zero thickness beta intensity I_o to the value $I_n = x^n I_o$. One then uses the n^{th} curve to find the value E_n (estimated upper energy of

1. Reference B5.
2. The reasons R_aE was originally chosen as standard were firstly, absence of gamma radiation, and, secondly, the comparative wealth of information on the disintegration energy.

Korrekturen für $Z \neq 20$.

$$\delta = \frac{d_n'(Z) - d_n'(20)}{d_n'(20)} = f(Z)$$

für $E_0/mc^2 = 1,3,10$.

Parameter: $n = 1,(2),3,5,7,9$.

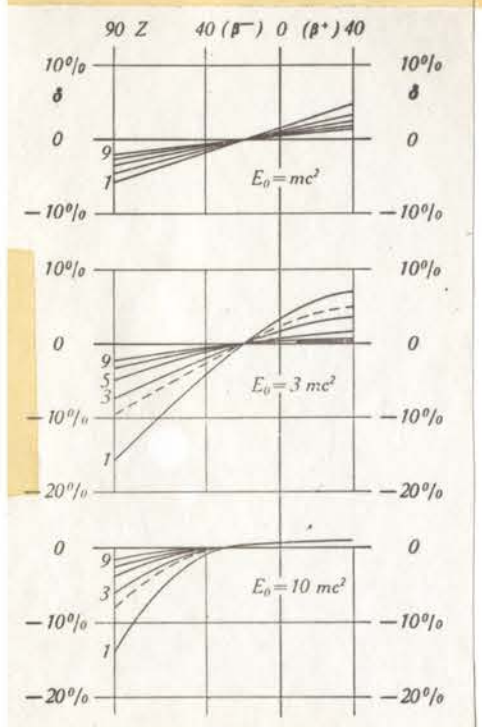

FIG. 4.2.

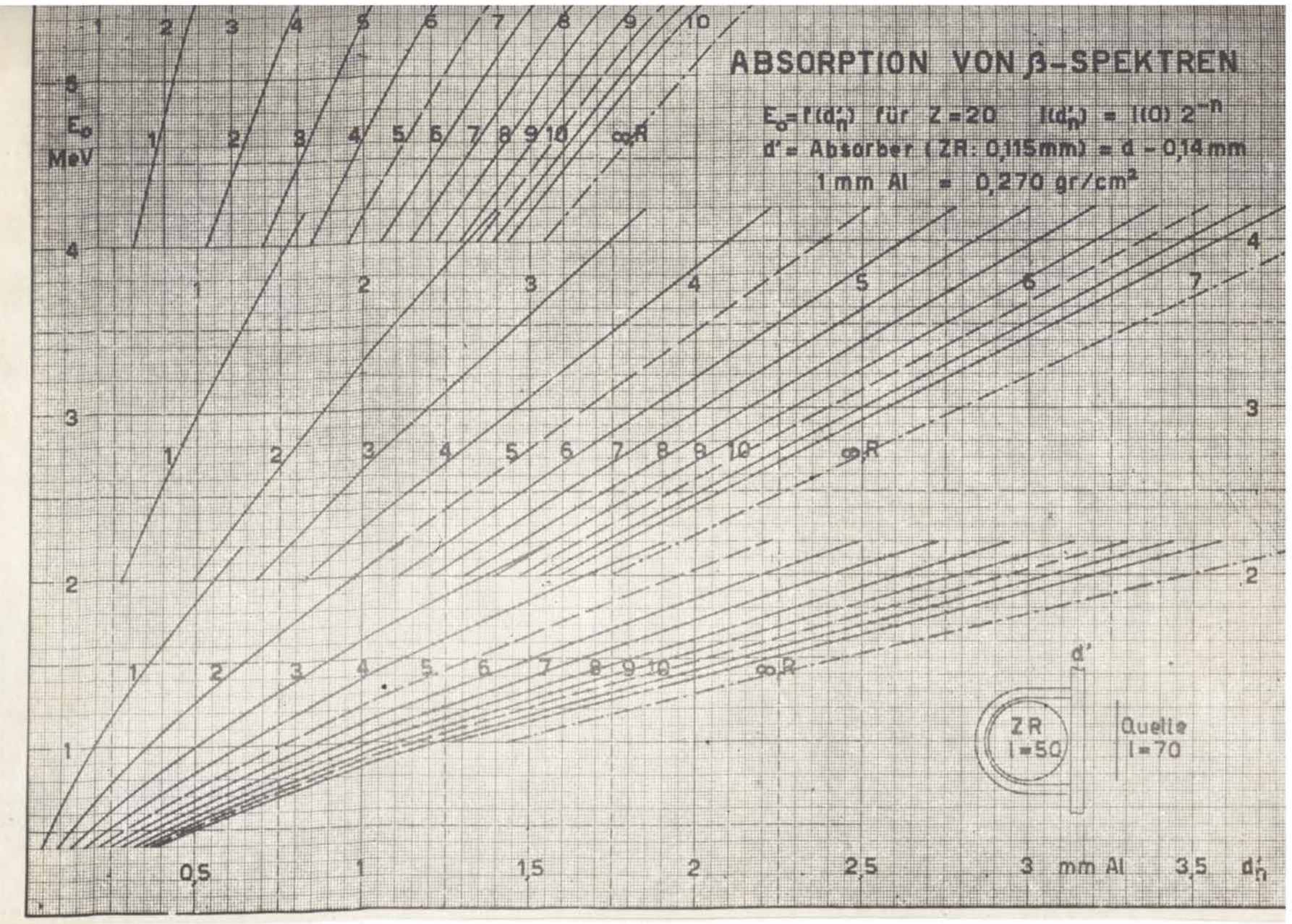

FIG. 4.1

the beta spectrum) corresponding to the value of α_n. If the spectrum is simple, the values of E_n are constant; if complex, they increase with n and an end value can be assigned to E_n by extrapolation to $n = \infty$. When the spectrum is complex, it may be possible to resolve the observed logarithmic absorption curve into several normal curves which yield the end points (constant E_n values) and relative intensities of the components. Changes of slope in the curve are frequently an aid to such a resolution.[1] For $Z \neq 20$ and for positron emission, the corrections of Fig. 4.2 may be applied. The limits of error quoted for these comparison curves are

$$\left.\begin{aligned} \delta &< 0.04 \text{ M.e.v.}, \quad \text{for } E_0 < 1 \text{ M.e.v.} \\ \delta &< 0.06 \text{ M.e.v.}, \quad \text{for } E_0 < 2 \text{ M.e.v.} \\ \delta &< 0.1 \text{ M.e.v.}, \quad \text{for } E_0 < 3 \text{ M.e.v.} \\ \delta &< 0.2 \text{ M.e.v.}, \quad \text{for } E_0 < 5 \text{ M.e.v.} \end{aligned}\right\} \quad (4.1, 6)$$

The effects of thick sources are discussed in References F2, C5 and B5. Since the gamma intensity from a source is roughly proportional to the thickness t of the source, and since the observed beta intensity does not increase proportionally with t, and attains a miximum value when t is equal to the range of the beta particles, thin sources should be used. The method used to obtain thin sources for the experiments described in Chapter 6 is outlined in Appendix 1.

4.2. Gamma Rays.

In Chapter 1 it was stated that the intensity of a homogeneous beam of gamma rays emerging from thickness x of absorber is given by the relation (1.1, 2)

$$I(x) = I_0 e^{-\mu x}$$

where μ consists of the three partial absorption coefficients given in equation (1.1, 3). Consequently, if one plots, for a

1. See, for example, the resolution of the beta absorption curve of Ag^{110} described in Chapter 6.

homogeneous beam of gamma rays, the logarithm of the intensity against the thickness of absorber, one obtains a straight line, the slope of which provides the value of μ. Then, from Fig. 1.1, one obtains the energy of the gamma radiation. Such a determination, however, gives an ambiguous result, for, in general, two values of gamma energy correspond to the same total absorption coefficient. To be sure which value is to be taken, one must plot the absorption curve in a different material and obtain the absorption coefficient for this material. Again, two values of energy are obtained, from Fig. 1.1, one of which agrees with one of the two values for the first absorber. The common value, then, is the energy of the gamma radiation.

When the gamma spectrum contains more than one component, a plot of log. I against x is not linear. However, provided the intensities are not too low, and the energies not too close, the plot may be able to be split up into its several linear components, and the energy of each component deduced. The relative intensities of each component can also be determined provided the efficiency v. energy curve for the counter is available so that the necessary corrections can be applied to the observations. The method of resolving the spectrum is similar to that used in Chapter 6 for resolving the observed beta absorption curve of Ag^{110}. Since an analysis of a gamma spectrum by this method was not undertaken in the experiments reported in Chapter 6, Fig. 4.3[1] is included. It shows the absorption curve for the first part of the gamma spectrum of Au^{198} and its subsequent resolution into linear components.

A second method for investigating γ spectra by the absorption technique has been described in Section 3.3. The energy of the hardest gamma ray may be obtained from Fig. 4.4 in which the experimental linear relation between quantum energy

1. Reference W3, Part II, Fig. 2.

and corresponding Compton electron range in aluminium is reproduced[1]. Another way in which the "Compton-coincidence"

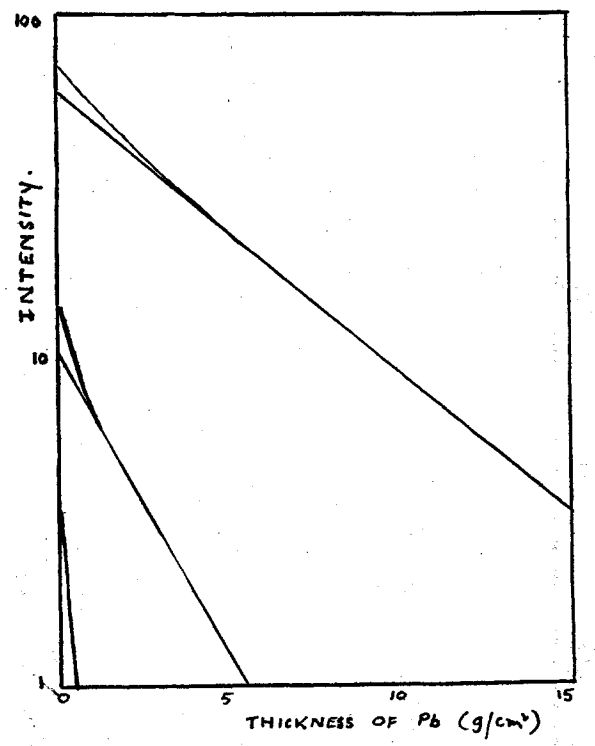

FIG. 4.3 Resolution of Absorption Curve of γ Rays from Au^{198}

results may be used is due to Bleuler and Zunti[2] who have calculated absorption curves for the Compton electrons ejected from aluminium and brass radiators. Their results are presented in Fig. 4.5 which may be used in precisely the same manner as Fig. 4.1 is used for determination of beta ray energies and for resolution of beta ray absorption curves into component curves. The factor k (Fig. 4.5) depends upon the geometry and experimental set up. These curves are used in Chapter 6 to resolve the experimental coincidence absorption curve for the Compton electrons produced by gamma rays from Co^{60}. In these experiments d was taken equal to d', thickness of absorber A (Fig. 3.1).

(The method due to Becker and Bothe (B6) and described by Mitchell (M2) is not a good one. The "constant", $C_{\gamma m}$, in

1. Reference C3., Fig. 10.
2. Reference B5.

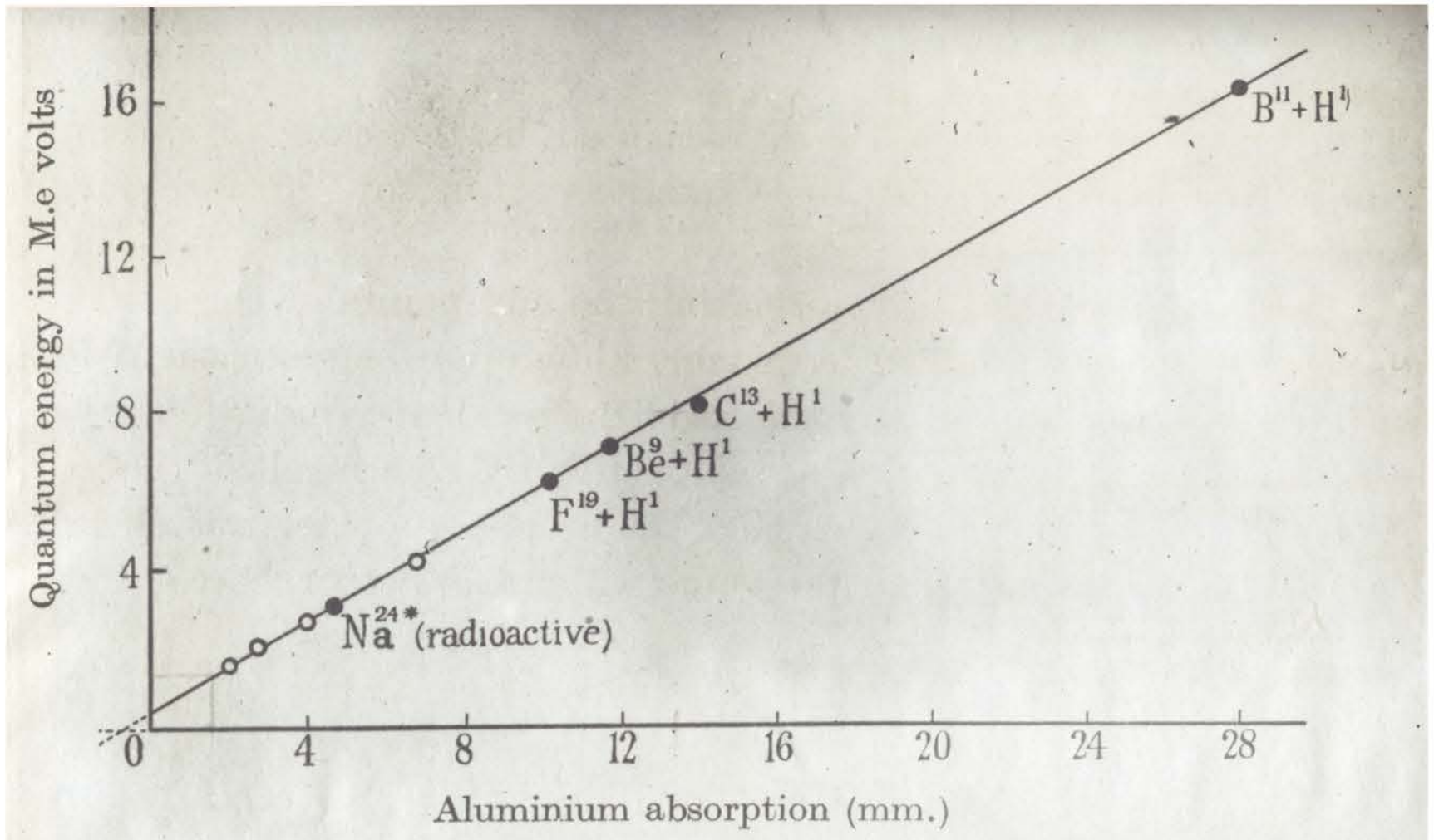

FIG. 10. ○, Bernardini and Franchetti. ●, Curran, Dee and Petržílka.

FIG. 4.4.

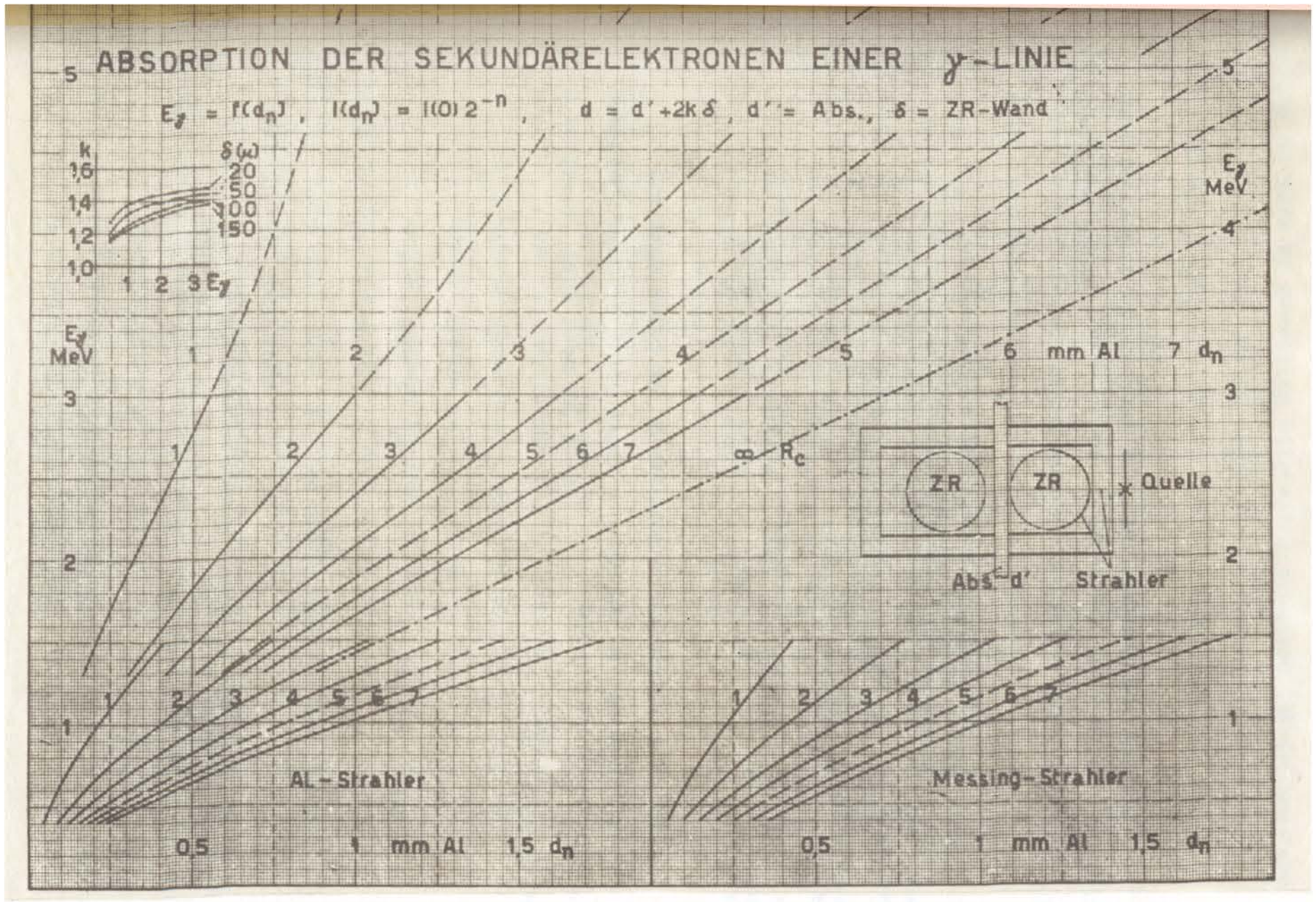
ABSORPTION DER SEKUNDÄRELEKTRONEN EINER γ-LINIE
$E_\gamma = f(d_n)$, $I(d_n) = I(0)\,2^{-n}$, $d = d' + 2k\delta$, d' = Abs., δ = ZR-Wand
k
δ(ω)
20
50
100
150
E_γ
E_γ MeV
mm Al
d_n
R_c
ZR
ZR
Quelle
Abs. d'
Strahler
Al - Strahler
Messing - Strahler

FIG. 4.5.

Mitchell's equation (1) varies considerably with energy. This may be seen by rewriting Mitchell's equation (1) in the form

$$C_{1/n} \doteq d_{1/n}\ \frac{2E+1}{4E^2}$$

by taking $m_0 c^2 = 1/2$ approx.

From the curve $n=1$, Fig. 4.5, one deduces the results tabulated below.

E	$d_{1/2}$	$C_{1/2}$	$C_{1/2}$
0.5 M.e.v.	0.065 mm. Al.	0.130 mm. Al.	0.035 g/cm²
1 "	0.215 "	0.160 "	0.043 "
1.5 "	0.420 "	0.187 "	0.050 "
2.6 "	0.93 "	0.211 "	0.057 "

The last value is in reasonable agreement with the "constant value", 0.063 gms./cm², quoted by Mitchell for the 2.62 M.e.v. line from Th. C".).

CHAPTER 5.

THE DESIGN OF EQUIPMENT

5.1. Introduction.

The first task in the project undertaken by the writer was to design a complete new electronic unit suitable for carrying out coincidence experiments. Briefly, the assignment might have been set out:

> "A Geiger counter furnishes an electrical impulse of the form of that shown in Fig. 2.5. The pulse height varies between about 0.5 and 2 volts. Design an arrangement which will count all the pulses occurring in each of two such counters and which will count, in addition, the number of pulses in one channel which occur within a time interval τ of pulses in the other channel. Choose a suitable value of τ, design the circuits and construct them. Plan experiments along the lines of the discussion in Chapters 3 and 4, and verify that the equipment works satisfactorily by checking the well known decay scheme of Co^{60}. Use the equipment to investigate the decay scheme of Ag^{110}."

5.2. Basic Design.

It was decided to mould the equipment round a coincidence circuit of medium resolution ($\tau \sim 2\,\mu secs.$). The disadvantages of such a circuit over one of shorter resolving time are

i) Larger chance coincidence rate (equation 3.2, 2)

ii) Longer time of experiment for given fractional accuracy (Section 3.6).

On the other hand, however, the advantages in the preliminary stages of the work were

i) Less critical circuitry. A well designed reliable unit could be constructed fairly quickly and put into operation.

ii) The operation of the circuit could be checked by the provision of test points at which the pulses would be suitable for presentation on the C.R.O. available.

iii) Genuine coincidences would not be missed due to chance fluctuations in the times of response of the Geiger counters.

iv) Resolving time experiments (a very important preliminary

task in a coincidence experiment) could be done quickly and checked.

v) The experience gained in the construction and operation could be used later in the design of a circuit of shorter resolving time.

vi) Some information on (iii) could be obtained by comparing results from a higher resolution circuit with those from the original medium resolution circuit.

Several methods of registering coincidences have been described[1]. One of the most reliable is the "Rossi Circuit"[2], which was chosen for use in these experiments and the operation of which may be understood from Fig. 5.1. Each tube is normally

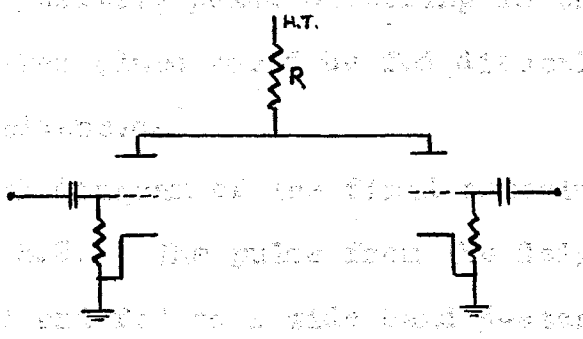

FIG. 5.1. Rossi Stage.

conducting heavily until a large negative pulse fed to the grid cuts it off. The common load R is large compared to the D.C. resistance of either tube when conducting. Thus, when only one tube is cut off, only a small pulse appears at the plate. But when both are cut off simultaneously, the plate voltage begins to rise towards the full H.T. supply and a large positive pulse may be taken from the plate to register a coincidence between pulses on the grids. Thus, in the Rossi stage of the Coincidence circuit of Fig. 5.5, the output pulse when only one tube is cut off is about 12 volts, but when both are cut off simultaneously, it is about 120 volts. Discrimination in favour of the latter is easily arranged.

1. Reference M3.
2. Reference R5.

It was apparent that a reliable coincidence circuit could be constructed by designing an arrangement which would preserve the fast initial rise of the Geiger pulse and amplify it to the point where it would trigger a fast one-shot multivibrator. With the latter, triggering could be initiated with a pulse as small as 5 volts. Further, very stable output pulses (stable in duration and in height) at 2 or 3 μsecs. and at 30 to 100 volts could be obtained. The large negative pulse (from the normally-off tube) could be fed directly to the Rossi stage and the large positive pulse (from the normally-on tube) could be fed directly to the scaling circuit counting the number of input pulses. The positive pulse occurring in the Rossi stage when a coincidence takes place could be fed directly to the scaler counting coincidences.

The block diagram of the final experimental set up is shown in Fig. 5.2. The pulse from the Geiger counter is differentiated and fed to a wide band 3-stage preamplifier close to the counter. The cathode follower output permits the use of a comparatively long lead to the appropriate channel of the Coincidence circuit without attendant distortion of the pulse. The latter is fed via another differentiating circuit and gain control to a wide band 3-stage amplifier (gain $\sim$ 100) giving a narrow positive output pulse of about 15 volts maximum. This pulse triggers the multivibrator, and a preset control enables the width of the output pulse from the multivibrator to be varied between approximately 1.5 and 3 μsecs. Thus the resolving time of the circuit can be varied over about 1.5 μsecs. (equation 3.2, 2). Cathode followers are provided at various points in the circuit to preserve pulse shape and to enable test points to be incorporated.

The scales-of-10 are a modification of a design by Rotblat[1]. They require a sharp input pulse of about 30 volts, and provide a sharp output pulse of about 50 volts.

1. Reference R3.

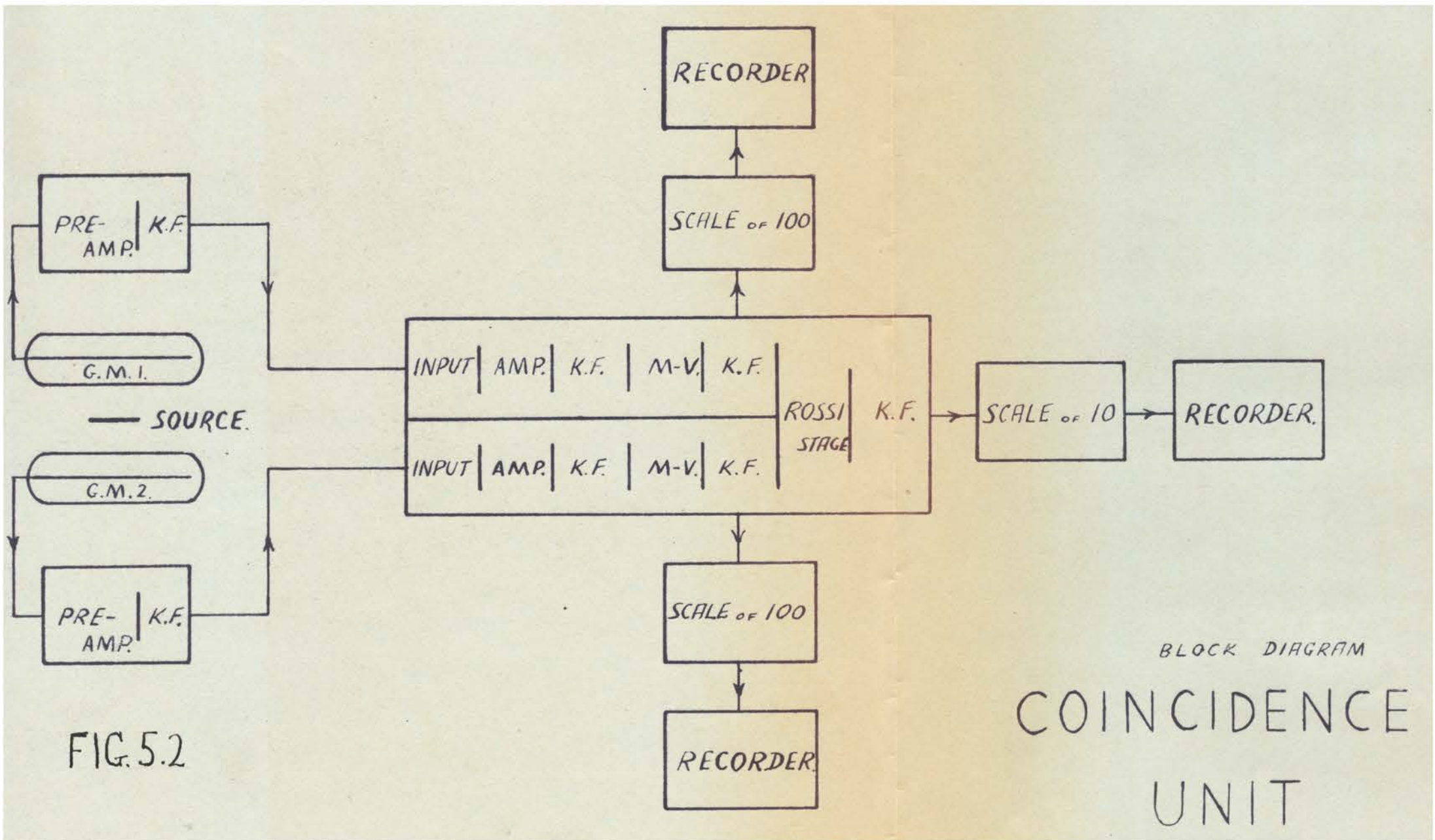

FIG. 5.2

BLOCK DIAGRAM

COINCIDENCE UNIT

The general purpose recording unit was designed by the writer and the developmental work was carried out by Mr. Bishop. It will operate directly from a Geiger counter or from a source of either negative or positive pulses. The circuit will drive any mechanical register operating on a pulse width between 5 and 30 milliseconds and a pulse current in the range 5 to 30 milliamps.

Detailed circuits and full discussions of them, together with instructions for operation and maintenance, are given in the Appendix.

5.3. Geiger Counters and Attachments.

Conventional Geiger counters with copper cathodes and filled with 9 cms. Argon and 1 cm. Alcohol were used for detecting gamma rays. G.E.C. end window counters, EHM2 and GM4, were used for detecting beta particles. Single window counters and double window counters of special design for Compton coincidence absorption measurements were constructed. These counters are reproduced in Plate 3.

Special supports and attachments for each of the two types of Coincidence Experiments undertaken were designed and constructed by the workshop staff. Plate 4a shows the arrangement for carrying out beta-gamma coincidence absorption measurements, and Plate 4b that for carrying out Compton coincidence absorption measurements. Miscellaneous items of equipment are reproduced in Plate 5.

CHAPTER 6.

EXPERIMENTAL RESULTS

6.1. Coincidence Resolving Time.

It was shown in Section 3.2. that the rate of chance coincidences in a twofold coincidence circuit is

$$C = N_1 N_2 . 2\tau \qquad (3.2,3)$$

in the usual notation. The validity of this formula has been established experimentally by Dunworth[1], and its importance has been emphasised. In the first place it may be used to determine the coincidence resolving time when each channel is actuated by separate sources, and, in the second place, it may be used to determine the "chance correction" to be made to the observed coincidence rate. Consequently, the first project in a coincidence experiment is to establish that the equipment has a constant resolving time, τ , and to measure it.

The Coincidence Circuit designed by the author and described in Chapter 5 is very suitable for "resolving-time experiments" since the pulse widths in each channel and hence the resolving time may be varied. The first series of experiments consisted in plotting, for particular settings of the pulse widths, the chance coincidence rate as a function of the product of the single channel counting rates. A typical result is shown in Fig. 6.1. where the coincidence resolving time is approximately 2.3 μ secs. The significance of this result is, firstly, that it shows that the coincidence resolving time for this equipment is constant, independent of the counting rate in either channel, and secondly, that it yields experimental confirmation of equation (3.2, 3) over a considerably wider range of values of the product $N_1 N_2$ than provided by the experiments of Dunworth.

1. Reference D3, Table II.

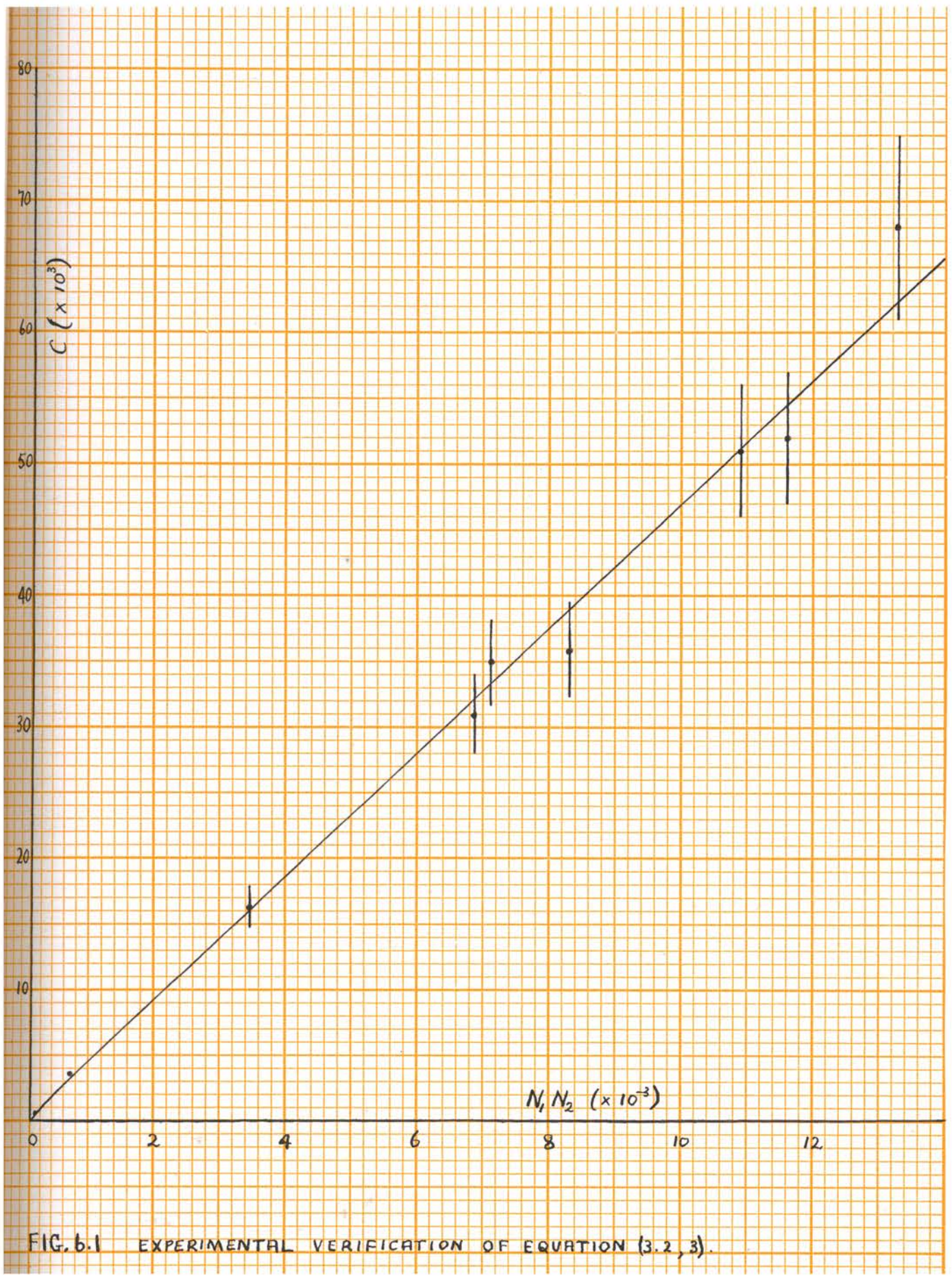

FIG. 6.1 EXPERIMENTAL VERIFICATION OF EQUATION (3.2, 3).

Further experiments carried out on the "Coincidence Resolving Time" involved the use of a cathode ray tube [1] in which the input to the Rossi stage from one of the channels was viewed on the "trace" triggered by a pulse from the same channel. Although the full input pulse was not displayed because of a delay of a microsecond or more in the triggering, the trailing edge could be seen, and, as the pulse length was varied, the shift in position of the trailing edge gave the change in width of the pulse; this change in width was compared with the change in resolving time determined from chance coincidences. Typical results are summarised in Table 6.1.

TABLE 6.1.

$(\tau_A + \tau_B)_1$ (CHANCE COINC.)	τ_A increased by (C.R.O.)	τ_B increased by (C.R.O.)	$(\tau_A + \tau_B)_2$ (CHANCE COINC.)
5.9 ± 0.3 μsecs.	0.5 μsecs.	0	6.6 ± 0.3 μsecs.
5.44 ± 0.32 "	0.5 "	0	5.66 ± 0.31 "
5.66 ± 0.31 "	1.0 "	0	6.99 ± 0.47 "
6.99 ± 0.47 "	0	- 1.0 μsecs.	5.95 ± 0.37 "
4.26 ± 0.24 "	1.0 "	0.5 "	5.90 ± 0.25 "

6.2. The Disintegration of Co^{60}.

The decay scheme of Co^{60} (Fig. 6.2) is well known and accordingly this radioactive isotope was used to test the equipment and to obtain practice in the experimental technique.

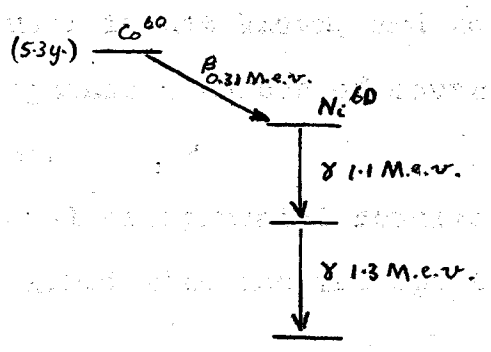

FIG. 6.2

1. A "time-calibrated" double beam Cossor C.R.O.

The absorption of the beta rays in aluminium is shown in Fig. 6.3 where the presence of a gamma ray background is observed and where the beta ray end point occurs at approximately 0.07 gm/cm^2. This absorption limit corresponds to an energy of 0.28 M.e.v.[1]

Gamma-gamma coincidences are also observed and the beta-gamma coincidence rate per beta particle, plotted in Fig. 6.4 against thickness of aluminium absorber, yields a straight line as expected. From the ratio

$$R = \frac{N^{\beta\gamma}}{N^{\beta}} \Big/ \frac{N^{\gamma\gamma}}{N^{\gamma}} = 1 - \frac{1}{n} , \qquad (3.4, 29)$$

one obtains for n, the number of gamma rays per disintegration, the value 2.10 ± 0.35, in good agreement with the expected value of 2. The plot of $N^{\beta\gamma} + N^{\gamma\gamma}$ against absorber thickness is almost identical in shape with the plot of $N^{\beta} + N^{\gamma}$ as may be seen from Fig. 6.3. where the former curve has been matched to the latter at absorber density 0.0053 gms./cm.^{2}. This is precisely what is expected (Section 3.4(IV)). Thus the decay scheme of Fig. 6.2, one beta ray followed by two gamma rays, is verified.

From the "Compton electron coincidence rate v. absorber thickness" curve[2] of Fig. 6.5, E_n values of 0.97 M.e.v., 1.06 M.e.v., 1.14 M.e.v., 1.19 M.e.v., 1.20 M.e.v are deduced. These values indicate that the gamma radiation consists of more than one component. That they are about 10% lower than the values one would have expected is probably due to the failure to add a correction term (C.f. $d = d' + 2k\delta$, Fig. 4.5) to the absorber density. The magnitude of such a correction for the experimental arrangement used is not known, and could only be determined by calibration against a number of sources yielding gamma rays of known energies.

Additional experimental results of considerable interest were also obtained with the isotope Co^{60}. Figure 6.6 shows the

1. This value is determined from the relation $R = 0.407\,E^{1.38}$ 0.15 M.e.v. $< E < 0.7$ M.e.v. (Reference F3). The underestimation illustrates the point discussed on p. 43, footnote 2. The curves of Bleuler and Zunti (Fig. 4.1) do not extend to 0.3 M.e.v.
2. Sections 3.3. and 4.2.

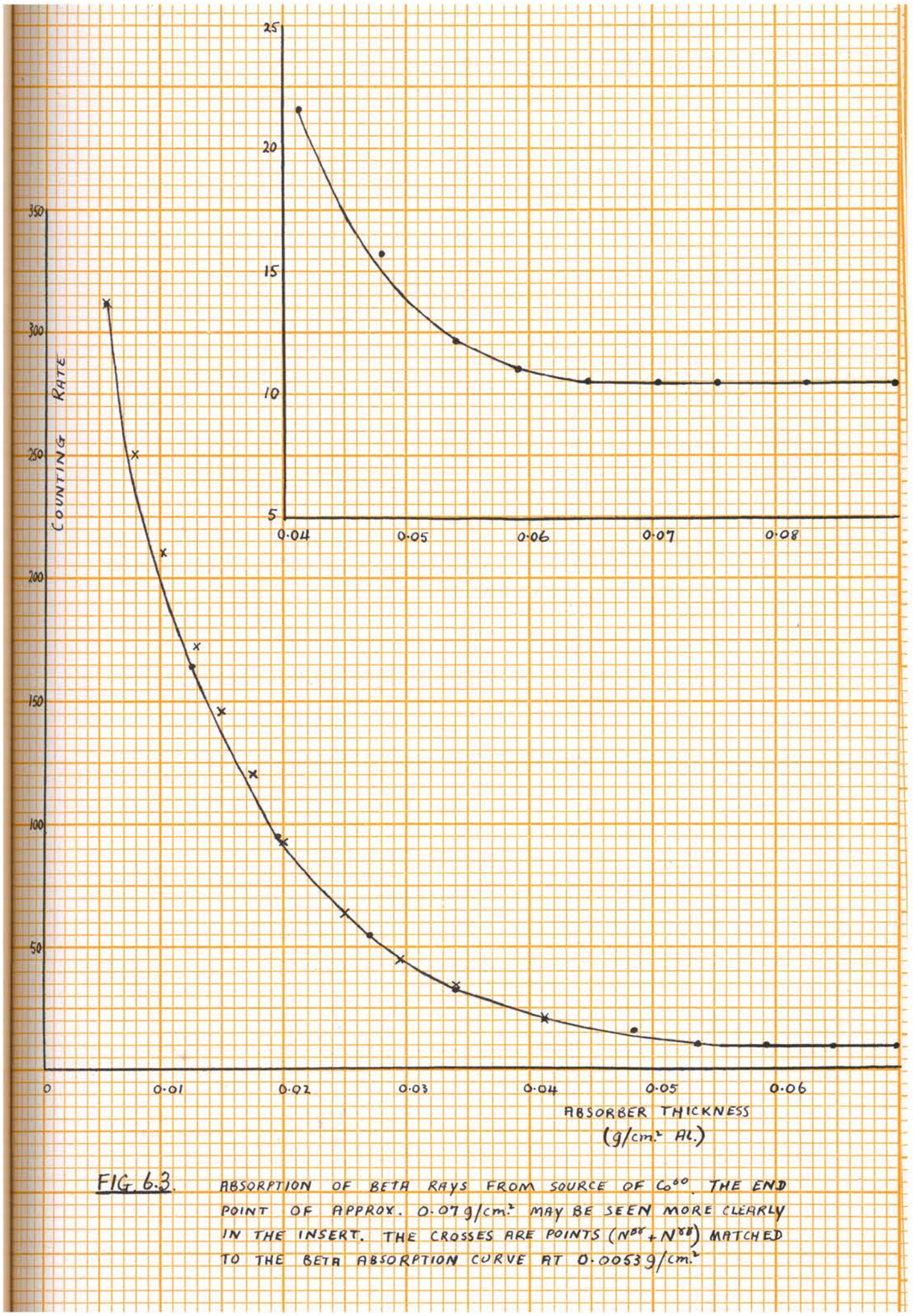

FIG. 6.3. ABSORPTION OF BETA RAYS FROM SOURCE OF Co^{60}. THE END POINT OF APPROX. 0.07 g/cm². MAY BE SEEN MORE CLEARLY IN THE INSERT. THE CROSSES ARE POINTS ($N^{BS} + N^{BB}$) MATCHED TO THE BETA ABSORPTION CURVE AT 0.0053 g/cm².

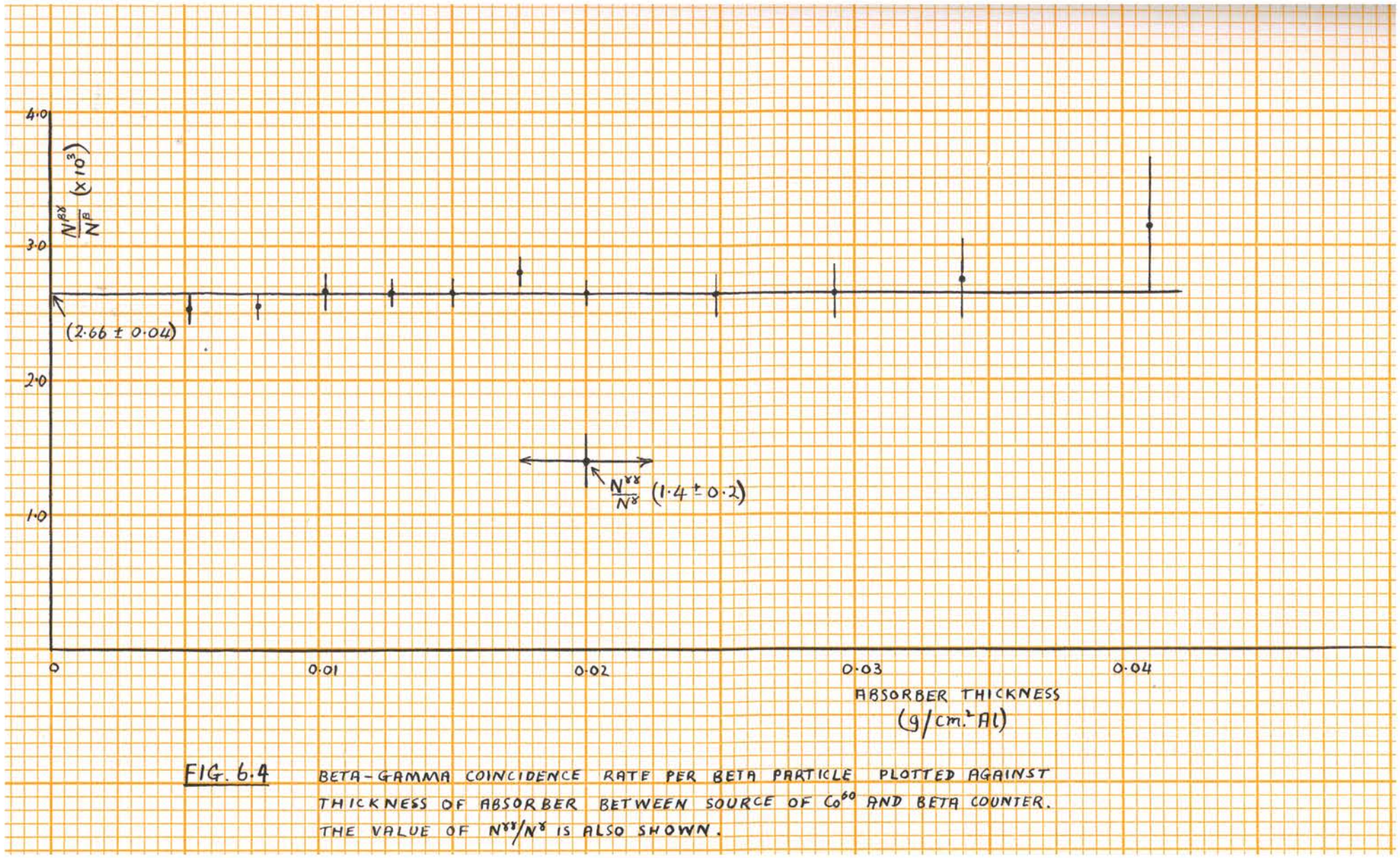

FIG. 6.4 BETA-GAMMA COINCIDENCE RATE PER BETA PARTICLE PLOTTED AGAINST THICKNESS OF ABSORBER BETWEEN SOURCE OF Co^{60} AND BETA COUNTER. THE VALUE OF $N^{\beta\gamma}/N^{\gamma}$ IS ALSO SHOWN.

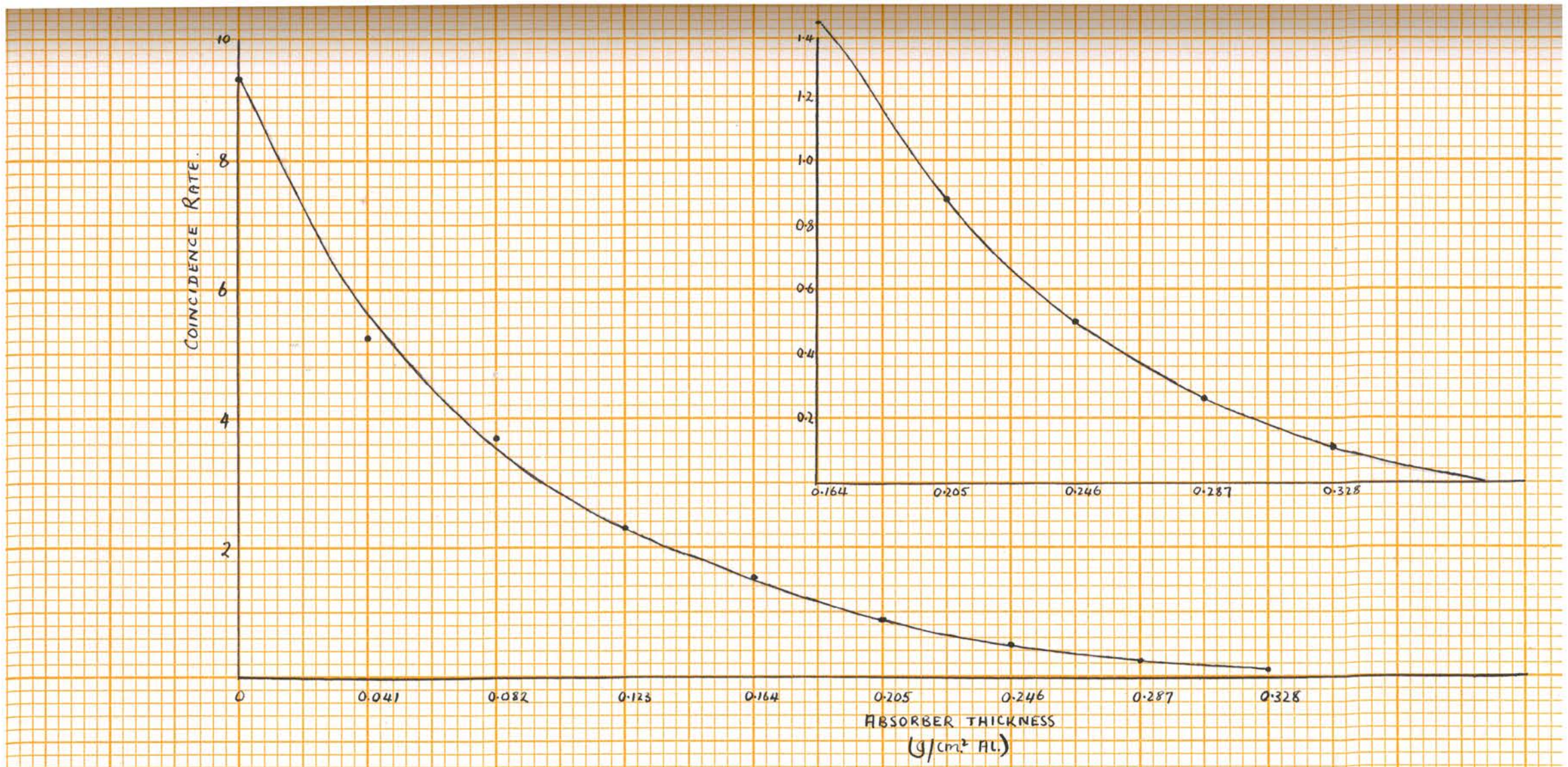

FIG. 6.5 COMPTON ELECTRON COINCIDENCE RATE AS A FUNCTION OF THICKNESS OF ABSORBER PLACED BETWEEN DOUBLE WINDOW BETA COUNTER AND SINGLE WINDOW COUNTER (FIG. 3.1) FOR SOURCE OF Co^{60}.

gamma counting rate plotted against thickness of aluminium absorber placed between a strong source of Co^{60} and a beta ray counter. One would expect the counting rate for gamma rays of a particular energy to increase with the thickness of absorber up to the absorption limit of the Compton electrons produced in the absorber, and then to decrease exponentially beyond this thickness; such is the case in Fig. 6.6. Using firstly Feather's relation[1] to determine the energy of the Compton electrons[2] corresponding to an absorption limit of approximately 0.3 gms/cm^2, and secondly the relation[3]

$$W_c = \frac{2W_\gamma^2}{m_0c^2 + 2W_\gamma}$$

connecting the upper limit of the Compton spectrum with the energy of the incident gamma ray, one obtains the value 1.1 M.e.v. for the mean gamma ray energy in good agreement with an expected value of 1.2 M.e.v.[4] Although the absorption curve has not been taken far enough to obtain a reliable estimate of the mean gamma ray energy, an absorption coefficient of approximately 0.17 may be deduced from the graph. This corresponds roughly to a mean energy of 0.9 M.e.v. (Fig. 1.1). Fig. 6.6 has been included to illustrate one of the chief difficulties in interpreting the beta absorption curve of a radioactive isotope. It will be remembered that the procedure involved the subtraction of the constant gamma background beyond the absorption limit of the hardest beta ray. Obviously such a procedure is only reliable when the absorption limit of the hardest detected beta ray is less than the point at which the gamma counting efficiency begins to increase appreciably. Consequently, when the spectrum is complex

1. Equation (4.1, 1)
2. Feather's relation holds strictly only for Beta rays, but the error is of no consequence to the point under consideration here.
3. Equation (1.1, 1)
4. The absorption limit of the Compton electrons may be seen from Fig. 6.5 to be about 0.42 gms/cm^2 (an extra 0.04 gms/cm^2 has been added for window thicknesses). Using the same procedure, one obtains a value 1.2 M.e.v. for the energy of the harder gamma ray.

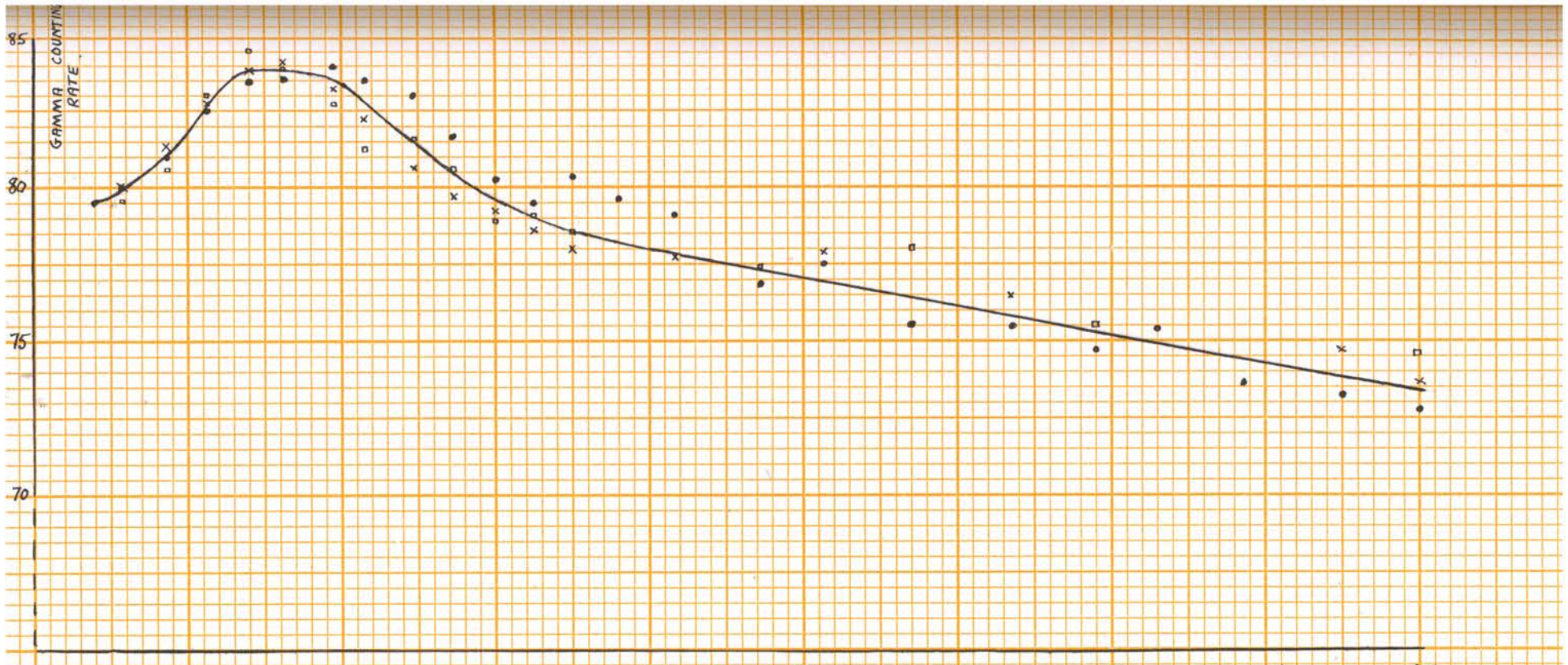

FIG. 6.6. GAMMA COUNTING RATE AS A FUNCTION OF THICKNESS OF ABSORBER PLACED BETWEEN SOURCE OF Co^{60} AND BETA COUNTER. NO BETA RAYS PENETRATE BEYOND 0.07 g/cm.². THE INITIAL RISE CORRESPONDS TO AN INCREASE IN EFFICIENCY UP TO THE ABSORPTION LIMIT OF THE COMPTON ELECTRONS PRODUCED IN THE ABSORBER. THE SUBSEQUENT FALL REPRESENTS THE ABSORPTION OF THE GAMMAS BEYOND THIS POINT.

and particularly when the gamma background is large it may be difficult to interpret the absorption curve. For example, where a low energy gamma ray is associated with a hard beta ray of comparatively low intensity, the small beta count may be difficult to determine accurately because of the initial increase in gamma efficiency and subsequent decrease with absorber thickness; and more so, when other gamma rays are present as in the case of Ag^{110} described in a later section

6.3. A New Method for Determining the Resolving Time of a Coincidence Circuit or the Strength of a Radioactive Isotope of Simple Decay Scheme.

For the disintegration scheme of Fig. 6.2, the following equations hold[1]:

$$N_1(x) = 2N\epsilon_1^{\gamma} + N\epsilon_1^{\beta}F(x) \qquad (6.3,1)$$

$$N_2 = 2N\epsilon_2^{\gamma} \qquad (6.3,2)$$

$$N_{12}(x) = N_{12}^{\beta\gamma}(x) + N_{12}^{\gamma\gamma} + N_1N_2\cdot 2\tau + K$$

$$= 2N\epsilon_1^{\beta}F(x)\epsilon_2^{\gamma} + 2N\epsilon_1^{\gamma}\epsilon_2^{\gamma} + 2N_1N_2\tau + K$$

$$= N_1N_2\left[\frac{1}{N} + 2\tau\right] + K - N_2\epsilon_1^{\gamma} \qquad (6.3,3)$$

Consequently, if $N_{12}(x)$ is plotted against $N_1(x)$, a straight line of slope $(\frac{1}{N} + 2\tau)$ and intercept (extrapolated to $N_1 = 0$), $K - N_2\epsilon_1^{\gamma}$, results. If one of the quantities, $N, 2\tau$, is known, the other may be deduced. Further, if K is known, ϵ_1^{γ} may be determined and checked against the value obtained from a measurement of $N_1(x)$ where $F(x) = 0$.

The advantage of using this method for determining the resolving time of a coincidence circuit, in place of that in which the chance coincidence rate and the single channel rates are determined when the two Geiger counters are placed some distance apart and actuated from separate sources, is that the counters need not be removed from the standard positions with the poss-

1. Section (3.4, IV). K = COSMIC RATE.

ibility of a subsequent change in the net efficiencies; in fact, the method enables the net efficiency of the beta counter for gamma rays of the appropriate energy to be checked.

The method has been used to determine the strengths of a strong and a weak source of Co^{60}. In the former case, illustrated in Fig. 6.7, chance coincidences contribute more to the total rate than do genuine coincidences. From the slope of the graph one obtains

$$2\tau + \frac{1}{N_0} = 9.4 \times 10^{-6}$$

and since 2τ has been determined previously,

$$2\tau = 5.4 \times 10^{-6}$$

one infers

$$N_0 = 0.25 \times 10^6 \text{ disintegrations per sec.}$$

From equation (6.3, 1) ϵ_1^γ may be calculated:

$$\epsilon_1^\gamma = 2.6 \times 10^{-4}.$$

From equation (6.3, 2)

$$\epsilon_2^\gamma = 3.5 \times 10^{-4}$$

Since K has been determined in a prior experiment, [1]

$$K = 0.011,$$

one calculates

$$-N_2 \epsilon_1^\gamma + K = -0.035$$

in excellent agreement with the value intercepted on the y-axis by the extrapolation of the straight line graph to $N_1 = 0$

The case of a weak source, illustrated in Fig. 6.8, is obtained from the measurements used in plotting Fig. 6.4. The net efficiency of the γ counter in this experiment was increased relative to that for the experiment illustrated in Fig. 6.7 by improving the geometry. As in the previous case one deduces

1. This is fortuitous in that several straight lines could be drawn through the four experimental points which would need to be determined with much smaller statistical error for reliance to be placed on the value of the intercept on the y-axis. Nevertheless, the fact that the intercept is negative for this strong source is well established.

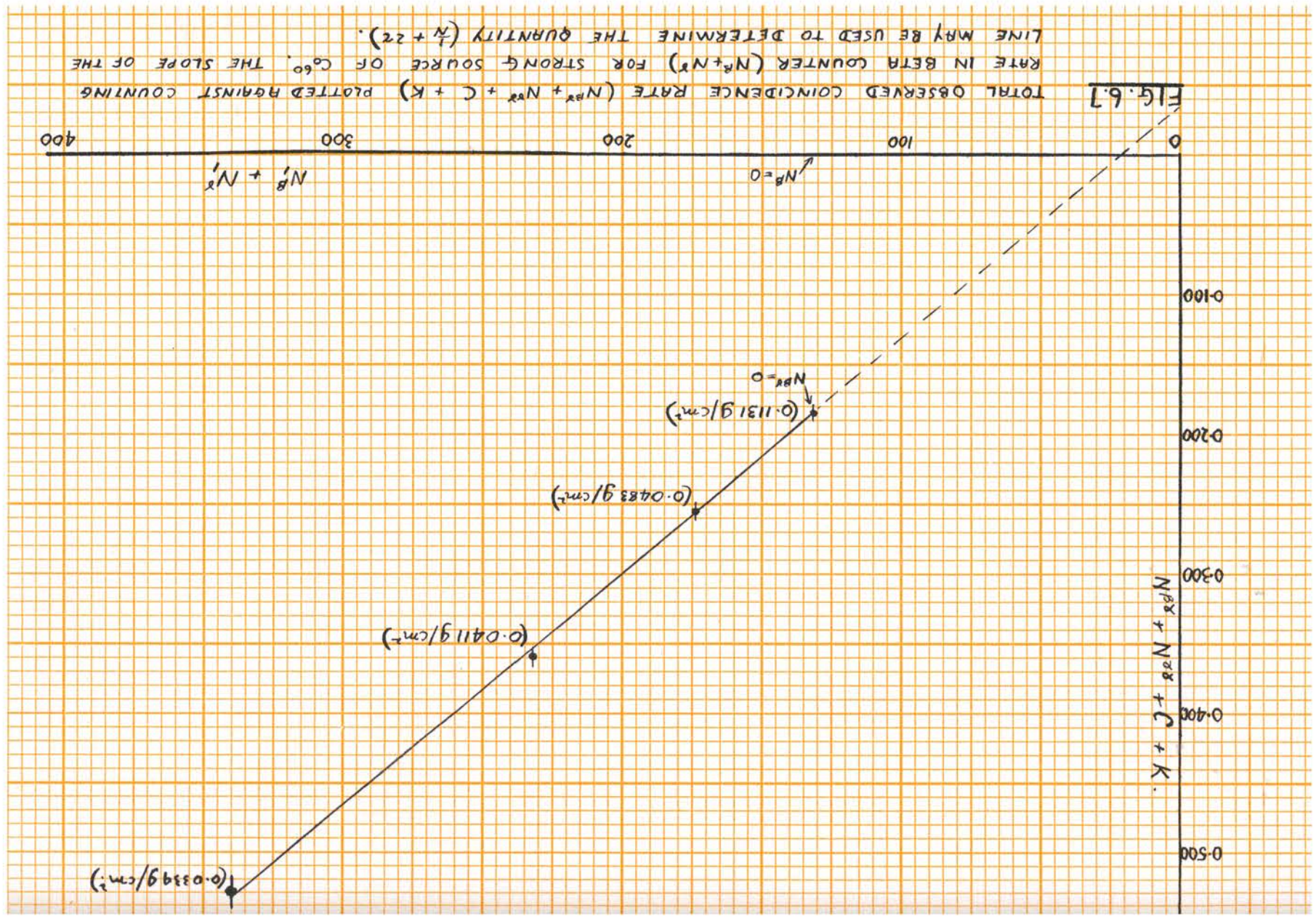

FIG. 6.7 TOTAL OBSERVED COINCIDENCE RATE $(N^{\beta\gamma} + N^{\alpha\gamma} + C + K)$ PLOTTED AGAINST COUNTING RATE IN BETA COUNTER $(N^\beta + N^\gamma)$ FOR STRONG SOURCE OF Co^{60}. THE SLOPE OF THE LINE MAY BE USED TO DETERMINE THE QUANTITY $(\frac{1}{N} + 2\tau)$.

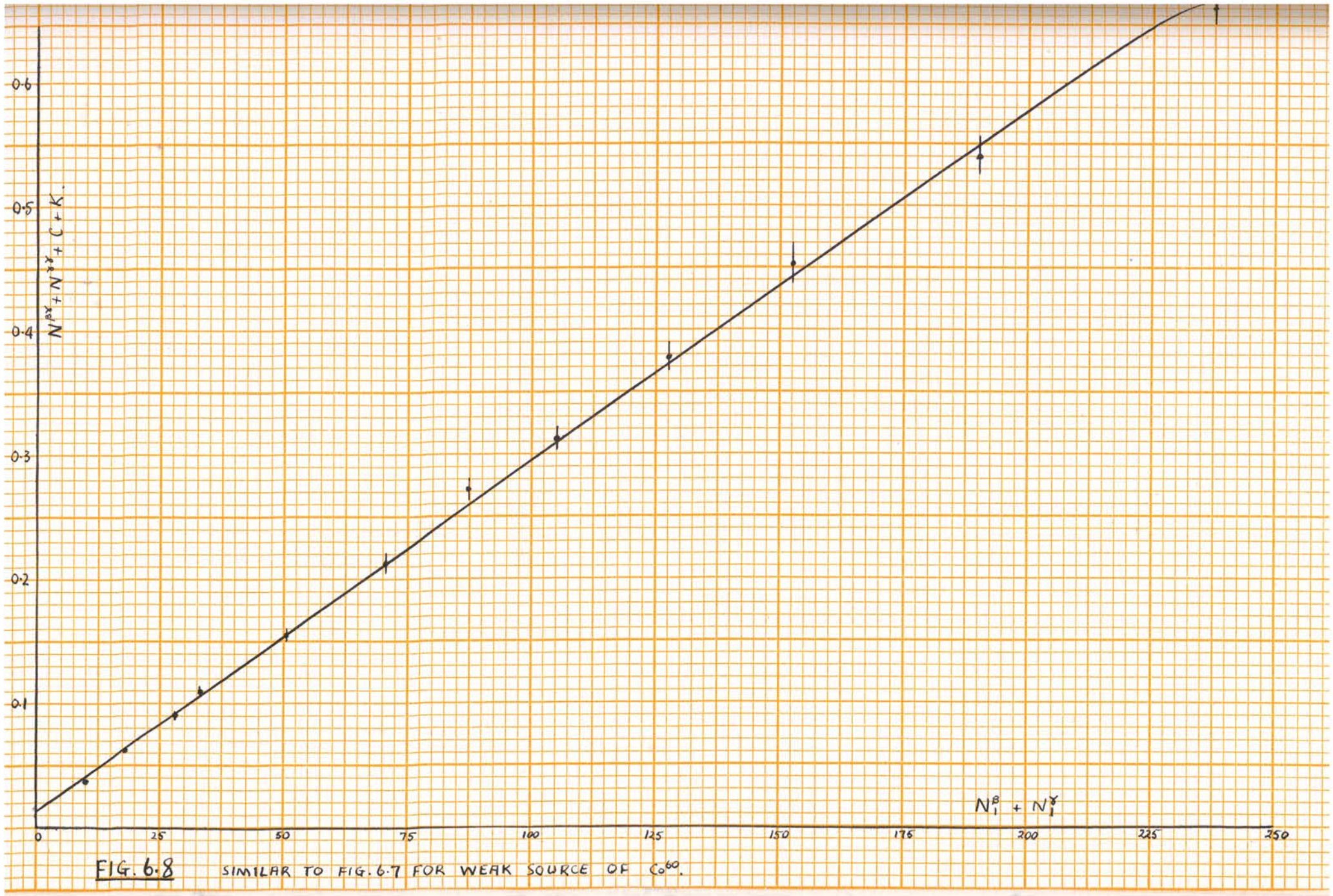

FIG. 6·8 SIMILAR TO FIG. 6·7 FOR WEAK SOURCE OF Co^{60}.

$$2\tau + \frac{1}{N_0} = 53.5 \times 10^{-6}$$

$$N_0 = 0.021 \times 10^{6}$$

$$\epsilon_1^{\gamma} = 2.4 \times 10^{-4}$$

$$\epsilon_2^{\gamma} = 13 \times 10^{-4}$$

and $K - N_2 \epsilon_1^{\gamma} = 0.004 \pm 0.002$, compared with the value 0.013 from the intercept. The positive value of this quantity for the weak source may be contrasted with the negative value for the stronger source of Fig. 6.7.

6.4. The Decay of Ag^{110}.

Fragmentary information on the decay scheme of Ag^{110} has been given by a number of authors. Measurements made by Siegbahn[1] with a magnetic analyser have shown the scheme to be very complicated. The disintegration pattern proposed by Siegbahn is reproduced in Fig. 6.9. (The more recent investigations by Rutledge and others - see Fig. 1.4 - do not add to the essential features of the scheme). Accordingly, initial experiments by the Coincidence-absorption technique were planned to test the pattern suggested in Fig. 6.9.

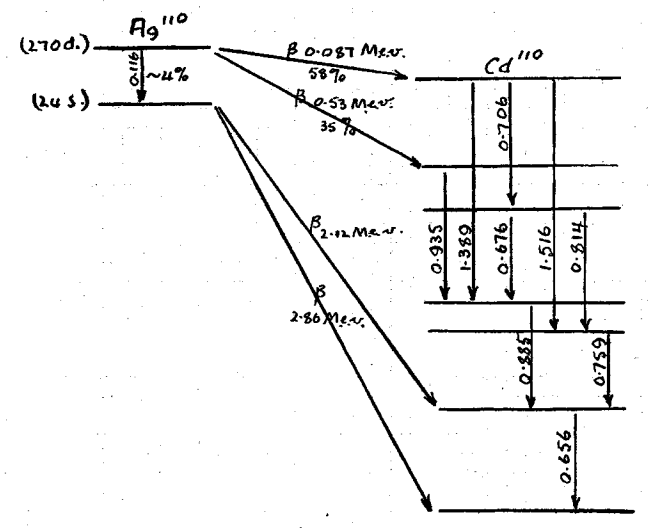

FIG.6.9 Ag^{110} Disintegration Scheme suggested by Siegbahn.

The absorption curve of the beta rays is shown in Fig. 6.10 and the first part of the curve may be seen more clearly in Fig. 6.11.[2] Beta rays of sufficient intensity to be measured

1. Reference S2.
2. The relation between density ρ, thickness t and surface density x is $\rho t = x$.

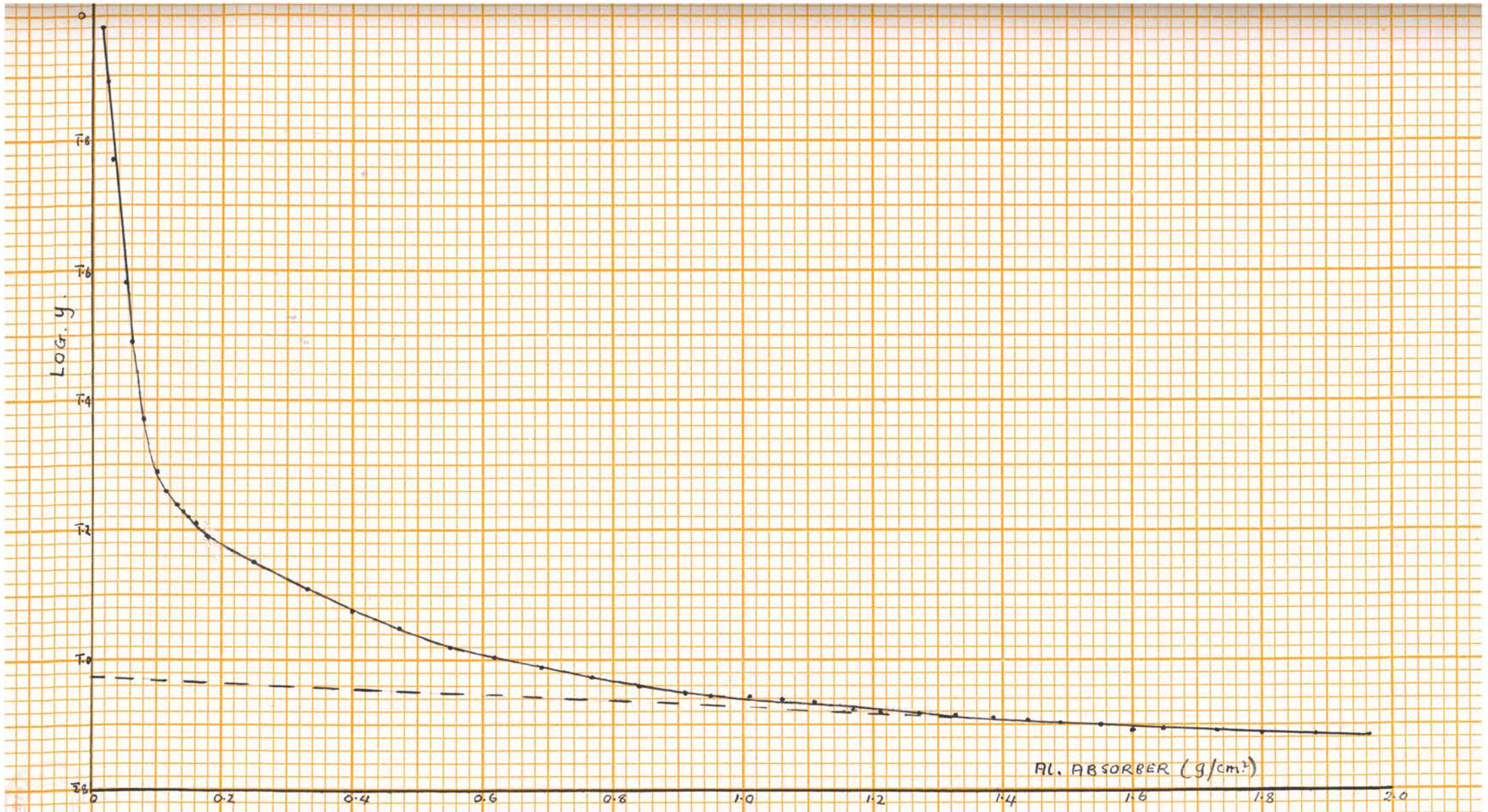

FIG. 6.10 EXPERIMENTAL CURVE OF LOG y. v. x FOR DISINTEGRATIONS FROM Ag^{110}.
$y(x)$ = FRACTIONAL TRANSMISSION THROUGH ABSORBER THICKNESS x.

among the gamma background do not appear to occur beyond an absorber surface density of 1.2 gms/cm^2. The subsequent linear absorption curve of the gamma rays may be projected back, and the true beta absorption curve obtained by difference. Whilst the gamma absorption curve has not been taken far enough to obtain a reliable value for the mean absorption coefficient a value of μ equal to 0.3 may be deduced from Fig. 6.10. One would have expected from Figs. 1.4 and 1.1 a value of about 0.2.

One notes the comparatively large gamma background. (In Fig. 6.10, $\frac{N^\gamma}{N} \sim 10\%$ for $x \sim 0.008$ gms/cm^2, whilst in Fig. 6.3, $\frac{N^\gamma}{N} \sim 4\%$ for $x \sim 0.008$ gms/cm^2). This is due partly to the many gamma rays associated with the decay of Ag^{110}, and partly to the total absorption of the softest beta ray (0.087 M.e.v.) in the window of the counter used for obtaining the curve of Fig. 6.10. A similar curve taken with a very thin window counter was parallel to and below that of Fig. 6.10, and, when superimposed on the latter, yielded the point marked X. This point indicates the presence of a very soft beta component, and, since an absorption curve for it could not be obtained, it is assumed that it is Siegbahn's 0.087 M.e.v. beta ray. The thin window counter was not used in any of the subsequent experiments, and consequently, effects due to the 0.087 M.e.v. beta ray were not observed.

After allowing for the gamma component of Fig. 6.10, one obtains the beta absorption curves of Figs. 6.12 and 6.13. A Bleuler and Zunti analysis[1] of the component β_2 yields the E_{∞} values: 2.52 M.e.v., 2.65 M.e.v., 2.76 M.e.v. One concludes that the β_2 component is complex and the E_{∞} values are consistent with values 2.12 M.e.v. and 2.86 M.e.v. proposed by Siegbahn. Further, the β_2 component represents about 10% of the activity $\beta_1 + \beta_2$. If one accepts Siegbahn's estimate of 35% for the activity β_1, then, on these measurements, β_2 comprises 4% of the total activity. This agrees well with the value 3% deduced by Siegbahn from his magnetic analysis.

1. Section 4.1.

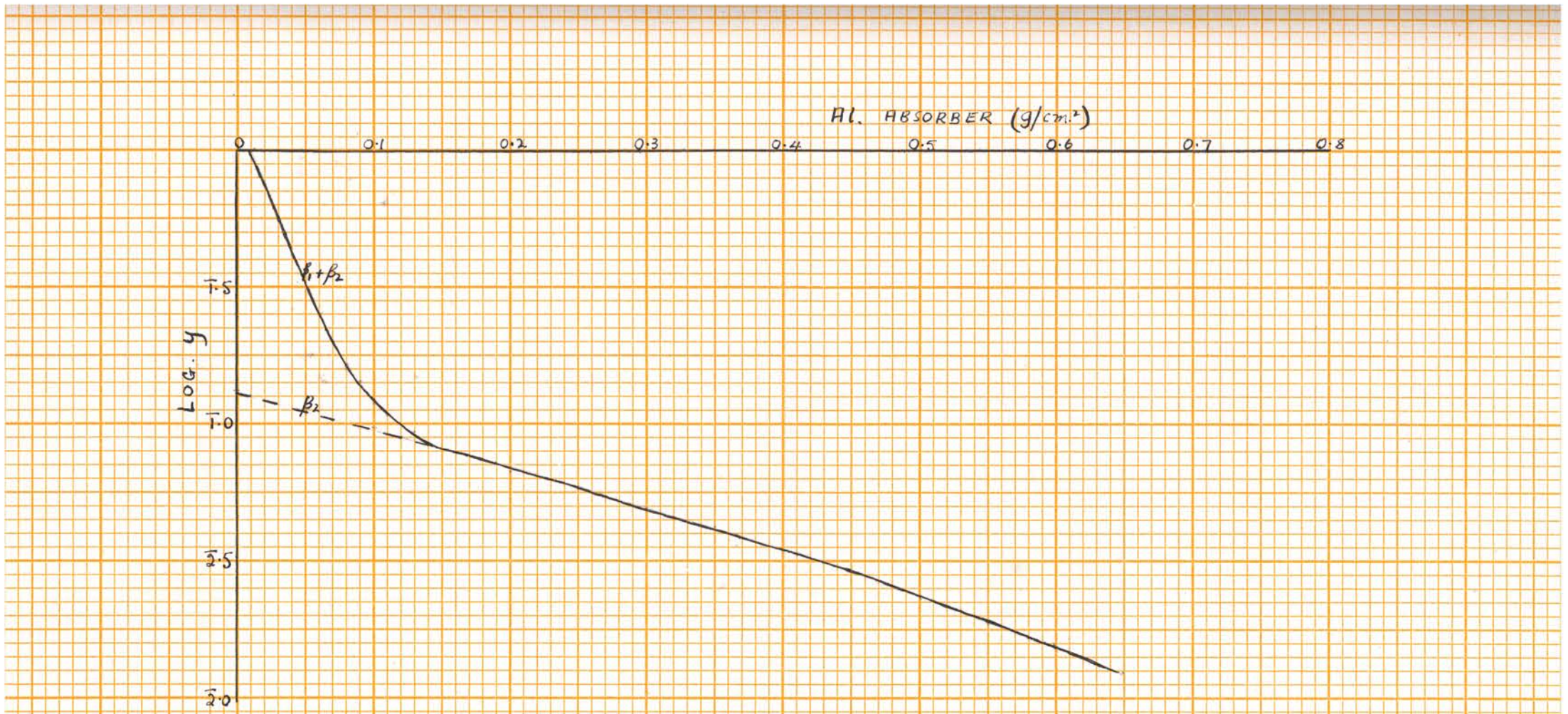

FIG. 6.12 BETA ABSORPTION CURVE FOR Ag^{110}, OBTAINED FROM FIG. 6.10 BY SUBTRACTING GAMMA BACKGROUND.

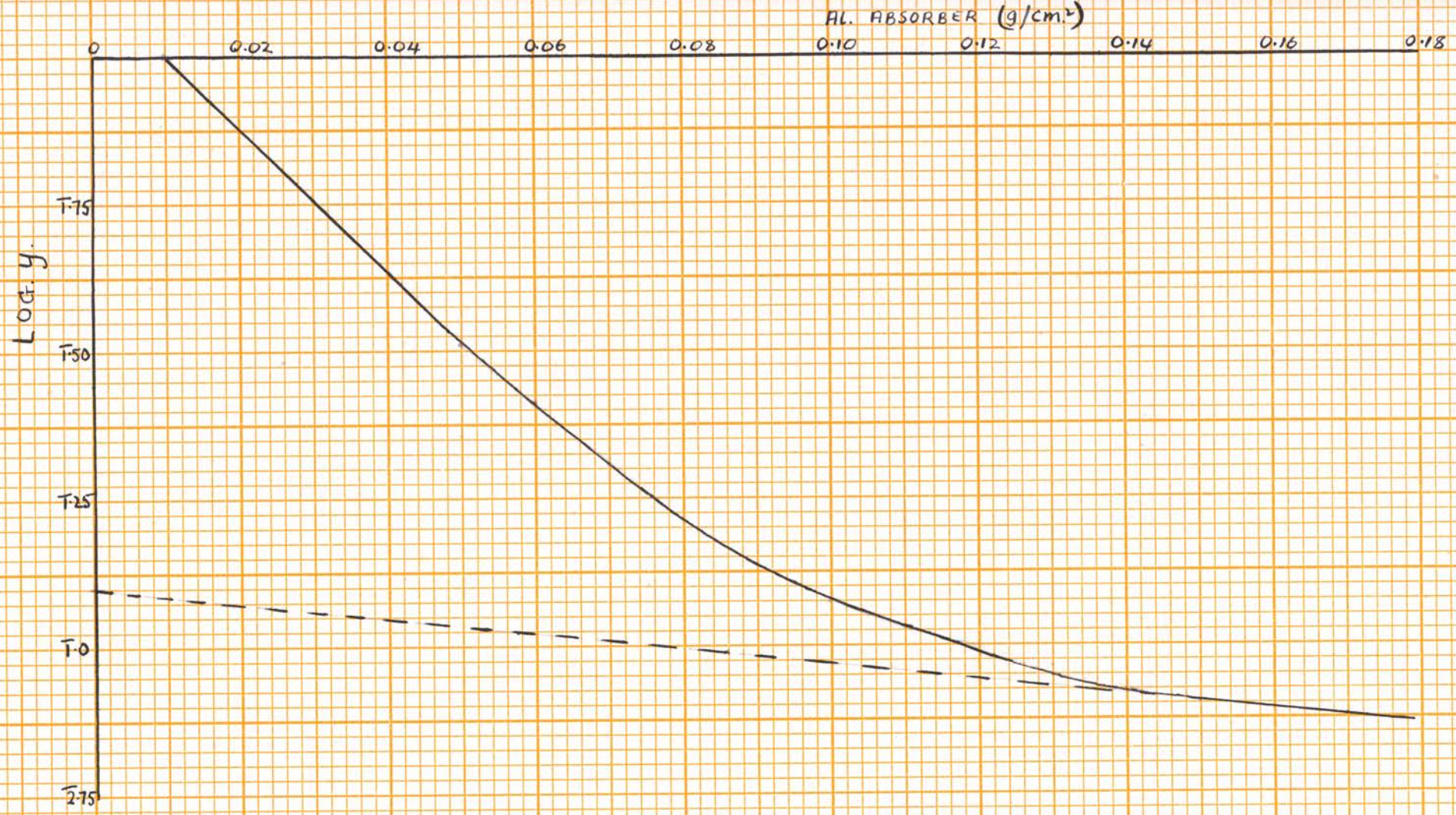

FIG. 6.13 FIRST PART OF FIG. 6.12 ON LARGER SCALE.

Figure 6.14 represents the absorption curve for β_1 . From a Bleuler and Zunti analysis, one deduces E_λ values: 0.55 M.e.v., 0.55 M.e.v., 0.55 M.e.v., 0.55 M.e.v. One concludes that β_1 is simple and has the energy 0.55 M.e.v., with error ± 0.04 M.e.v.[1] This value agrees well with the value 0.53 M.e.v. quoted by Siegbahn.

A gamma-gamma coincidence rate of 0.0460 was also obtained. The observed beta gamma coincidence rate is plotted against thickness of absorber placed between the source and beta counter in Fig. 6.15, and the corresponding beta-gamma coincidence rate per beta particle is shown in Fig. 6.16. On the average, 900 coincidences were obtained for each point plotted. The large standard errors shown in Fig. 6.16 are due to the fact that the observed coincidence rate at each point comprises a beta-gamma rate, a gamma-gamma rate, a cosmic rate and a chance rate. The magnitude of the beta-gamma rate over the region 0.15 to 0.8 gms/cm^2 is roughly of the same order as that of the cosmic rate and that of the chance rate, and considerably less than that of the gamma-gamma rate. In the subtraction, the absolute errors mount and the fractional errors become very large. The gamma-gamma rate was measured accurately at 1.5471 gms/cm^2 and the rate to be subtracted for $N^{\beta\gamma}$ at any other absorber thickness was computed from this value by allowing for a mean absorption coefficient of 0.2 cm^{-1} for the gamma rays.

The initial rapid fall in the curves of Figs. 6.15 and 6.16 and the abrupt change in slope at about 0.15 gm/cm^2 may be compared with the corresponding behaviour of Fig. 6.12. Thus the presence of β_1 and its end point are confirmed. β_1 leads to an excited state of the product which loses its excess energy by radiating one or more gamma rays. If β_2 leads to the ground state of the product one would expect $\frac{N^{\beta\gamma}}{N^{\beta}}$ to fall to zero at an absorber thickness of approximately 0.15 gms/cm^2.[2] On the

1. See the relations quoted in (4.1, 6).
2. Section 3.4.

FIG. 6.14 ABSORPTION CURVE FOR β_1, Ag^{110}, OBTAINED FROM FIG. 6.12 BY SUBTRACTING β_2 FROM $(\beta_1 + \beta_2)$

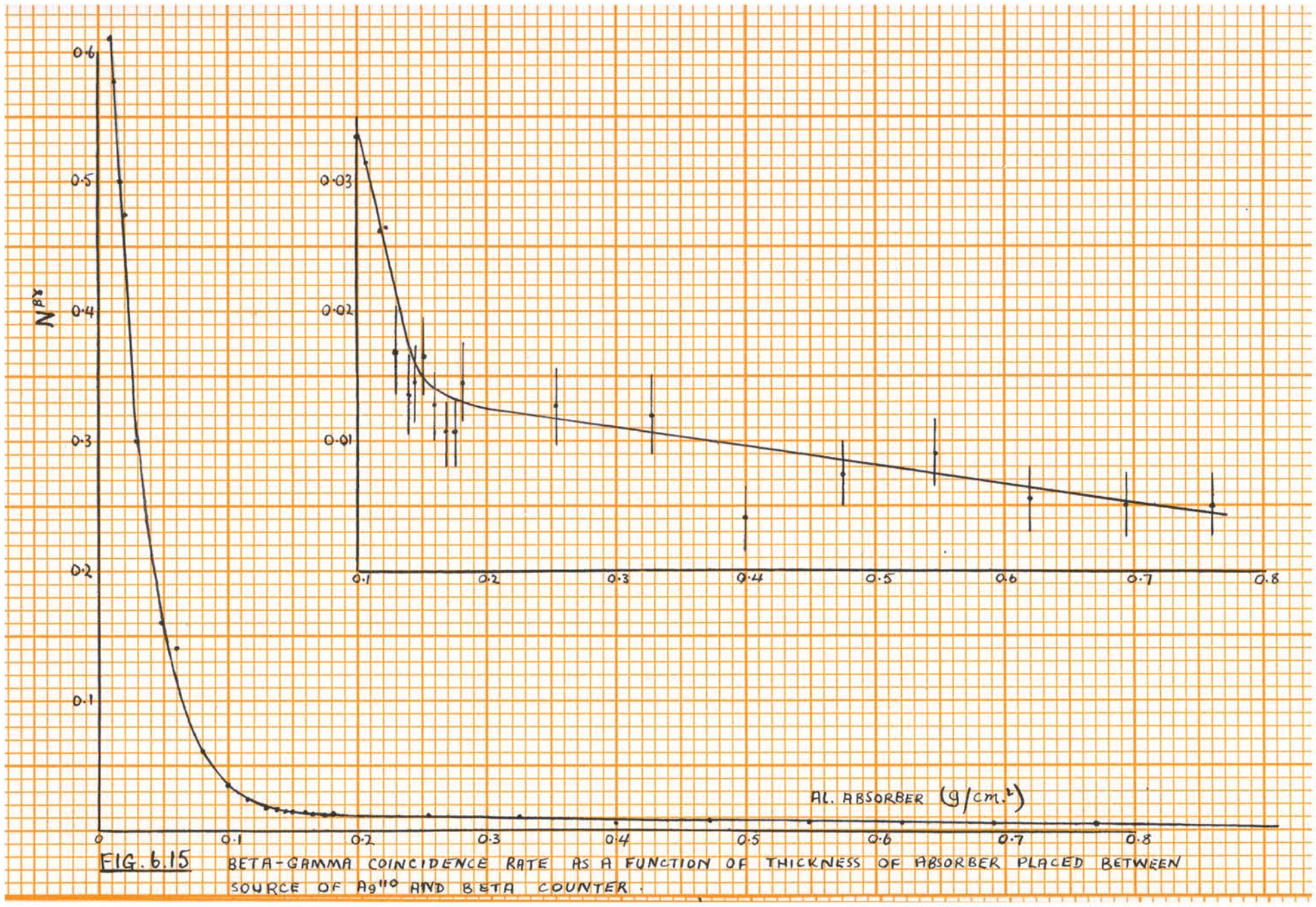

FIG. 6.15 BETA-GAMMA COINCIDENCE RATE AS A FUNCTION OF THICKNESS OF ABSORBER PLACED BETWEEN SOURCE OF Ag^{110} AND BETA COUNTER.

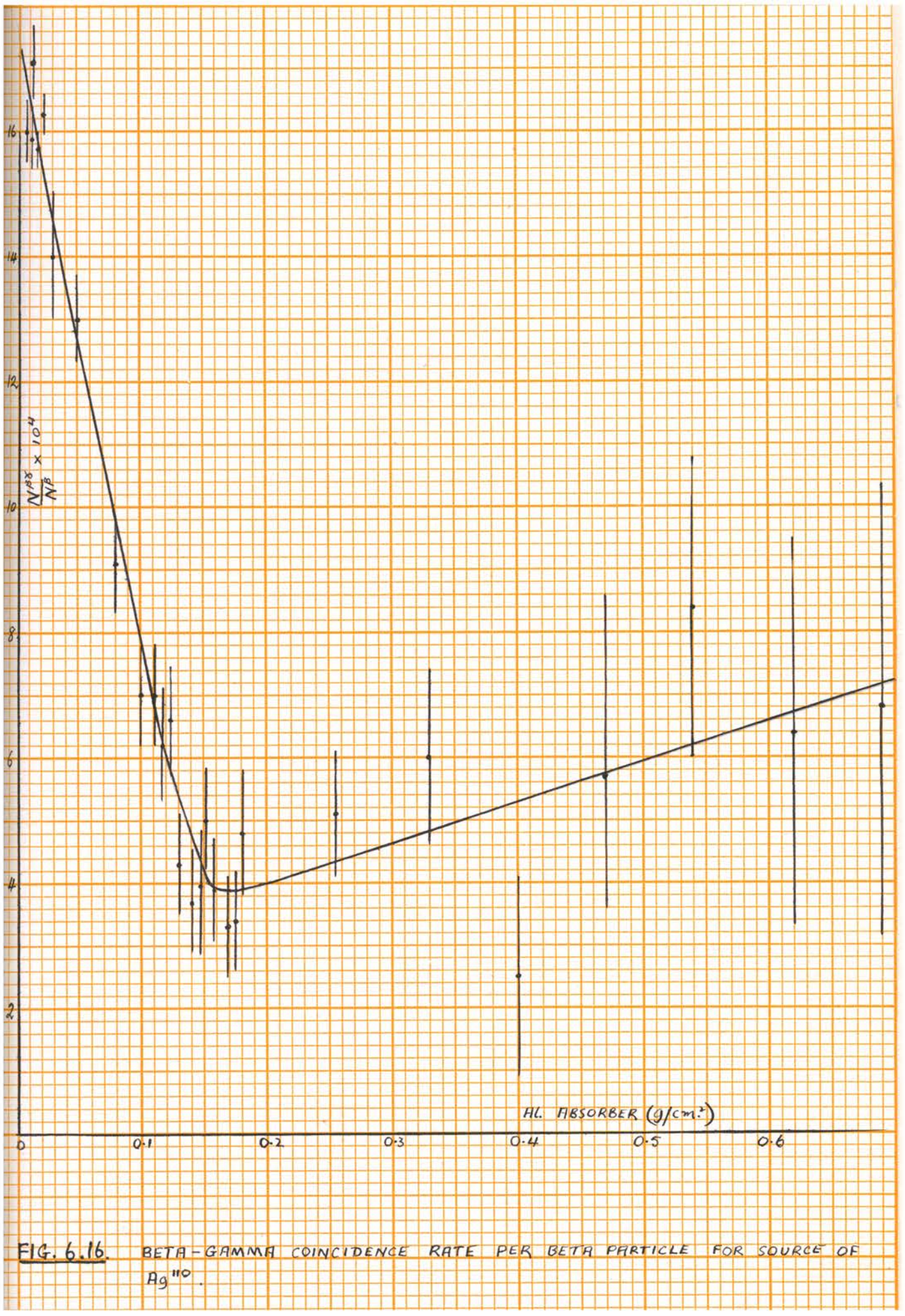

FIG. 6.16. BETA-GAMMA COINCIDENCE RATE PER BETA PARTICLE FOR SOURCE OF Ag^{110}.

other hand, if β_2 is simple and leads to an excited state of the product, $\frac{N^{\beta\gamma}}{N^{\beta}}$ should decrease with absorber density to 0.15 gms/cm^2 and should then remain constant; if, however, β_2 is complex, $\frac{N^{\beta\gamma}}{N^{\beta}}$ would fall away slowly beyond 0.15 gms/cm^2 if the harder part of β_2 were the less intense, and more rapidly, if the softer part were the less intense. One would not expect $N^{\beta\gamma}/N^{\beta}$ to increase beyond the end point of β_1.

Some conclusions may be drawn from the behaviour of the first part of the curve of Fig. 6.15. Let us assume that the disintegration scheme takes the form of Fig. 6.17[1].

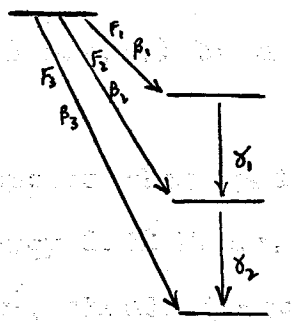

FIG. 6.17

Suppose $$\epsilon^{\gamma_1} = k\,\epsilon^{\gamma_2} = k\epsilon^{\gamma} \qquad (6.4,1)$$

Then one deduces

$$N^{\beta\gamma}(x) = N_0\,\epsilon^{\beta}\epsilon^{\gamma}\left[F_1(x)\cdot(1+k) + F_2(x)\right] \qquad (6.4,2)$$

$$N^{\beta}(x) = N_0\,\epsilon^{\beta}\left[F_1(x) + F_2(x) + F_3(x)\right] \qquad (6.4,3)$$

where the figures quoted in Table 6.2 hold:

TABLE 6.2

Absorber (x)	$F_1 + F_2 + F_3$	F_1	$N^{\beta\gamma}$
0.01 gm/cm^2	1	0.88	0.61
0.14 gm/cm^2	0.084	0	0.014

Consequently one has

$$\frac{0.88\,(1+k) + F_2(0.01)}{F_2(0.14)} = 44$$

and, since[2] $F_2(0.01) \approx F_2(0.14)$,

$$F_2(0.14) = 0.020\,(1+k) \qquad (6.4,4)$$

1. Since the beta component of energy 0.087 M.e.v. does not contribute to the shape of Fig. 6.14, it is omitted from Fig. 6.17.
2. Fig. 6.12.

where[1] $0 < k \leq 3.2$ (6.4, 5)

If one uses the "counter efficiency v. quantum energy" curve of Bradt and his associates,[2] and assumes that Siegbahn's scheme is correct, one deduces that $k \approx 4$. Hence the conclusion to be drawn from the above observations (equations 6.4, 4 and 6.4, 5) is that $F_3 << F_2$. This would be consistent with a constant value for $N^{\beta\gamma}/N^{\beta}$ beyond absorber thickness 0.14 gms/cm^2. Since, according to Siegbahn, β_2 contains the components 2.86 M.e.v. and 2.12 M.e.v., and since, on the above analysis, the former component is only a small fraction of β_2, one would have expected E_n values closer to 2.12 M.e.v. than the three values deduced (2.52, 2.65, 2.76 M.e.v.) by a Bleuler and Zunti analysis of (Fig. 6.12).

If one supposes that β_2 is simple and represents the radiation of energy 2.12 M.e.v., the curve $N^{\beta\gamma}(x)$, for $x > 0.15$ gms/cm^2, should trace out the shape of the absorption curve for β_2, and, when analysed by the method of Bleuler and Zunti, should yield E_n values of approximately 2.1 M.e.v. Fig. 6.18 shows the behaviour of log. $\left[N_{12}(x)/N_{12}(0)\right]$. An end point of about 1.1 gms/cm^2 is observed for the beta ray contributing to the $N^{\beta\gamma}$ rate beyond 0.15 gms/cm^2. This represents an energy of 2.2 M.e.v. If, however, the gamma rate is subtracted from $\beta_2 + \gamma$, the resulting absorption curve falls somewhat more slowly than that of β_2 in Fig. 6.12 and very much more quickly than that of γ in Fig. 6.10. Thus the fall of the coincidence rate in Fig. 6.17 beyond 0.15 gm/cm^2 is attributed to the absorption of a beta ray. It does appear, however, both from this rate of fall and from the fact that $N^{\beta\gamma}/N^{\beta}(x)$ increases, that the observed $N^{\beta\gamma}$ rate is too high. It has been explained that, in these measurements, a very small $N^{\beta\gamma}$ rate is being obtained by subtracting rates C ($\sim N^{\beta\gamma}$), K ($\sim N^{\beta\gamma}$) and $N^{\gamma\gamma}$ ($\sim 5 \times N^{\beta\gamma}$) from an observed rate,

1. $F_1(0.14) \leq F_2(0.14) + F_3(0.14) = 0.084$
2. Reference B8.

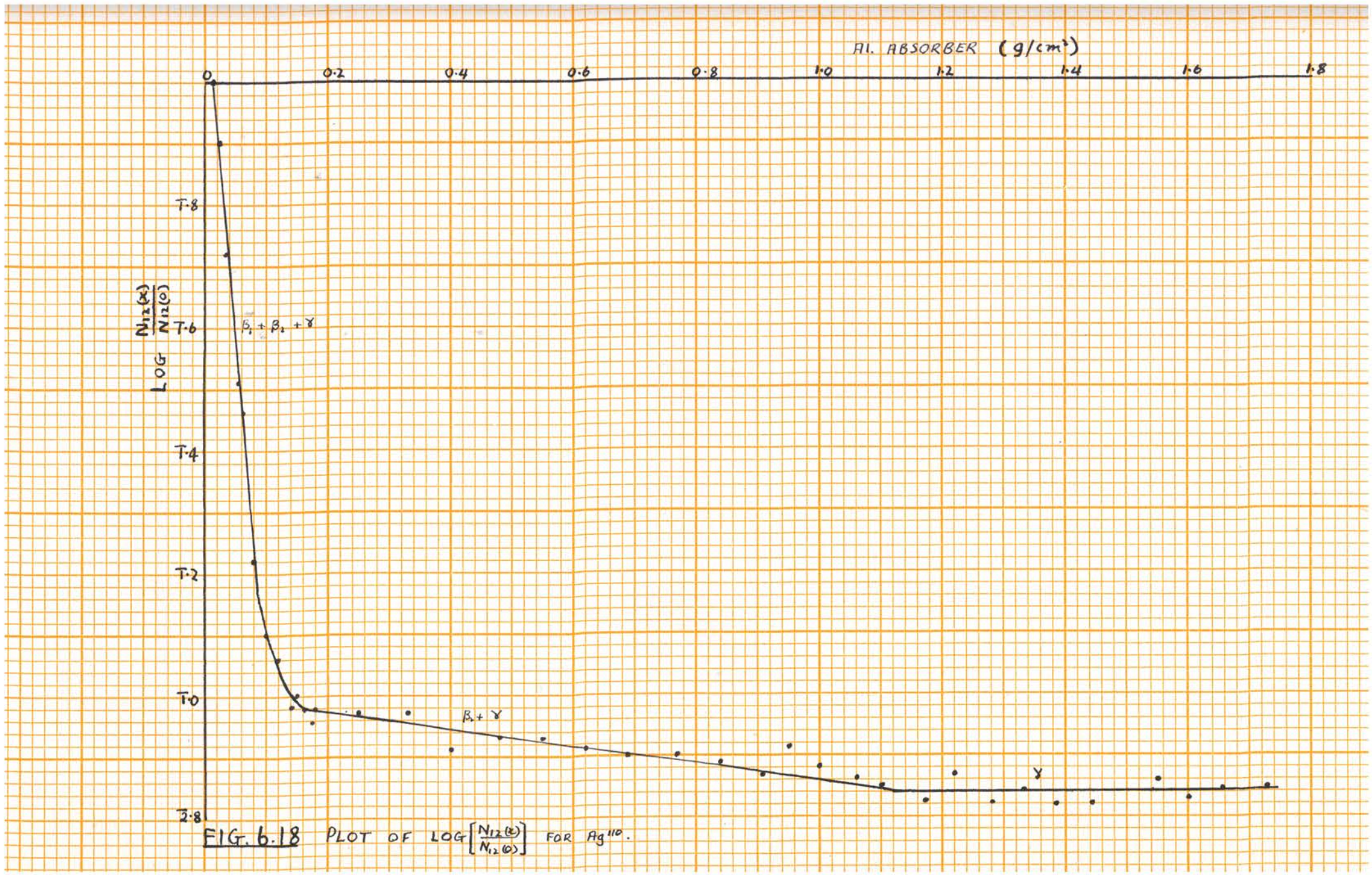

FIG. 6.18 PLOT OF LOG $\left[\frac{N_{12}(x)}{N_{12}(0)}\right]$ FOR Ag^{110}.

and that, consequently, only a small systematic error would be needed to alter the courses of several of the curves.

These experiments may be summarised as having confirmed the disintegration scheme suggested by Siegbahn for Ag^{110}. The only point of difference lies in the determination of the ratio $F_1(0) : F_3(0)$. A method[1] has been devised by the writer for determining this ratio and, on the measurements reported here, it has been deduced that $F_1(0) + F_3(0) \approx 4\%$ of the total disintegrations, and that $F_1(0) \gg F_3(0)$. Several apparent inconsistencies have been pointed out. These can only be resolved by repeating the experiments and by aiming at increased accuracy. The detailed results included here will serve as a guide to the course of these new experiments.

6.5. Future Experiments.

Of immediate interest is the decay scheme of Ag^{110}. It has been pointed out in the preceding section that the chief requirement in further experiments is an increase in the accuracy. This, of course, means that, with the present arrangement, the time of experiment must be increased[2]. It is desirable, therefore, that the apparatus be improved so that the time required be not prohibitive. Two courses are open.

1) Improvement in net efficiencies of counters.

2) Reduction in Resolving Time of Coincidence circuit.

With regard to the first of these, it does not seem possible that the geometry[3] could be much improved. The intrinsic efficiency of the gamma ray counters, however, could be increased by a factor of two or more by the use of lead cathodes which are recommended for incorporation in new counters. Further, the construction of a coincidence circuit of resolving time $\sim 10^{-7}$ sec. is now desirable. The original coincidence circuit can be

1. Equations (6.4, 4) and (6.4, 5) and the attendant discussion.
2. Section 3.6.
3. See equation (3.4, 1)

used to ensure that genuine coincidences are not being lost in the new circuit.

The amount of information that can be obtained from experimental results of $N^{\beta}, N^{\gamma}, N^{\beta\gamma}$ is increased considerably if the efficiencies of the counters are known. It is desirable, therefore, that calibration curves for the gamma counters be obtained. The obvious procedure is to check the efficiency-energy curve of Bradt and his colleagues[1] for the counters in use[2]. Once the shape of this curve has been confirmed, only one point on it need be obtained for the calibration curve of a new counter to be drawn. Experiments on the efficiency of thin window beta counters of standard design for detecting gamma rays are recommended. In particular, information is desirable on the way the efficiency varies as aluminium absorber in front of the window is increased. Since these experiments require known source strengths, the technique described in Section 6.3 may be found useful.

A circuit suitable for measuring delayed coincidences would double the usefulness of the Coincidence Unit. In an experiment involving delayed coincidences, the only alteration to the Unit would be the replacement of the circuit of fixed τ by the new circuit. It may also be possible to use the Unit in conjunction with other equipment at present under construction and designed for investigating isomeric states produced by neutron activation.

1. Reference B8.
2. It is assumed that the counters are used in a standard position.

APPENDIX

1. Preparation of Sources.

The following method provides sources suitable for use in the experiments described in this paper. The active material is converted to powdered form, suspended in collodion and a drop allowed to fall on a sheet of aluminium which has been cleaned thoroughly with amyl acetate. If the sheet is still wet with amyl acetate when the drop of active material is allowed to fall on it, the active material spreads out evenly and does not peel off when it dries. Sources as thin as 2 or 3 milligms./cm^2 can be obtained in this way.

The Co^{60} obtained for the experiments described in Section 6.2 was received in the form of Cobalt oxide, a black powder. The Ag^{110}, however, was received in the form of small silver sheets. Sufficient silver was dissolved in nitric acid and excess sodium hydroxide added to precipate silver oxide, a dark brown powder. The silver oxide was filtered off, washed with alcohol into a test tube, and separated in a centrifuge. The alcohol was poured off and collodion added.

2. Detailed Circuits, Wiring Diagrams etc.

(a) Coupling Unit.

The coupling unit (Fig. 5.3) differentiates the pulse from the Geiger counter and the size of the differentiated pulse fed to the preamplifier can be varied by means of the potential divider R_2. The high voltage supply fed to the Geiger counter through the coupling unit is obtained from a 0-1650 volts power pack which has been in the Nuclear Physics Laboratory for some years and which is of quite conventional design. Voltage stabilisation is effected by a series of V.R. 150's.

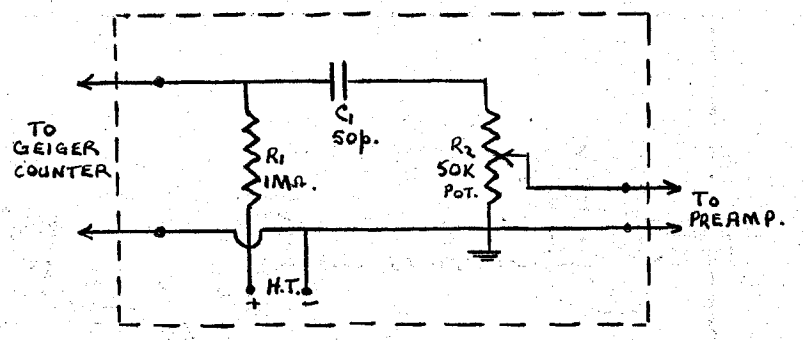

FIG. 5.3. Coupling Unit

(b) Preamplifier[1]

Circuit and Wiring diagrams are shown in Fig. 5.4, and a photograph is included in Plate 1. The potential divider on the Coupling Unit is adjusted so that the negative output pulse of about 10 volts from the Preamplifier (viewed on the Cossor C.R.O.) just shows saturation and is not followed by positive "throw back".

(c) Coincidence Circuit.

The operation of this circuit has been outlined in Chapter 5 by reference to the Block Diagram of Fig. 5.2. The circuit diagram is shown in Fig. 5.5, the wiring diagram in Fig. 5.6, and the Power Supply in Fig. 5.12. Photographs may be seen in Plates 1 and 2.

The following description of the circuit operation amplifies the discussion in Chapter 5:

Negative pulses from the cathode follower in the Pre-amplifier are differentiated in an R-C circuit of time constant 0.2 or 2 μsecs. The differentiated pulses pass through a three stage wide band amplifier having a gain ~ 100. The wide band characteristic which is necessary to preserve the sharp rise of Geiger pulses, is obtained by the use of video amplifiers 6AC7 having low plate loads and by the incorporation of a high degree of negative feed-back from the cathode of V_3 to the cathode of

1. The Preamplifier and the amplifier in the Coincidence circuit are modifications of circuits described in Reference J1.

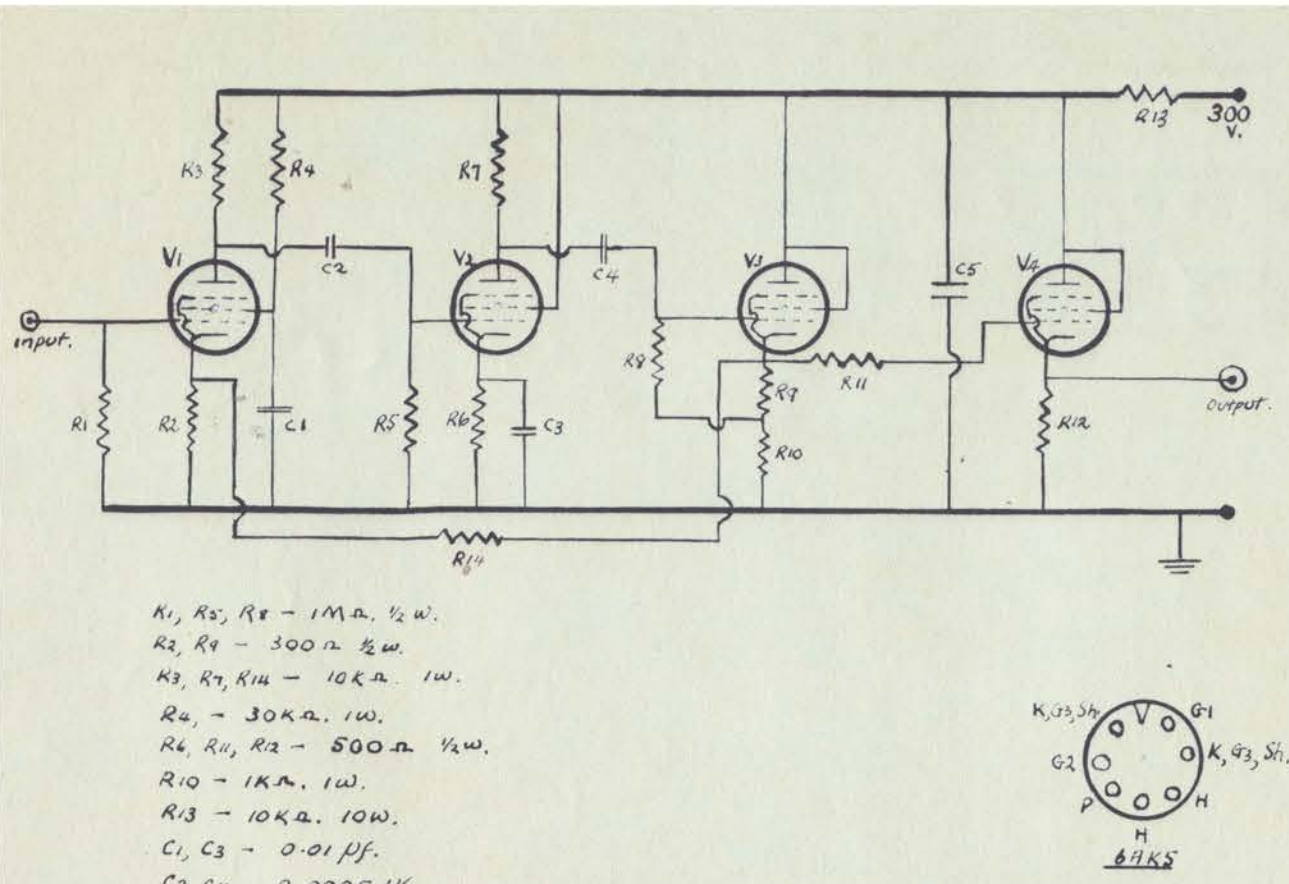

K1, R5, R8 – 1MΩ. ½ w.
R2, R9 – 300Ω ½ w.
K3, R7, R14 – 10KΩ. 1w.
R4, – 30KΩ. 1w.
R6, R11, R12 – 500Ω ½w.
R10 – 1KΩ. 1w.
R13 – 10KΩ. 10W.
C1, C3 – 0.01 μf.
C2, C4 – 0.0005 μf.
C5 – 14 μf.
V1, V2, V3, V4 – 6AK5.

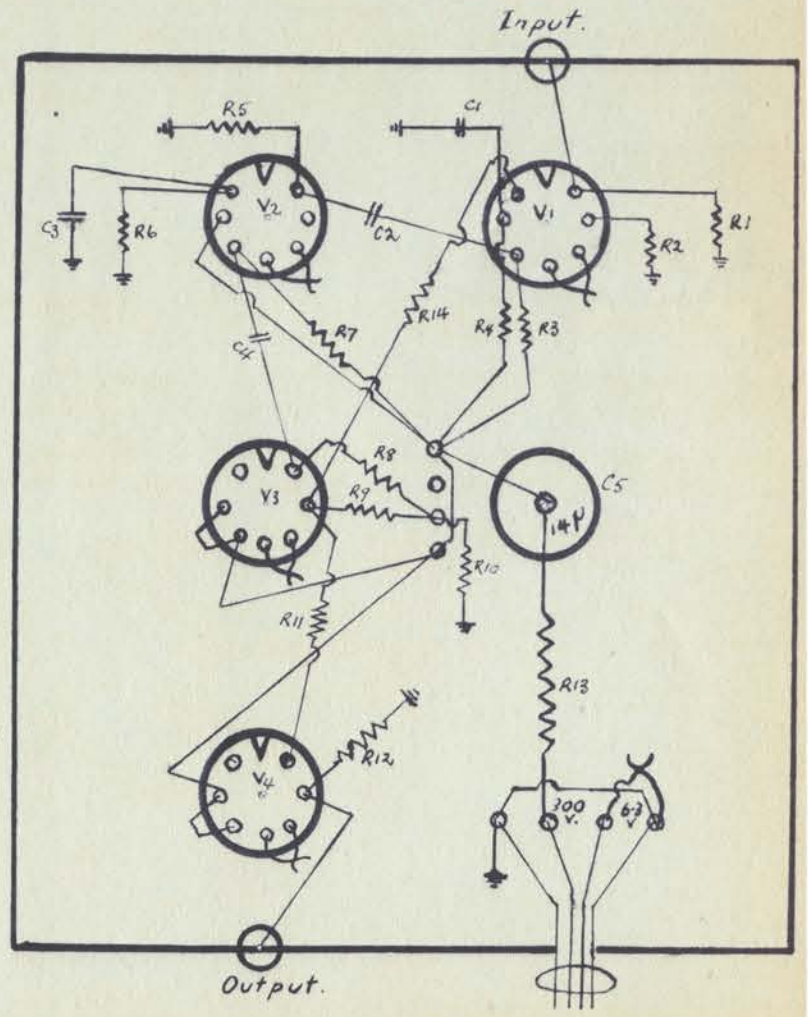

FIG. 5.4. PREAMPLIFIER CIRCUIT and WIRING DIAGRAM.

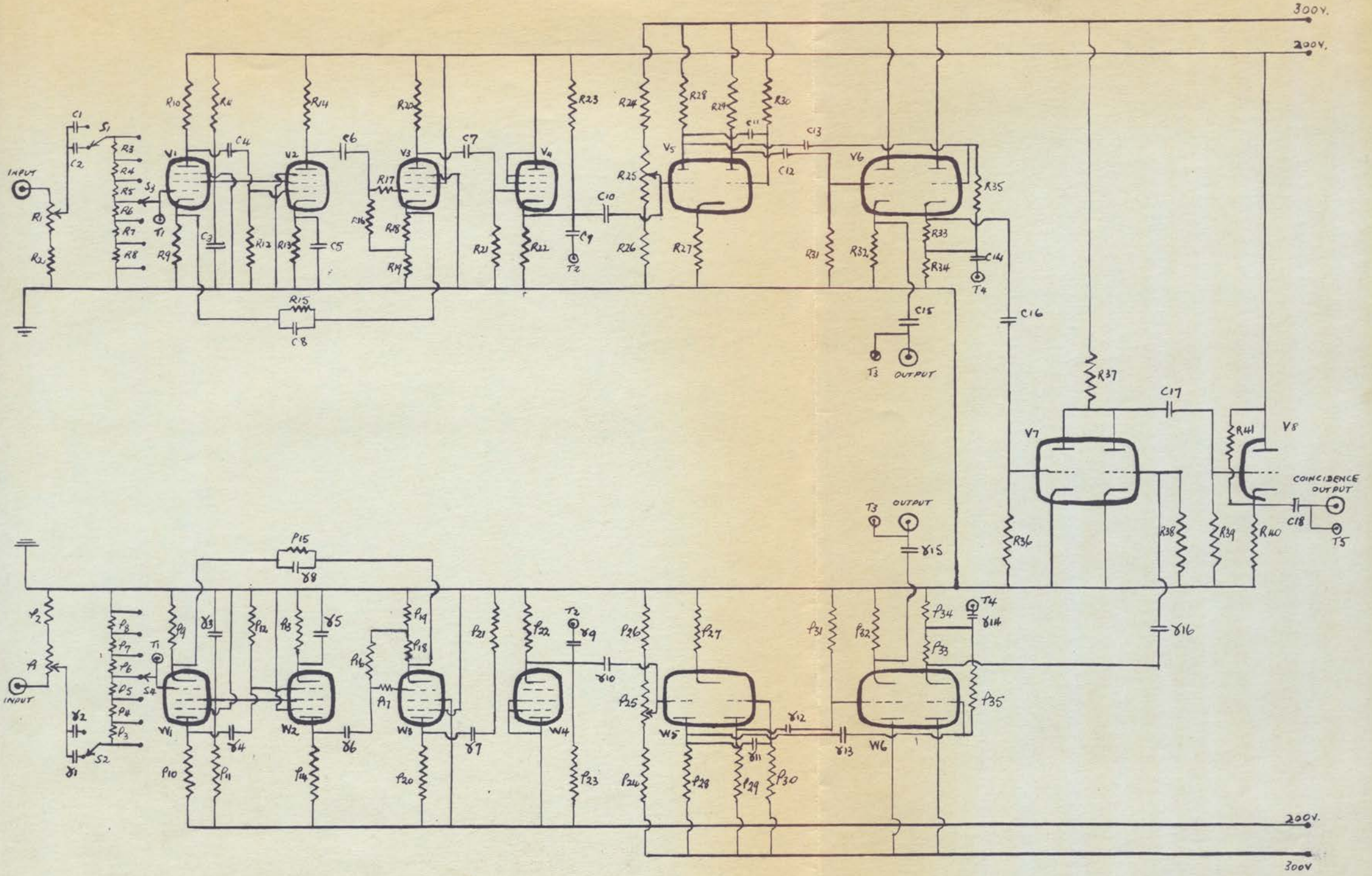

FIG. 5.5 COINCIDENCE CIRCUIT

$V_1, V_2, V_3, V_4, W_1, W_2, W_3, W_4$ 6AC7; V_5, W_5 6J6; V_6, V_7, V_8, W_6 6SN7.

S_1, S_2, single pole 2-position switch; S_3, S_4, single pole 7-position switch.

T C.R.O Test points — T_1, INPUT; T_2, Amplifier output; T_3, channel output; T_4, 'Rossi' input; T_5, Coinc. output.

$R_n = P_n$; R_1 1000Ω Pot.; R_2, R_3, R_{33} 1000Ω 1w.; R_4, 500Ω 1w.; R_5 250Ω 1w.; R_6 100Ω 1w.; R_7, R_8 50Ω 1w.; R_9, R_{18} 150Ω 1w.; R_{10}, R_{14} 10K. 2w.; R_{11} 15K 2w.; R_{12} 250K 1w.; R_{13}, R_{19} 300Ω 1w.; $R_{15}, R_{17}, R_{26}, R_{38}$ 20K 1w.; $R_{16}, R_{21}, R_{35}, R_{39}$ 0.5M 1w.; R_{20}, R_{22}, 2.5K 1w.; R_{21}, R_{28}, R_{40} 5K. 1w.; R_{23}, R_{37} 50K. 2w.; R_{24} 1M. ½w.; R_{25} 0.5M Pot.; R_{26} 0.5M ½w.; R_{27} 12.5K 2w.; R_{29} 7.5K 2w.; R_{30} 2M 1w.; R_{32}, R_{34} 10K. 1w.

$C_n = \gamma_n$; C_1 100μf.; $C_2, C_4, C_{12}, C_{16}, C_{17}$ 0.001 μf.; C_3 14μf.; $C_5, C_6, C_9, C_{10}, C_{14}, C_{15}$ 0.01 μf.; C_7, C_{13} 250μf.; C_8, C_{11} 10μf.; C_{18} 0.05μf

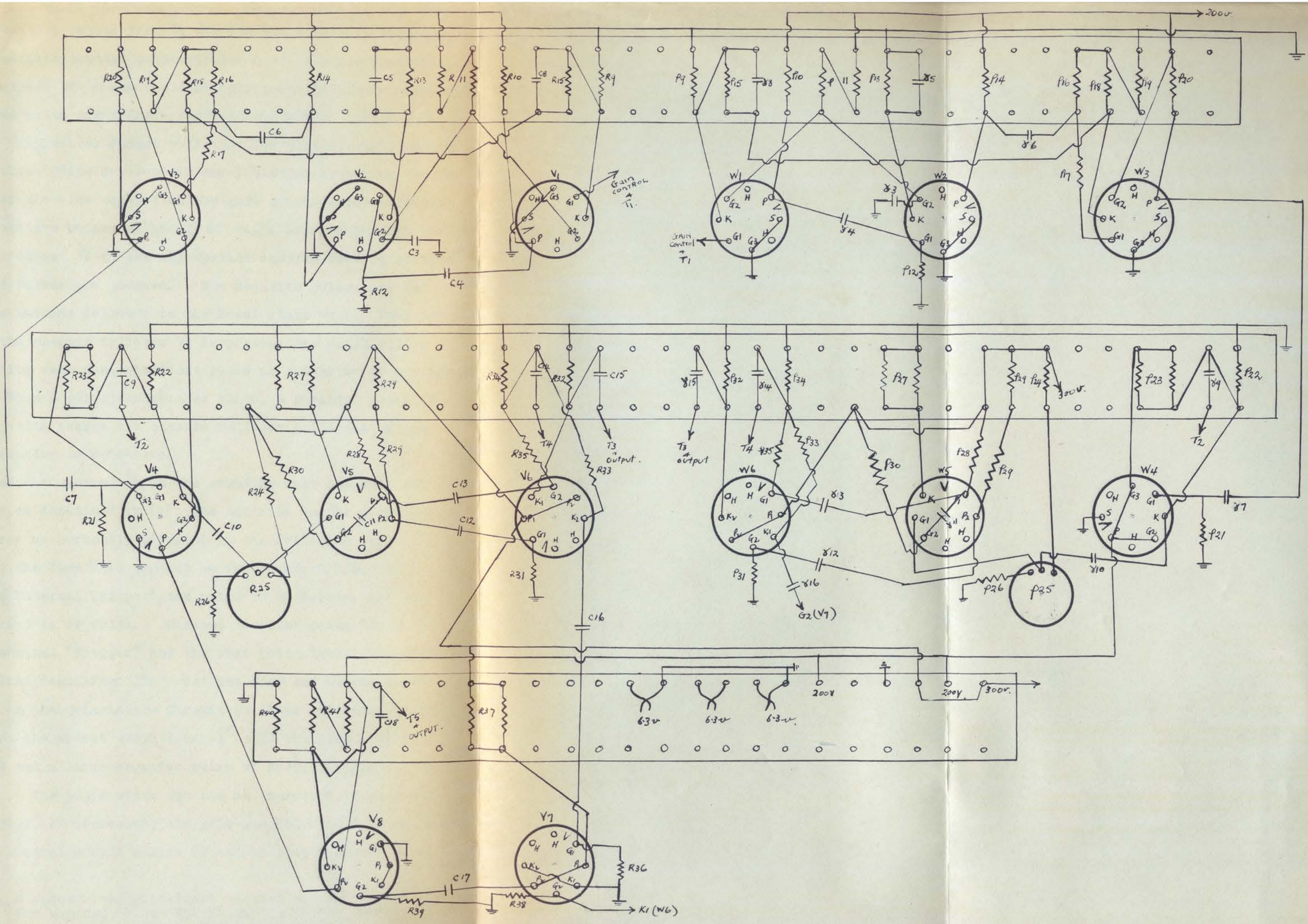

FIG. 5.6. COINCIDENCE CIRCUIT WIRING DIAGRAM.

V_1. Positive pulses from V_3 are fed via a cathode follower V_4 to a cathode coupled multivibrator V_5. A bleed from H.T. to the cathode of V_4 ensures that only positive pulses larger than a few volts are transferred from V_3 to V_5. The multivibrator V_5 produces square pulses at its plates, the duration of the pulses lying between 1.5 and 3 μsecs. according to the setting of the bias control on the grid of the first triode in V_5. Positive pulses of about 65 volts are fed through the cathode follower V_6 to the appropriate scaling circuit so that the input pulses are counted. The negative pulses are fed through a cathode follower to the Rossi stage V_7. Positive bias on the cathode follower V_8 suppresses the small pulses accompanying each non-coincident pulse on the grids of the Rossi tubes. When a coincidence takes place, a positive pulse of about 70 volts passes the cathode follower and actuates the scaler counting coincidences.

When the control R_2 on the coupling unit has been set correctly as explained in (b), the controls on the Coincidence Circuit may be correctly adjusted in the following way:

Set the Time Base control on the Cossor C.R.O. to "Positive External Trigger", the range to 15 μsecs. and the Gain control to 50 volts. Connect the Test point "Output" to the terminal "Trigger" and the Test point "Rossi Input" to the terminal "Amplifier 1". Set the Fine and Coarse gain controls on the Coincidence Circuit to their mid range positions and adjust the preset width control[1] till the time base is triggered and a large negative pulse of about 1.2 μsecs. is observed. The pulse width can now be increased or decreased as desired. If decreased, the gain control should be advanced. The gain control should always be set so that a steady Rossi

1. A screwdriver adjustment located on top of the chassis. The control "Pulse Width" on the front panel adjusts the width (and size) of the input pulse to the Coincidence Circuit by altering the capacity in the differentiating circuit (R.C., 0.2 or 2 μsecs.)

input pulse with no flutter is observed. This will usually be the case when the gain controls are set not too far above the point at which the multivibrator is just triggered. (It should be noted that, if the preset width control is set too low, the amplifier gain is not sufficient to trigger the multivibrator, and, if too high, the multivibrator free-runs.)

The appearance of the pulses at the several test points is shown in Fig. 5.7. Slight "ringing" in the amplifier is not objectionable. It could be eliminated, if desired, by altering the Capacity Cg.

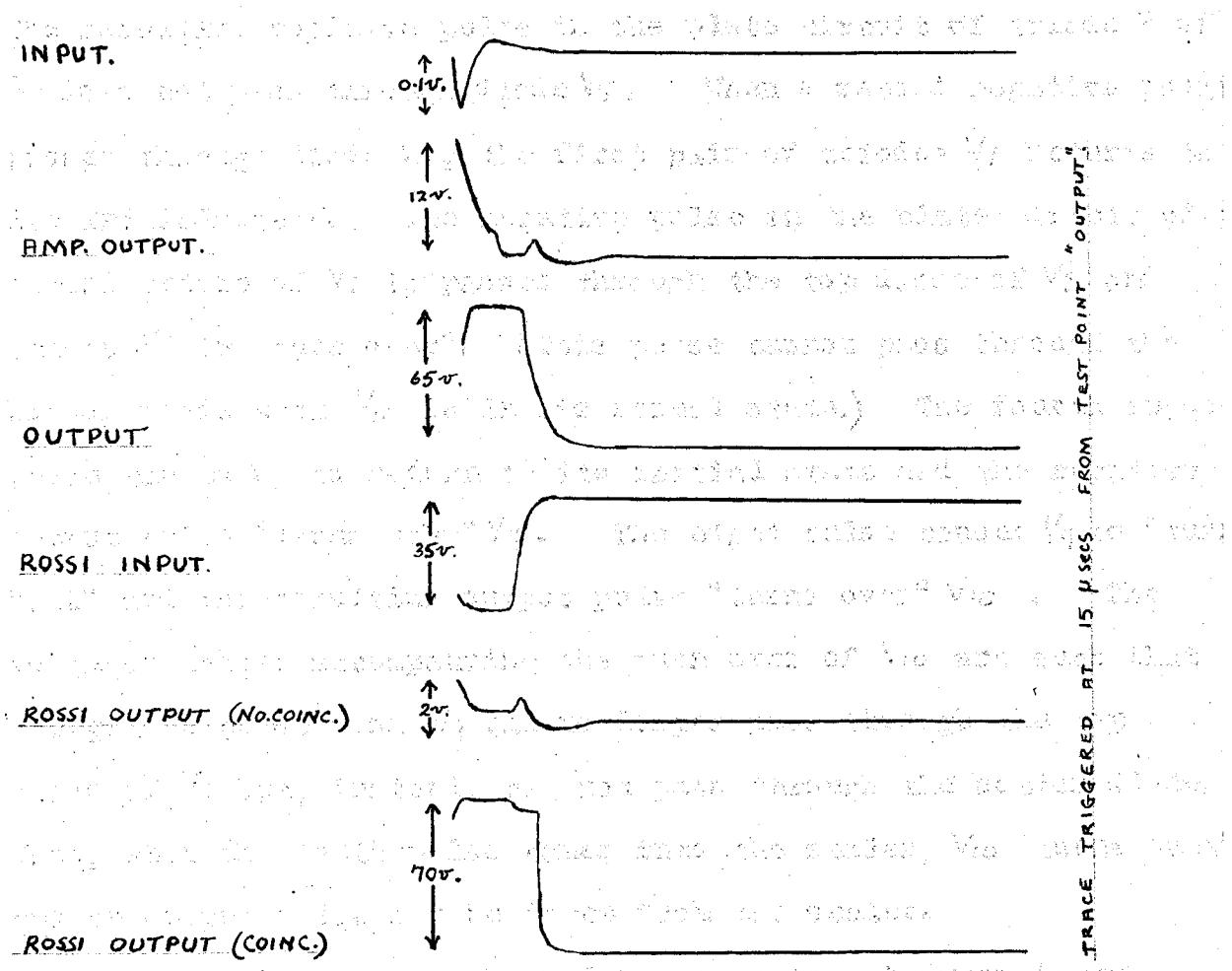

FIG. 5.7 Pulse Shapes at Test Points on Coincidence Circuit.

Maintenance on the Coincidence circuit involves checking the pulses of Fig. 5.7 and Checking the Resolving Time. Faults may be localised by checking the pulses of Fig. 5.7.

(d) Scaling Circuit.

Circuit and wiring diagrams are shown in Figs. 5.8 and 5.9 respectively and photographs are incorporated in Plate 2. The Power supply is drawn in Fig. 5.13.

The operation of the circuit may be described briefly in the following way:

When the reset control is operated, the right hand members of the twin triodes conduct and the left hand members are biassed beyond cut-off. A sufficiently large negative pulse through the first diode cuts off triode 2 of V_7 and triode 1 comes on. The resulting positive pulse in the plate circuit of triode 2 of V_7 does not pass through diode V_5. When a second negative pulse passes through diode V_1, the first pair of triodes V_7 returns to its initial state. The negative pulse in the plate circuit of the second triode of V_7 is passed through the top diode of V_5 and causes V_8 to "turn over". (This pulse cannot pass through the bottom diode when V_{10} is in its normal state.) The fourth input pulse causes V_8 to return to its initial state and the negative output pulse "turns over" V_9. The eight pulse causes V_9 to "turn back" and the resulting output pulse "turns over" V_{10}. The voltage changes accompanying the turn over of V_{10} are such that a negative pulse from V_7 can no longer pass through the top diode of V_5 but, instead, can now pass through the bottom diode. Thus, when the tenth pulse comes into the scaler, V_{10} "turns back" and an output pulse may be taken from the scaler.

The scaler may be checked by observing the neon interpolating lights as they register the background count of a Geiger counter. Alternatively, pulses can be fed into the scaler and these can be compared on the double beam Cossor with the output pulses at the plates of the triodes. If the lead to the C.R.O. from the plates incorporates a differentiating circuit (e.g. a condensor of 50 p.f. and a resistor of 100 K), the patterns of Fig. 5.10 should be observed.

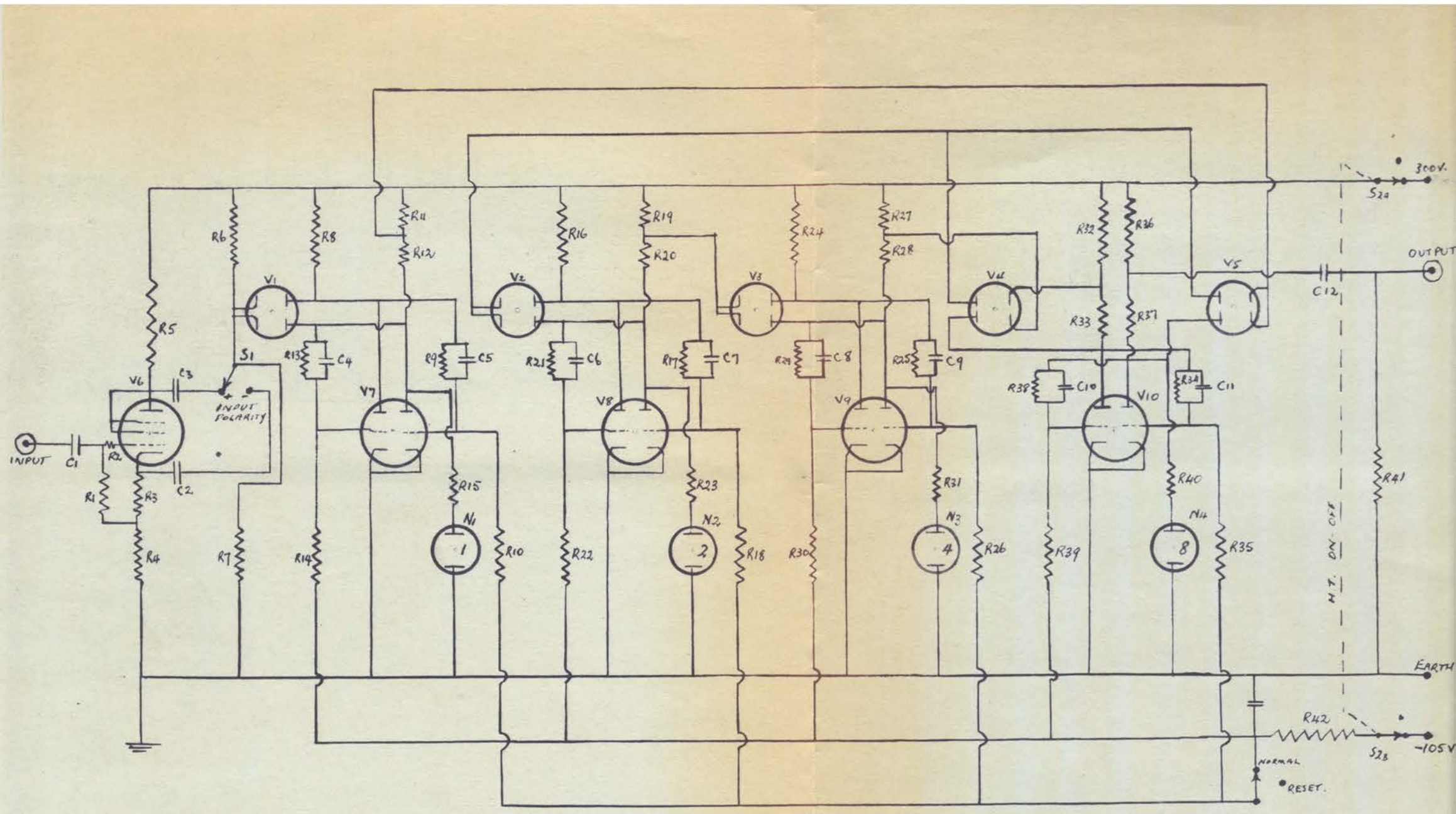

FIG. 5.8 SCALE-OF-TEN.

V1, V2, V3, V4, V5 6H6 ; V6 6J7 ; V7, V8, V9, V10 6SN7; N1, N2, N3, N4 200V. NEON LAMPS;
S1 Single pole 2-position switch ; S2 Double pole 2-position switch.
R1, R15, R23, R31, R40 0·5M 1w. ; R2, R5 10K 1w. ; R3 1K 1w. ; R4, R19, R27 5K 1w. ; R6 13K 1w. ;
R7 0·25M 1w. ; R8, R16, R24 20K 1w. ; R9, R13, R17, R21, R25, R29, R34, R38 0·3M 2w. ;
R10, R14, R18, R22, R26, R30, R35, R39 0·15M 1w. ; R11 4·3K 1w. ; R12, R20, R28, R33 15K 3w. ;
R32 67K 2w. , R36, R37 10K 2w. ; R41 100K 1w. ; R42 1·5K 1w
C1, C2, C3 0·1 μf. ; C4, C5 0·0005 μf. ; C6, C7, C8, C9, C10, C11, C12 50μ.μf.

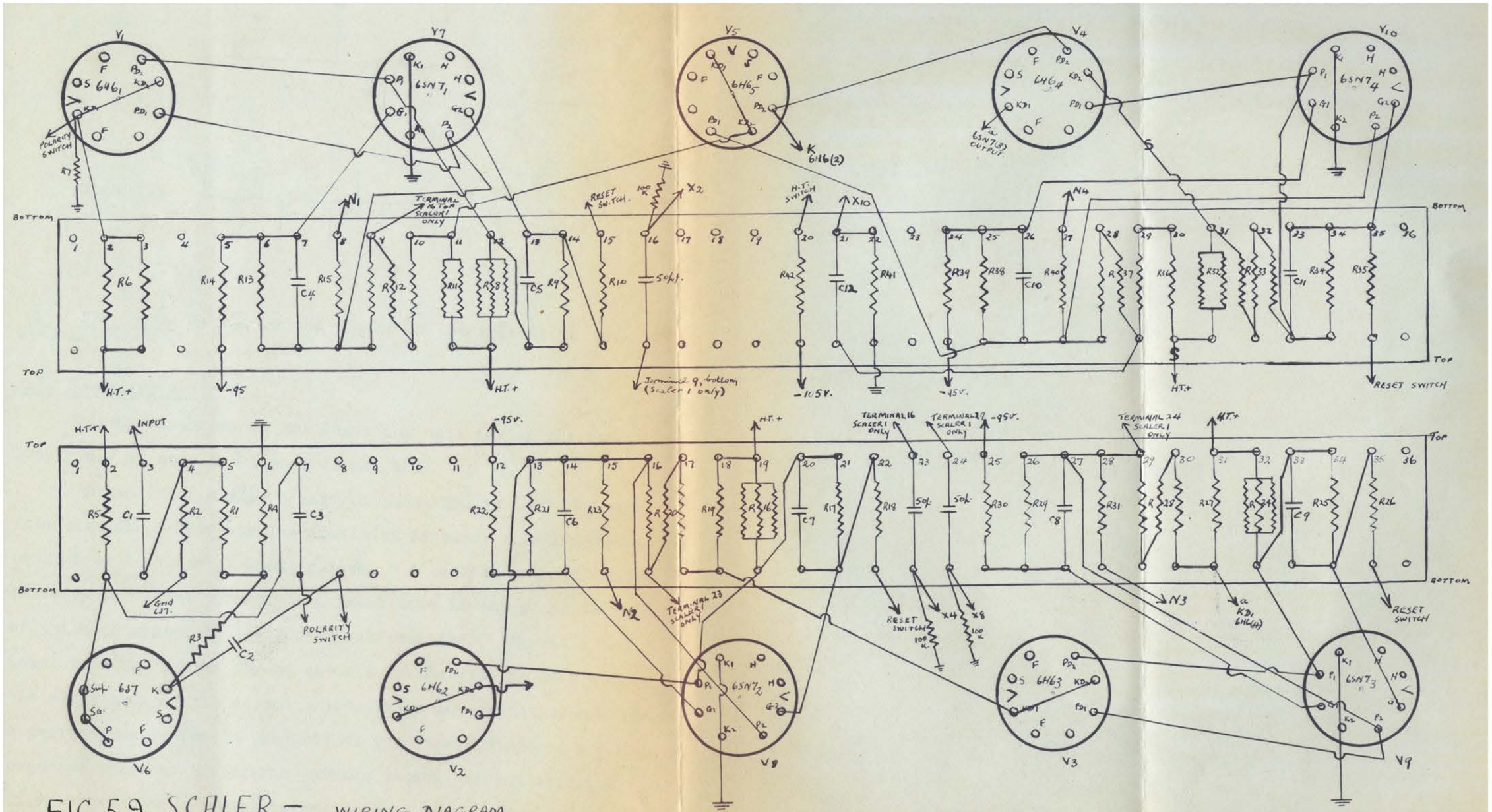

FIG. 5.9. SCALER – WIRING DIAGRAM.

X OUTPUT.

S DOUBLE POLE - 2 POSITION SWITCH. CLOSED - SCALE BY 10. OPEN – SCALE BY 2, 4, 8 (SCALER 1 ONLY).

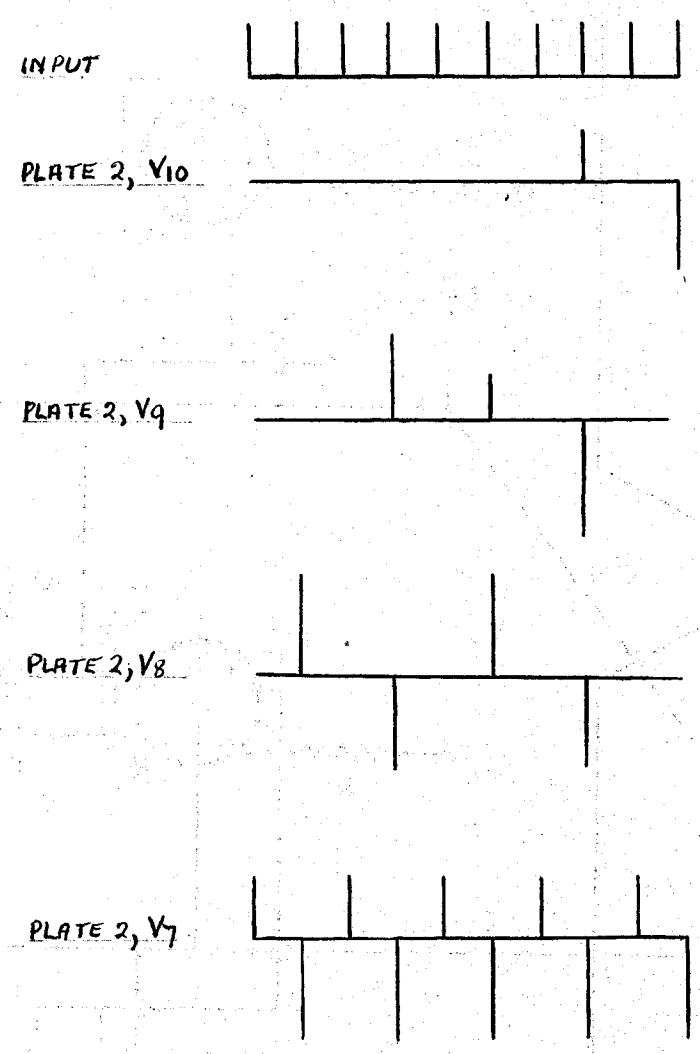

FIG. 5.10 Pulses at the plates of the triodes in the Scaling Circuit.

(e) Recording Unit.

Circuit diagrams of the Recording unit and of the Power Supply may be seen in Figs. 5.11 and 5.12.

An amplifier having a gain of about 100 is included in this circuit. This enables operation directly from a Geiger counter or a source of small pulses. A cathode coupled multivibrator is direct coupled to a power tube in the plate circuit of which is connected the mechanical recorder. Normally the power tube is biassed beyond cut off by the voltage drop across the plate load of the second triode which is conducting heavily. A positive pulse fed to the grid of the first triode or a negative pulse to the common cathode causes the multivibrator to flip over for a time interval determined by the setting of

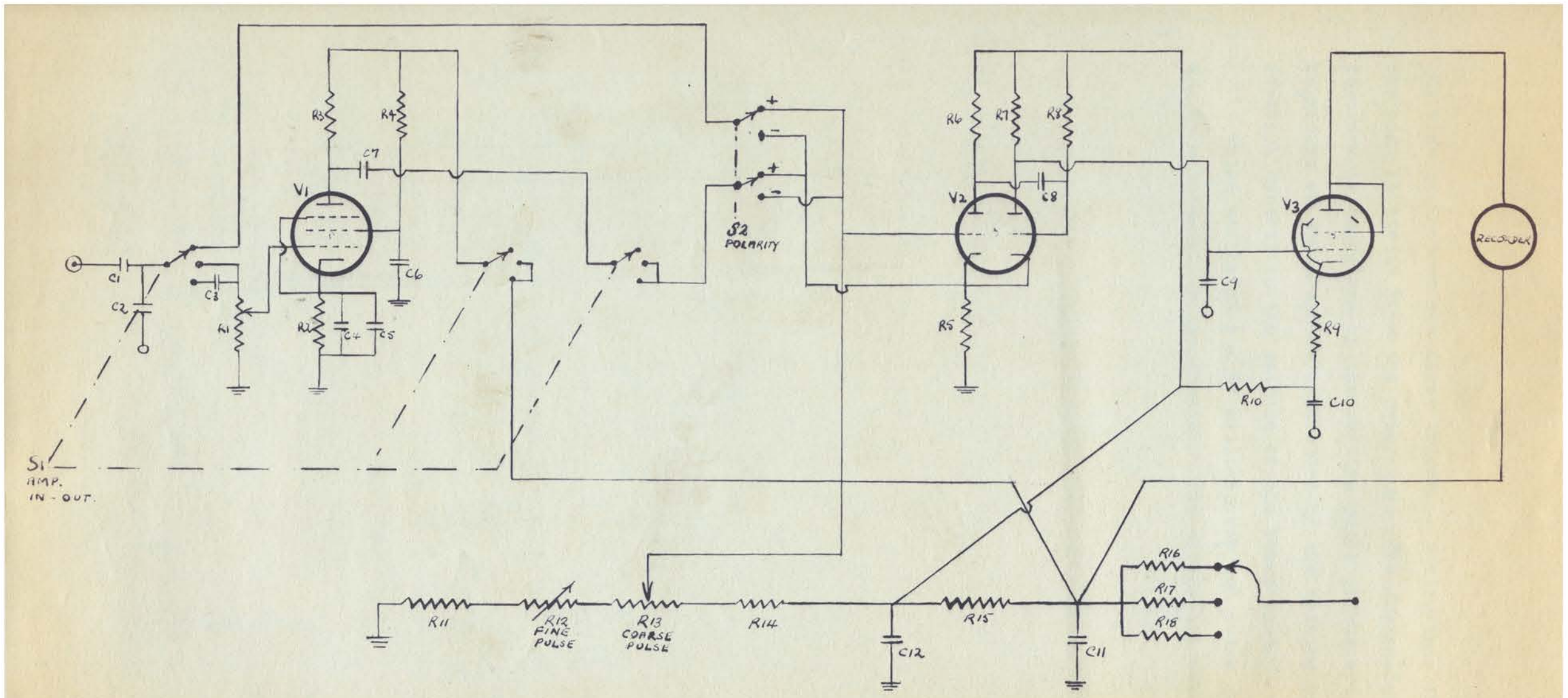

FIG. 5.11. RECORDING UNIT

V1 6AC7 ; V2 6SN7 ; V3 6V6 ; R1, R13 100K POT. ; R2 200Ω 1W. ; R3, R5 20K 1W. ; R4 60K 1W. ; R6 30K 1W. ; R7, R17 10K 1W. ; R8 1MΩ 1W. ; R9 500Ω POT. ; R10 150Ω 1W. ; R11 10K 1W. ; R12 25K POT ; R14 375K 1W. ; R15 45K 1W. ; R16 15K 2W. ; R18 3K 1W. ; C1, C2 0·05μf. ; C3 0·01μf. ; C3 500μf. ; C5 25μf ; C6, C11, C12 14μf. ; C7, C8 0·1μf. ; C9 0·25μf ; C10 0·25μf.

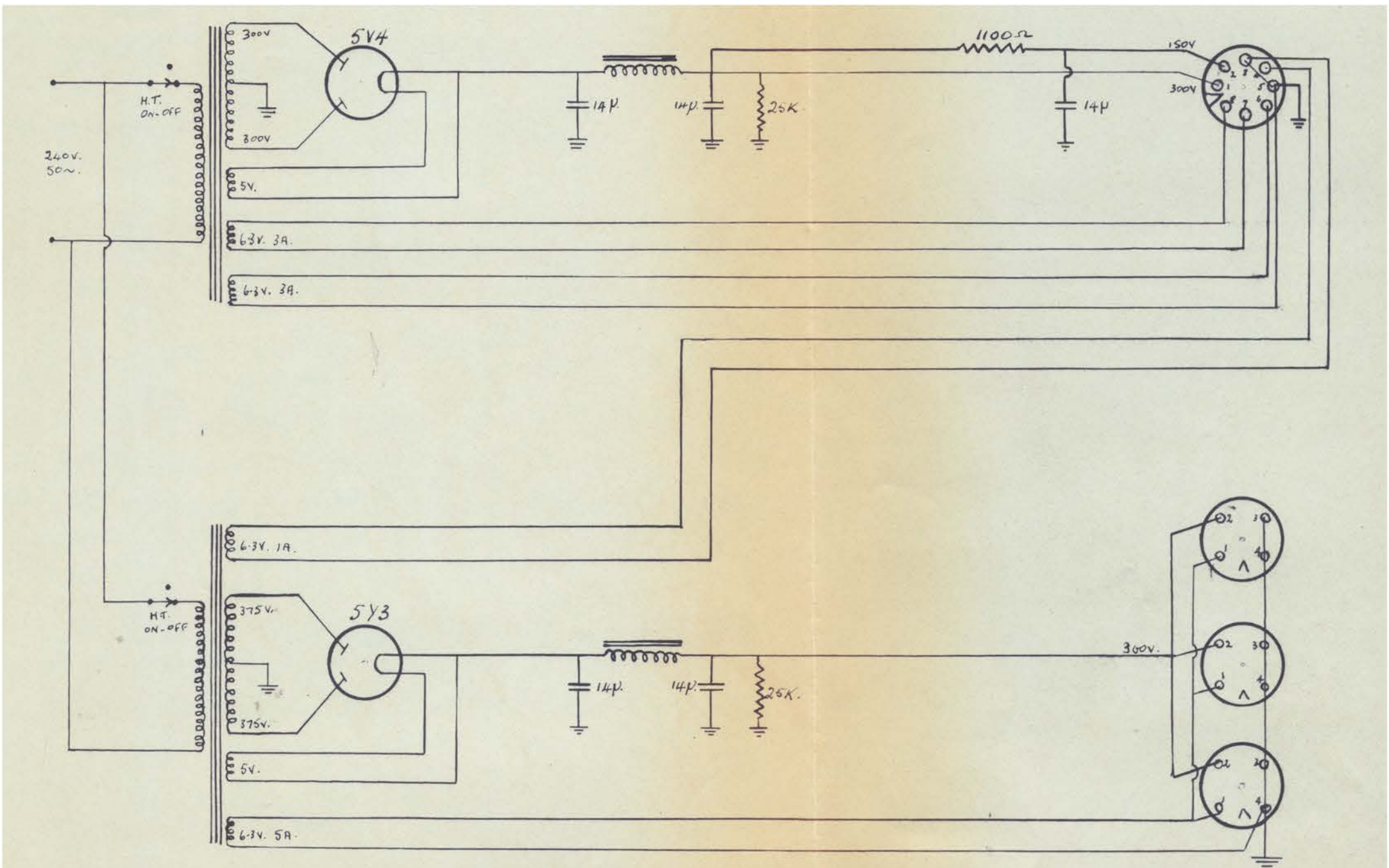

FIG. 5.12. POWER SUPPLY — COINCIDENCE UNIT AND RECORDERS.

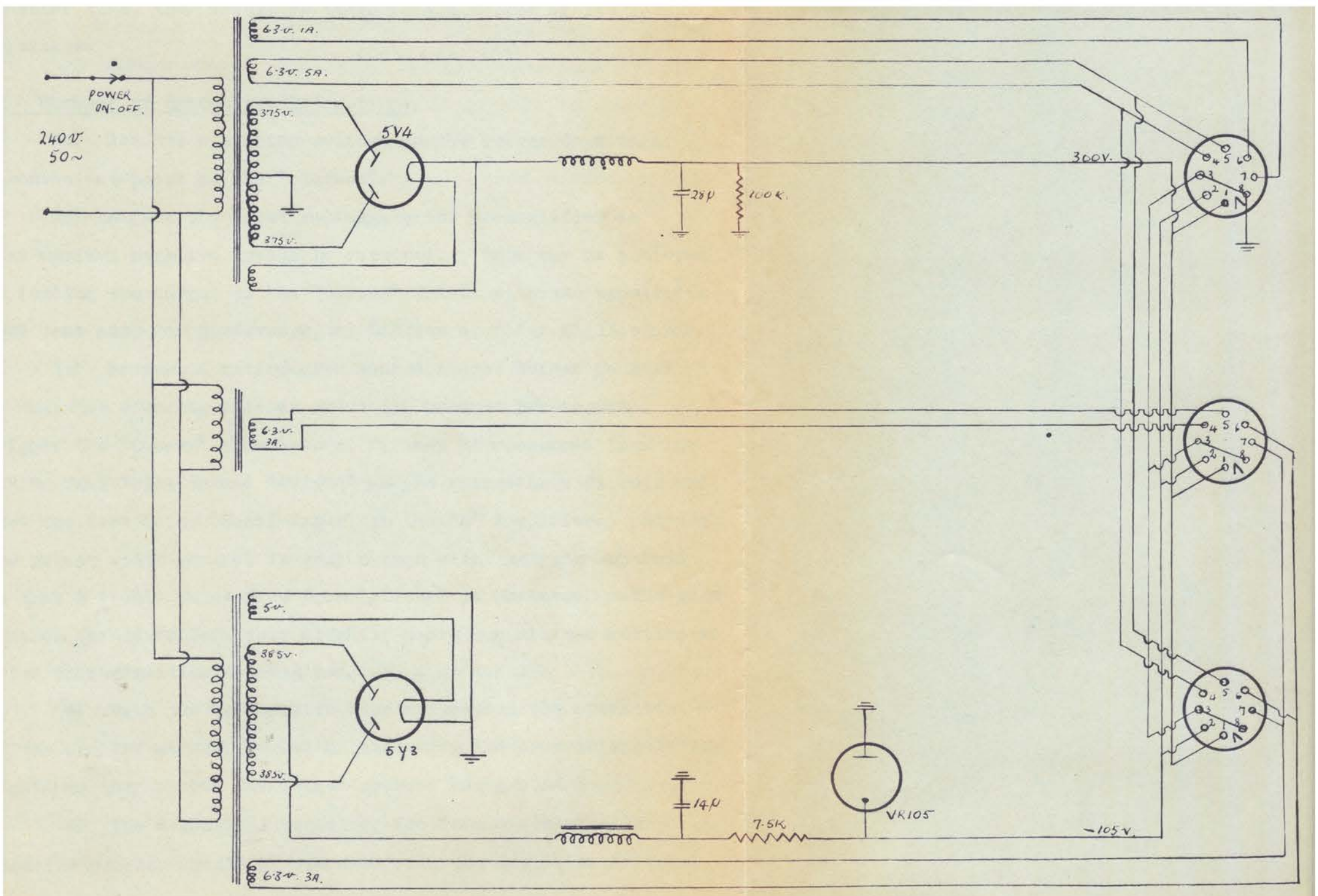

FIG. 5.13

POWER SUPPLY FOR SCALERS.

the bias control on the first triode. During this interval, the bias is lifted from the power tube, and the mechanical recorder is energised by the ensuing pulse of current, the magnitude of which can be controlled by the setting of the feedback control in the cathode of the power tube.

Pulse widths of 5 - 30 milliseconds and pulse currents of 5 - 30 milliamps. are available. The circuit is best operated by feeding positive pulses to the grid of the first triode. If negative pulses are fed directly to the cathode of the multivibrator tube, they should be taken from a source of low output impedance.

(f) Summary of Operating Instructions.

(a) Set the operating voltage on the Geiger Counter at a convenient point on the "plateau".

(b) Adjust the input voltage to the preamplifier so that maximum negative output is obtained. This may be achieved by feeding the output to the "Cossor" C.R.O. with the repetitive time base set, for preference, at fifteen or fifty milliseconds.

(c) Present a radioactive source to the Geiger Counter so that the counting rate is about two hundred per second. Trigger the "Cossor" time base at fifteen microseconds from the C.R.O. Test Point marked "Output" on the Coincidence Circuit and feed the Test Point "Rossi Input" to the "A" Amplifier. Adjust the preset width control in conjunction with the gain controls so that a steady pulse free from "jitter" is observed. The gain control should be left only slightly above the minimum setting at which this condition is obtained.

(d) With the radioactive source removed, the operation of the scalers may be checked by observing the neon interpolating lights as they record the Geiger counter background.

(e) The mechanical register, fed from a scaler with negative pulses, should be operated with the amplifier switched

in. The gain control should be set slightly above the minimum setting at which the register pointer advances each time neon interpolating light "8" extinguishes. If the register is driven directly by positive pulses from an output terminal on the coincidence circuit, the amplifier should be switched out.

3. Acknowledgements.

The work reported here has been financed by a Commonwealth Research Grant and has been carried out under the general supervision of Professor V. A. Bailey whose constant encouragement is gratefully acknowledged. Dr. R. E. B. Makinson was originally in charge of the project and the writer is greatly indebted to him for ready advice and active co-operation in problems involving all aspects of the work. Dr. G. Builder assumed responsibility for the project when Dr. Makinson departed for England in September.

Many of the writer's associates and many members of the staff have made valuable contributions. In particular, Dr. K. Landecker was always a willing listener and a helpful critic, and, besides making many valuable suggestions, gave active assistance in solving many of the problems that arose in the course of the work. Mr. Guest also came to the rescue on more than one occasion. Mr. Bishop did most of the developmental work on the Recorder and together with Mr. Murdoch gave general assistance. Mr. Dehlsen constructed four scalers, a Recording Unit and two mechanical recorders, welded the racks on which the whole assembly is mounted and maintained power from a local generating set during interruptions on the Council mains. Mr. French constructed a Recording Unit and gave advice and assistance with the photography. Mr. Winn also helped with the photography and with the design of Geiger counters. Mr. Arthur made a number of valuable suggestions concerning the rack mounting and gave

assistance in other phases of the work. It is a pleasure to record the friendly co-operation of Mr. Hutchinson and his associates. In particular, Mr. Finlayson who cut a number of front panels and engraved them, and Mr. Marley who constructed several of the attachments and supports should be mentioned.

The author also acknowledges gratefully advice and assistance received from Dr. D. Mellor on chemical problems. Lastly, the author acknowledges the assistance of his wife who, among other things, typed this manuscript.

4. Summary of the Author's Work.

I Overall design of equipment.

II Original design of Coincidence circuit and Recording Unit and modification of Rotblat's Scale-of-10 to suit this equipment.

III Design of layout and wiring, and construction of

- 2 Preamplifiers
- Coincidence Circuit
- 1 Scaling Circuit
- 1 Power Supply for Coincidence Circuit and 3 Recording Units
- 1 Power Supply for 3 Scalers

IV Design of special types of beta counters.

V Planning of experiments to determine decay schemes of Co^{60} and Ag^{110}

VI The Development of a new method for determining the resolving time of a Coincidence circuit or the strength of a source of simple decay scheme.

VII Partial confirmation of Siegbahn's decay scheme for Ag^{110}. A method was devised for estimating the relative numbers of disintegrations proceeding via the 2.12 and 2.86 M.e.v. beta rays.

REFERENCES

A1. Alaoglu and Smith, Phys. Rev., 53, 832.

B1. Becquerel, Comptes Rendus, Vol. 122. (1896).
B2. Bunyan et al., Proc. Phys. Soc., 61, 300. (1948).
B3. Bunyan et al., Proc. Phys. Soc., 62, 253. (1949).
B4. Bleuler and Zunti, H.P.A., 19, 137. (1946).
B5. Bleuler and Zunti, H.P.A., 19, 375. (1946).
B6. Becker and Bothe, Zeits. f. Physik, 76, 421. (1932).
B7. Bradt and Scherrer, H.P.A., 16, 251. (1943).

C1. Curie and Joliot, Comptes Rendus, 198, 254, 559. (1934).
C2. Cook and Owen, Am. Journ. Phys., 18, 453. (1950).
C3. Curran, Dee and Petrzilka, Proc. Roy. Soc. A, 169, 269. (193
C4. Churchill R.V., "Modern Operational Mathematics in Engineering" (McGraw-Hill, 1944).
C5. Champion and Widdowson, Proc. Phys. Soc., 50, 185. (1938).

D1. Devons, S., "Excited States of Nuclei" (Cambridge, 1949).
D2. De Benedetti and McGowan, Phys. Rev., 74, 728. (1948).
D3. Dunworth, Rev. Sci. Insts., 11, 167 (1940).

E1. Elmore, Nucleonics, 6, 26, (1950).
E2. Eckart and Shonka, Phys. Rev., 53, 752. (1938).
E3. Eccles and Jordan, Radio Rev., 1, 143. (1919).

F1. Feather, Proc. Camb. Phil. Soc., 27, 430. (1931).
F2. Feather, Proc. Camb. Phil. Soc., 34, 599. (1938).
F3. Fermi, "Nuclear Physics" (Chicago Univ., 1950).

G1. Gum et al., Phys. Rev., 76, 184. (1949).

H1. Hoag, "Electron and Nuclear Physics" (Van Nostrand, 1938).
H2. Heitler, "Quantum Theory of Radiation" (Oxford, 1936).
H3. Hirzel et al., H.P.A., 20, 241. (1947).

J1. Jordan and Bell, Rev. Sci. Insts., 18, 703. (1947).

K1. Konopinski, Rev. Mod. Phys., 15, 209. (1943).
K2. Korff, "Electron and Nuclear Counters" (Van Nostrand, 1946).
K3. Katz et al., Phys. Rev., 77, 289. (1950).

L1. Lewis, "Electrical Counting" (Cambridge, 1942).

M1. Moon, "Artificial Radioactivity" (Cambridge, 1949).
M2. Mitchell, Rev. Mod. Phys., 20, 296. (1948).
M3. Mandeville and Scherb, Nucleonics, 3, 2. (1948).

N1. Neher, Rev. Sci. Insts., 10, 29. (1939).

P1. Pearson, "Tables of the Incomplete Gamma Function" (Cambridge, 1934).

R1. Rutledge et al., Phys. Rev., 80, 286. (1950).
R2. Reich, "Theory and Application of Electron Tubes" (McGraw-Hill, 1939).
R3. Rotblat, Journ. Sci. Insts., 25, 33. (1948).
R4. Rotblat, Proc. Roy. Soc. A, 177, 260. (1941).

S1. Stranathan, "Particles of Modern Physics" (Blakiston, 1942).
S2. Siegbahn, Phys. Rev., 75, 1277. (1949).
S3. Spatz, Phys. Rev., 64, 236. (1943).
S4. Stevenson and Getting, Rev. Sci. Insts., 8, 414. (1937).
S5. Shumard, Elec. Eng., 57, 209. (1938).

T1. Tuck, Journ. Sci. Insts., 13, 366. (1936).
T2. Terman, "Radio Engineers' Handbook" (McGraw-Hill, 1943).

W1. Wynn-Williams, Proc. Roy. Soc. A, 136, 312. (1932).
W2. Wynn-Williams, Proc. Roy. Soc. A, 132, 295. (1931).
W3. Wiedenbeck and Chu, Phys. Rev., 72, 1164. (1947).

RS. ROSSI, ZEITS. f. PHYSIK, 68, 64 (1931).

BB. BRADT ET AL. H.P.A., 19, 77 (1946)

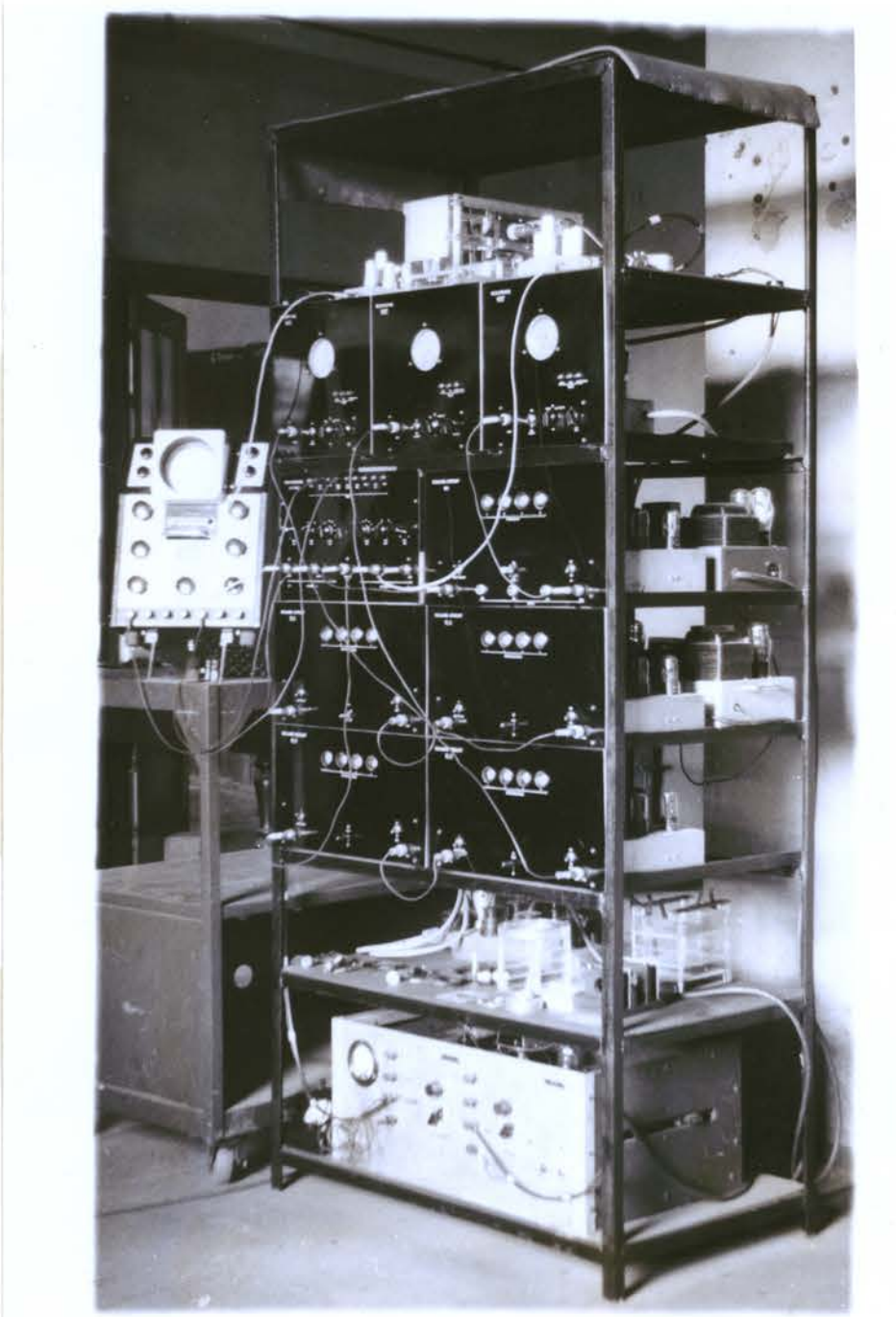

PLATE I. COINCIDENCE UNIT.

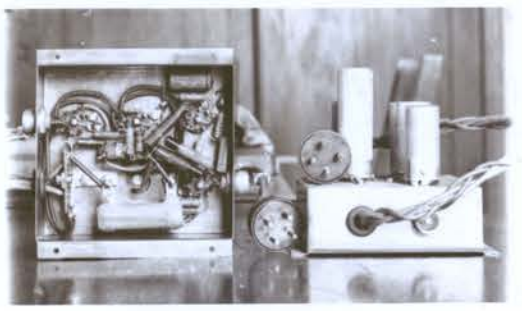

a. PREAMPLIFIER.

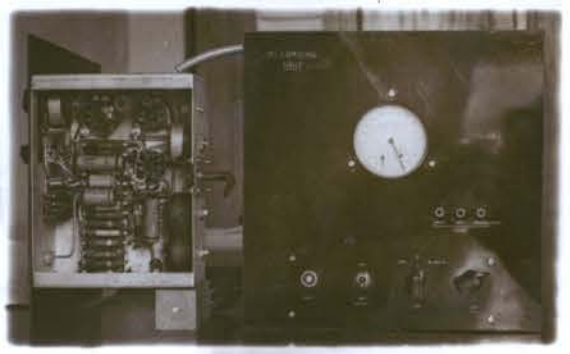

f. RECORDER

b. COINCIDENCE CIRCUIT.

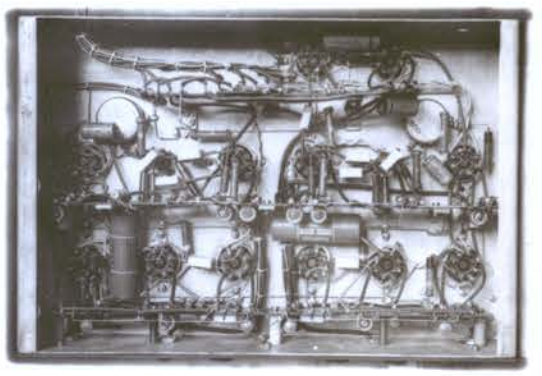

c. COINCIDENCE CIRCUIT.

d. SCALER

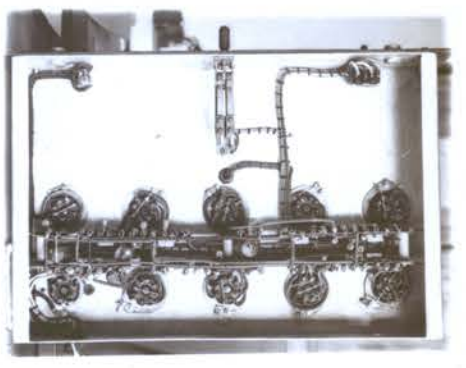

e. SCALER.

PLATE 2.

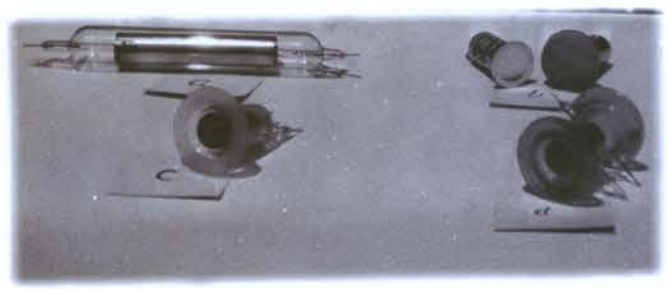

PLATE 3.

a. Cu-CATHODE GAMMA COUNTER
b. G.E.C. BETA COUNTERS, EHM2 and GM4.
c. BETA COUNTER, PHYSICS DEPT., SYDNEY
d. DOUBLE WINDOW BETA COUNTER.

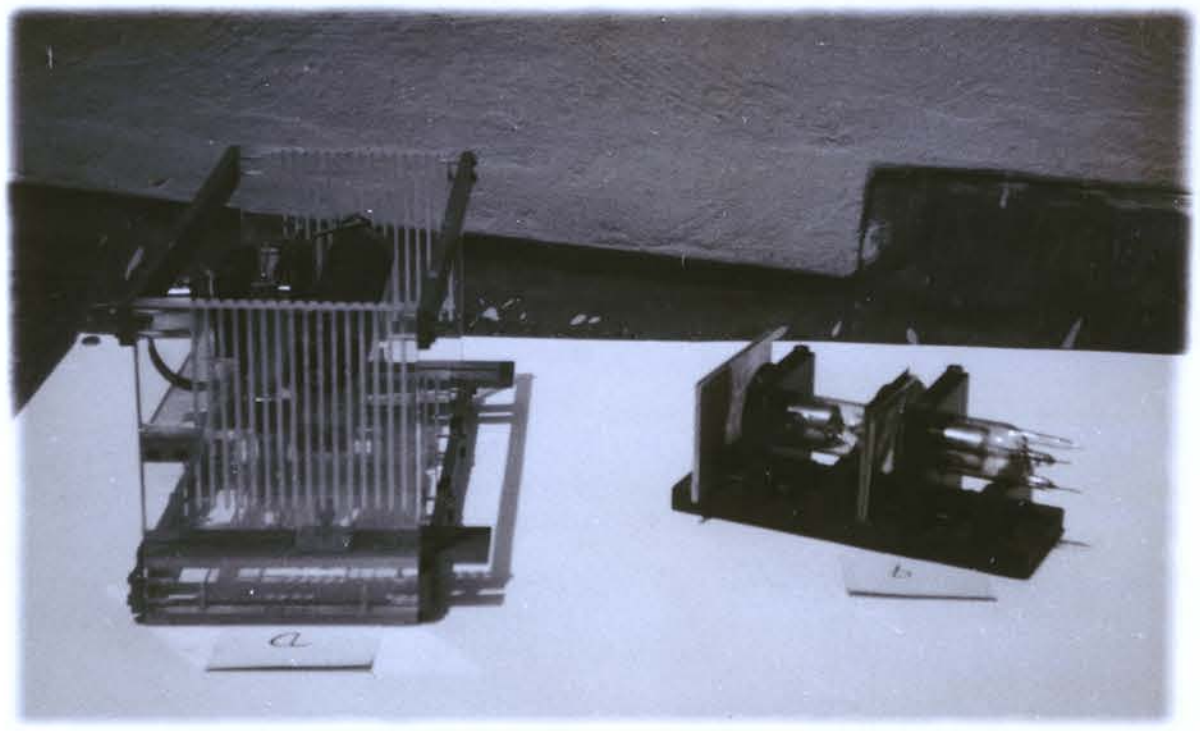

PLATE 4.

a. EXPERIMENTAL SET-UP FOR β-γ COINCIDENCES.
b. EXPERIMENTAL SET-UP FOR COMPTON COINCIDENCES.

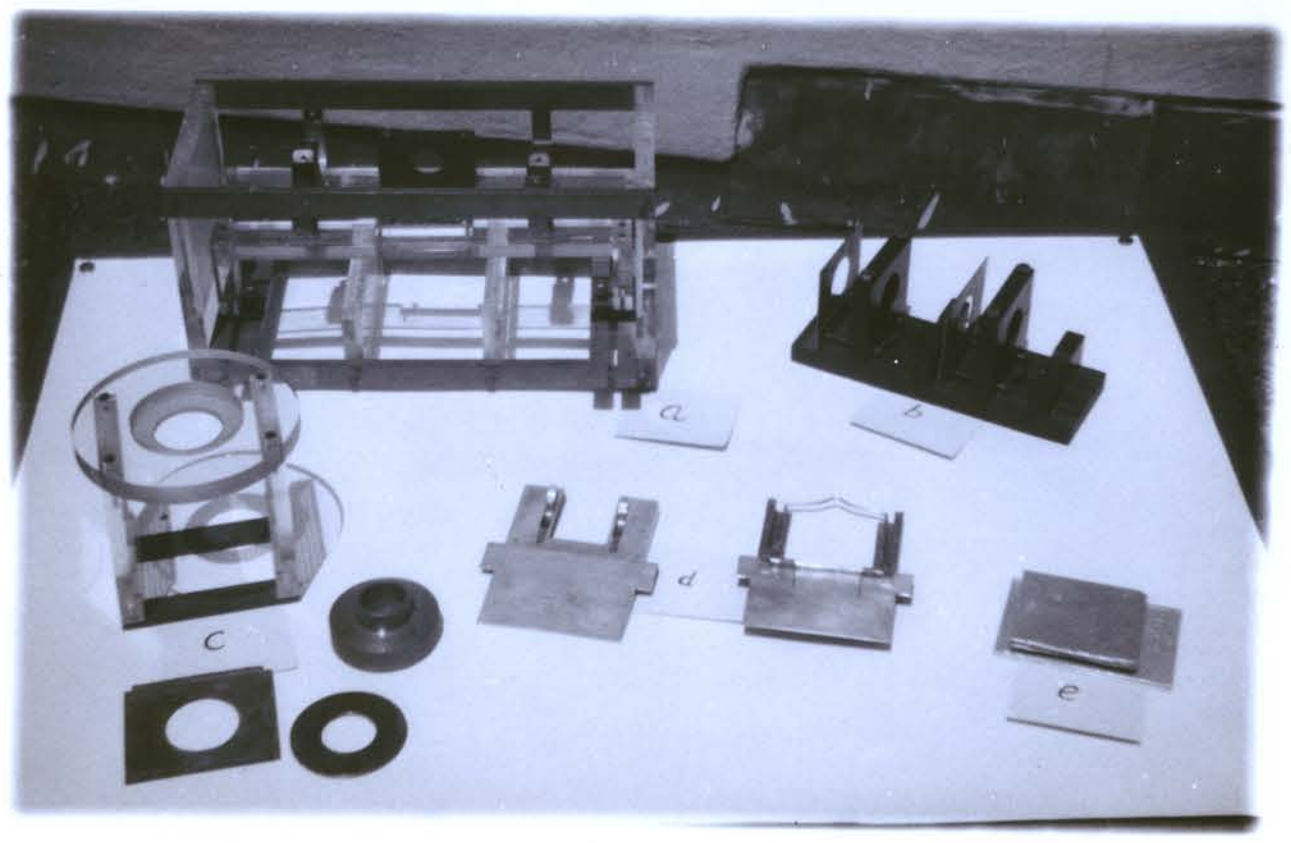

PLATE 5.

a. SUPPORT FOR COUNTERS – β-δ MEASUREMENTS.
b. SUPPORT FOR COUNTERS – COMPTON COINCIDENCES
c. SUPPORT FOR END WINDOW BETA COUNTER AND FITTINGS
d. SOURCE HOLDER AND ABSORBER HOLDER.
e. ABSORBER.